Technological University Dublin
ARROW@TU Dublin

Doctoral

Engineering

2021

# Inter-Microgrid Operation: Power Sharing, Frequency Restoration, Seamless Reconnection and Stability Analysis

Sandipan Patra
*Technological University Dublin*, patra.sandipan@gmail.com

Follow this and additional works at: https://arrow.tudublin.ie/engdoc

Part of the Electrical and Computer Engineering Commons

## Recommended Citation

Patra, S. (2021). Inter-Microgrid Operation: Power Sharing, Frequency Restoration, Seamless Reconnection and Stability Analysis. Technological University Dublin. DOI: 10.21427/NP9F-HD93

This Theses, Ph.D is brought to you for free and open access by the Engineering at ARROW@TU Dublin. It has been accepted for inclusion in Doctoral by an authorized administrator of ARROW@TU Dublin. For more information, please contact arrow.admin@tudublin.ie, aisling.coyne@tudublin.ie, gerard.connolly@tudublin.ie.

This work is licensed under a Creative Commons Attribution-Noncommercial-Share Alike 4.0 License

# Inter-Microgrid Operation: Power Sharing, Frequency Restoration, Seamless Reconnection and Stability Analysis

Sandipan Patra

A thesis submitted in fulfilment of the requirements for the degree of

Doctor of Philosophy

School of Electrical and Electronic Engineering

Technological University Dublin

2021

Under the Supervision of

Dr. Malabika Basu

*To Dadu and Dida*

# Abstract

Electrification in the rural areas sometimes become very challenging due to area accessibility and economic concern. Standalone Microgrids (MGs) play a very crucial role in these kinds of a rural area where a large power grid is not available. The intermittent nature of distributed energy sources and the load uncertainties can create a power mismatch and can lead to frequency and voltage drop in rural isolated community MG. In order to avoid this, various intelligent load shedding techniques, installation of micro storage systems and coupling of neighbouring MGs can be adopted. Among these, the coupling of neighbouring MGs is the most feasible in the rural area where large grid power is not available. The interconnection of neighbouring MGs has raised concerns about the safety of operation, protection of critical infrastructure, the efficiency of power-sharing and most importantly, stable mode of operation.

Many advanced control techniques have been proposed to enhance the load sharing and stability of the microgrid. Droop control is the most commonly used control technique for parallel operation of converters in order to share the load among the MGs. But most of them are in the presence of large grid power, where system voltage and frequency are controlled by the stiff grid. In a rural area, where grid power is not available, the frequency and voltage control become a fundamental issue to be addressed. Moreover, for accurate load sharing a high value of droop gain should be chosen as the R/X ratio of the rural network is very high, which makes the system unstable. Therefore, the choice of droop gains is often a trade-off between power-sharing and stability. In the context, the main focus of this PhD thesis is the fundamental investigations into control techniques of inverter-based standalone neighbouring microgrids for available power sharing. It aims to develop new and improved control techniques to enhance performance and power-sharing reliability of remote standalone Microgrids.

In this thesis, a power management-based droop control is proposed for accurate power sharing according to the power availability in a particular MG. Inverters can have different power setpoints during the grid-connected mode, but in the standalone mode, they all need their power setpoints to be adjusted according to their power ratings. On the basis of this, a power management-based droop control strategy is developed to achieve the power-sharing among the neighbouring microgrids. The proposed method helps the MG inverters to share the power according to its ratings and availability, which does not restrict the inverters for equal power-sharing.

The paralleled inverters in coupled MGs need to work in both interconnected mode and standalone mode and should be able to transfer between modes seamlessly. An enhanced droop control is proposed to maintain the frequency and voltage of the MGs to their nominal value, which also helps the neighbouring MGs for seamless (de)coupling. This thesis also presents a mathematical model of the interconnected neighbouring microgrid for stability and robustness analysis. Finally, a laboratory prototype model of two MGs is developed to test the effectiveness of the proposed control strategies.

# Keywords

Community Microgrid

Energy Community

Isolated Microgrid

Rural Distributed Generation

Photovoltaic Generation

Power Sharing

Power Management

Droop Control

Modified Droop Control

Frequency Control

Frequency Restoration

Reconnection

Stability Analysis

Eigenvalue analysis

Islanding

Voltage Source Inverter

Grid Supporting Inverter Control

# Declaration

I hereby certify that this thesis which I now submit for examination for the award of Doctor of Philosophy is entirely my own work and has not been taken from the work of others, save and to the extent that such work has been cited and acknowledged within the text of my work.

This thesis was prepared according to the regulations for postgraduate study by research of the Technological University Dublin and has not been submitted in whole or in part for another award in any Institute.

The work reported in this thesis conforms to the principles and requirements of the Technological University Dublin's guidelines for ethics in research.

Technological University Dublin has permission to keep, lend or copy this thesis in whole or in part, on condition that any such use of the material of the thesis is duly acknowledged.

……Sandipan Patra…….. Date: 01.09.2021

Sandipan Patra

# Acknowledgement

First and foremost, I would like to express my sincere gratitude to my supervisor Dr. Malabika Basu, for her patience, motivation, enthusiasm to support me throughout my doctoral research. Her guidance helped me in all the time of research and writing of this thesis, and one thing I would like to mention about her motivating power and soothing nature, which brought the best out of me. Her meticulous guidance, constructive and valuable suggestions, timely discussions and clarifications of my doubts increased my cognitive awareness and helped me make a deeper analysis of the research.

I would like to thank the Technological University Dublin for providing me the opportunity of doctoral research here. I also thank the graduate research school and the School of Electrical and Electronic Engineering for providing research resources and financial support.

I thank especially all my colleagues from the School of Electrical and Electronic Engineering. To name a few, Chittesh, Shahab, Shuo, Sreedhar, Arsalan, Zeeshan, Paul and Roberto, I cherished your camaraderie. Chittesh gave me a warm welcome to Ireland, and I am thankful to him for his support during my research. I am indebted to Sreedhar and Shahab for their valuable technical suggestion and kind support towards developing laboratory prototype.

I am also indebted to Finbarr O Meara, Andrew Dillon and Martin Sorohan for their kind support in every difficult situation in the laboratory.

I thank my parents for their support and unconditional love, and I miss so much being around you. Family responsibilities are as significant as research work to a researcher. My dear Sudha, I am so thankful to you for your tremendous support, understanding and motivation. I am very sorry for not being there with you. I would also like to thank all my family members for your support and encouragement during this period.

# Abbreviations List

| | |
|---|---|
| Distributed Energy Resources | DER |
| Solar Photovoltaic | SPV |
| Microgrid | MG |
| Renewable Energy Sources | RES |
| Interconnecting Static Switch | ISS |
| Coupled Microgrids | CMG |
| Power Management | PM |
| State of Charge | SoC |
| Battery Energy Storage System | BESS |
| Hardware in Loop | HIL |
| Intelligent Power Module | IPM |
| Enhanced Pulse Width Modulation | epwm |
| micro storage | MS |
| Microgrid Central Controller | MGCC |
| Small Signal Model | SSM |
| Energy Community | EC |

# Table of Contents

## Contents

Inter-Microgrid Operation: Power Sharing, Frequency Restoration, Seamless Reconnection and Stability Analysis ..... i
Abstract ..... i
Keywords ..... ii
Declaration ..... iii
Acknowledgement ..... iv
Abbreviations List ..... v
Table of Contents ..... vi
List of Figures ..... viii
List of Tables ..... viii
Chapter 1 ..... 1
Introduction ..... 1
1.1 Background ..... 1
1.2 Aims, objectives and research question ..... 5
1.3 Thesis organization ..... 7
Chapter 2 ..... 9
Review of Active Power-sharing and Frequency Control Strategies for Isolated Microgrids ..... 9
2.1 Introduction ..... 9
2.2 Different MG configurations ..... 10
2.3 Power sharing issues in rural, isolated MGs ..... 12
2.3 Review of frequency regulation of rural, isolated MGs ..... 18
2.4 Identification of research gap & proposed solution ..... 20
2.5 Novel contributions of the thesis ..... 22
Chapter 3 ..... 24
Building A Laboratory Scale Microgrid ..... 24
3.1 Introduction ..... 24
3.2 Overview of experiment setup ..... 25
3.3 IGBT module with gate driver ..... 28
3.4 Voltage and current measurements ..... 30
3.5 Controllers ..... 34
3.6 Real-time simulators ..... 39
3.7 Summary ..... 43
Chapter 4 ..... 44
Interconnection of Standalone Neighbouring Microgrids for Power-sharing ..... 44
4.1 Introduction ..... 44
4.3 Power management based droop control strategy ..... 46
4.4 The proposed control topology ..... 51
4.5 Working principle ..... 52
4.6 Simulation studies ..... 55

4.7 Experimental results ..... 60
4.8 Conclusions ..... 63
Chapter 5 ..... 65
Frequency Restoration and Seamless Reconnection of Neighbouring MGs for Power-sharing ..... 65
5.1 Introduction ..... 65
5.2 Proposed methodology for frequency/voltage regulation ..... 68
5.3 System structure ..... 73
5.4 Control topology for seamless (de)coupling of neighbouring MGs ..... 74
5.5 Working principle ..... 80
5.6 Simulation results ..... 80
5.7 Experimental validation ..... 86
5.8 Conclusion ..... 91
Chapter 6 ..... 92
Stability Analysis of Autonomous Microgrid with Proposed Droop Control ..... 92
6.1 Introduction ..... 92
6.2 Equivalent circuit diagram of coupled MG ..... 93
6.3 Inverter control structure of standalone MG ..... 94
6.4 Small signal modelling of the proposed system ..... 96
6.5 Eigenvalue analysis ..... 98
6.6 Simulation results ..... 103
6.7 Conclusion ..... 105
Chapter 7 ..... 107
Conclusions and Future Work ..... 107
7.1 General conclusions ..... 107
7.2 Future work ..... 109
Appendix A: Use of Signal Processing Methods for Efficient Islanding Detection in Static DG and a Parallel Comparison with DWT Method ..... 112
A.1 Introduction ..... 112
A.2 Proposed matrix pencil (MP) method and its application ..... 113
A.3 DWT-based islanding detection method ..... 117
A.4 System under investigation ..... 118
A.5 Simulated results with discussion ..... 120
A.6 Real-time results with discussion ..... 128
A.7 Conclusion ..... 130
Appendix B: Detail Control Technique of Inverters ..... 132
B.1 Detail inverter control topology ..... 132
Appendix C: List of Publication ..... 134
References ..... 135

# List of Figures

Figure 1.1 The monitoring and control functionalities of Microgrids ..... 6
Figure 2.1 Two islanded inverters connected to load ..... 14
Figure 3.1 Recommended laboratory test for the microgrid controller [148] ..... 24
Figure 3.2 Schematic diagram of the laboratory setup, connecting two neighbouring MG for power-sharing ..... 26
Figure 3.3 Proposed system experimental setup ..... 26
Figure 3.4 Layout of chapter 5 experimental work. ..... 27
Figure 3.5 Experimental setup for the PHIL test ..... 27
Figure 3.6 Internal circuit diagram of PM25CL1A120 [149] ..... 29
Figure 3.7 PM25CL1A120 module ..... 29
Figure 3.8 BP7B gate driver for IPM [150] ..... 29
Figure 3.9 Internal configuration of LV 25 P [151] ..... 30
Figure 3.10 Internal configuration of LA 55P [152] ..... 31
Figure 3.11 Performance of low pass filter in the current sensor board ..... 31
Figure 3.12 Schematic diagram of PCB for voltage and current sensor board ..... 32
Figure 3.13 Designed PCB for voltage and current sensor board ..... 33
Figure 3.14 FPGA based National Instrument sbRIO 9606 [153] ..... 34
Figure 3.15 Graphical interface of the proposed controller in LabView platform ..... 35
Figure 3.16 NI 9683 pinout [154] ..... 37
Figure 3.17 Stacked sbRIO 9606 on GPIC 9683 mezzanine card ..... 38
Figure 3.18 Evaluation board of F28335 controller [155] ..... 39
Figure 3.19 Front panel of OP5600 simulator [156] ..... 40
Figure 3.20 PLECS RT box with controller and I/O card [157] ..... 41
Figure 3.21 PLECS C2000 Launchpad development kit ..... 42
Figure 4.1 Proposed system configuration ..... 47
Figure 4.2 Proposed droop control ..... 48
Figure 4.3 Inverter control topology ..... 50
Figure 4.4 Flow chart to calculate power setpoints in different modes of operation ..... 52
Figure 4.5 Power flow for operation mode A ..... 53
Figure 4.6 Power flow for operation mode B ..... 53
Figure 4.7 Power flow for operation mode C ..... 54
Figure 4.8 Power flow for operation mode D ..... 54
Figure 4.9 Power flow for operation mode E ..... 55
Figure 4.10 System parameters for case study A ..... 55
Figure 4.11 Illustration of MG 1 overloading ..... 56
Figure 4.12 Illustration of MG 2 overloading ..... 57
Figure 4.13 Illustration of MG 1 & MG 2 both are overloaded ..... 58
Figure 4.14 Illustration of BESS charging situation ..... 59
Figure 4.15 Experimental prototype of the proposed system ..... 60
Figure 4.16 MGs operating condition- (a) in decoupled mode and (b) effect of a sudden load change 61
Figure 4.17 MGs power-sharing - (a) symmetric and (b) asymmetric power-sharing ..... 62
Figure 4.18 Power transfer between the MGs (a) power from MG1 to MG2 (b) Power from MG2 to 1. IPCC ..... 62
Figure 5.1 Conventional droop control (a) p-f droop control (b) V-Q droop control ..... 69
Figure 5.2 Proposed improved double layered droop control ..... 70
Figure 5.3 Block diagram of the proposed control topology. ..... 72
Figure 5.4 Structures of MGs understudy ..... 73
Figure 5.5 Proposed frequency-voltage controller for seamless connection ..... 74
Figure 5.6 Layout of the coupling controller ..... 76
Figure 5.7 Connection criteria ..... 76
Figure 5.8 Layout of the decoupling controller ..... 77

Figure 5.9 Disconnection criteria ..... 78
Figure 5.10 Final setpoint calculation ..... 78
Figure 5.11 Integration technique of the controllers ..... 79
Figure 5.12 Voltage and current profile of MG1 ..... 81
Figure 5.13 Microgrid 1 load demand and frequency profile ..... 82
Figure 5.14 Microgrid 1 load demand and frequency profile ..... 82
Figure 5.15 Illustration of the seamless interconnection of MGs ..... 83
Figure 5.16 Power sharing performance in interconnected mode ..... 84
Figure 5.17 Illustration of seamless decoupling ..... 85
Figure 5.18 Reconnection of MGs after decoupling ..... 85
Figure 5.19 MG1 and MG2 are operating in islanded mode ..... 87
Figure 5.20 Illustration of frequency restoration controller ..... 87
Figure 5.21 Illustration of seamless coupling of MGs ..... 88
Figure 5.22 Illustration of MG coupling without activating the coupling controller ..... 89
Figure 5.23 Illustration of seamless decoupling of MGs ..... 89
Figure 5.24 Illustration of seamless reconnection of MGs ..... 90
Figure 6.1 Equivalent circuit and power flow of coupled MG ..... 93
Figure 6.2 Single-phase to d-q transformation ..... 95
Figure 6.3 Proposed standalone MG controller ..... 96
Figure 6.4 Eigenvalue locus with real power droop gain change ..... 101
Figure 6.5 Eigenvalue locus with reactive power droop gain change ..... 101
Figure 6.6 Eigenvalue locus with load variation ..... 102
Figure 6.7 Eigenvalue locus with the variation of transmission line parameter ..... 102
Figure 6.8 Voltage drop analysis in a 50 KM rural network with an R/X ratio of 1.5 ..... 103
Figure 6.9 Voltage drop analysis in an 80 KM rural network with an R/X ratio of 1.5 ..... 104
Figure 6.10 Power sharing performance of MGs with different line impedance ..... 105
Figure A.0.1 Behaviour of frequency at PCC ..... 113
Figure A.0.2 Flow chart of proposed islanding detection with MP method ..... 116
Figure A.0.3 Flow chart of DWT based islanding detection method ..... 118
Figure A.0.4 System configuration and control strategy of inverter ..... 119
Figure A.0.5 Simulation result of large negative power mismatch with (a) proposed MP method (b) DWT method ..... 121
Figure A.0.6 Simulation result of close to zero power mismatch with (a) proposed MP method and (b) DWT method ..... 122
Figure A.0.7 load switching (non-islanding event) with (a) proposed MP method and (b) DWT method ..... 123
Figure A.0.8 Simulation result of nonlinear load switching with (a) proposed MP method and (b) DWT method ..... 124
Figure A.0.9 Capacitor switching (non-islanding event) with (a) proposed MP method and (b) DWT method ..... 125
Figure A.0.10 Effect of 13 and 17 order harmonics on (a) proposed MP method and (b) DWT method ..... 127
Figure A.0.11 Effect of load quality on (a) proposed MP method (b) DWT method ..... 127
Figure A.0.12 Opal- RT laboratory setup ..... 129
Figure A.0.13 Real-time result of close to zero power mismatch with (a) proposed MP method (b) DWT method ..... 129
Figure A.0.14 Real time result of the effect of non-linear load (non-islanding event) with (a) proposed MP method (b) DWT method ..... 130
Figure A.0.15 Real time result of effect of 13 and 17 order harmonics on (a) proposed MP method and (b) DWT method ..... 130
Figure B.0.1 Detail inverter control topology for the standalone mode of operation ..... 132
Figure B.0.2 Detail inverter control topology for the interconnected mode of operation ..... 133

# List of Tables

Table 2.1 Summary of different droop control methods ..... 17
Table 2.2 Summary on the literature of frequency regulation in MGs ..... 19
Table 3.1 Specification of PM25CL1A120 module ..... 28
Table 4.1 MG Parameters ..... 51
Table 5.1 Assumed System parameters ..... 80
Table 6.1 Nominal system parameters ..... 99
Table 6.2 System eigenvalues ..... 100
Table A.1 Parameters of the studied system ..... 120
Table A.2 Power mismatch and estimated parameters ..... 120

Chapter 1

# Introduction

## 1.1 Background

Renewable energy resources will constitute the backbone of the sustainable energy systems of the future and, due to their different characteristics and dependence on climate and geography, they will be scattered throughout host power systems. Most of them must be interfaced with the host grids via power electronic converters. Climate change issues and security of supply have been the driving force for significant changes in electricity generation and consumption.

The penetration level of Distributed Energy Resources (DER) (like Solar Photovoltaic (SPV), wind, fuel cells, micro-hydro etc.) and plug-in hybrid electric vehicles is increasing day by day, and the requirements of community-based microgrids in a rural area or in a commercial building is also becoming a new trend in modern electricity markets. According to the Ireland Government Climate Action Plan 2019 [1], 70% of the total electricity should be generated from the renewables by 2030. In order to achieve that the government planned to increase the number of sustainable energy communities to 1500.

A Microgrid (MG) is a combination of DERs with electrical storage (battery, diesel generator etc.), operating as a coordinated system, is able to function in parallel with the main utility grid or in island mode. As of 2019, 3,869 microgrids or 60.8 GW of total microgrid capacity have been either planned, proposed, under construction or in operation, worldwide [2], [3]. Greentech and other media houses predicted the capacity

of community microgrids in the United States will increase from 3.2 to 6.5 GW in 2017-2027, which will involve an investment of $12.5B [4]–[6].

Amongst Renewable Energy Sources (RESs), small to large scale installations of SPV plants have been developed in the last few years all over the world. The European Commission established a motivating goal that 20% of primary energy should be generated by using RESs by 2020 and 27% by 2030 and this target needs to be implemented in all member countries [7]. According to the last report from the International Energy Agency (IEA-PVPS), the total installed photovoltaic capacity in the EU exceeded 200 GW at the end of the year 2017. The advantage of using multiple RESs together like PV-PV, PV-wind, can offer some seasonal and diurnal balancing properties in relation to the reliability of the system.

The technical requirement for the connection of DER based MGs with the utility grid is provided in IEEE 1547-2018 standards [8], in order to maintain the stability, reliability and power balance during any grid-fault or unintentional islanding. The IEEE standard recommends isolating the DERs from the grid during any grid fault. This approach is adequate only when there is a proper power balance between the generation and load demand.

But the electrification of remote and rural areas has always been a significant challenge due to a variety of constraints such as the area accessibility and economic factors. The electricity demand in these areas can be supplied with the help of DERs in an islanded scheme. Thus, the power system of the remote regions can be considered as a MG that operates in islanded mode. The MGs should be formed such that there is enough generation capacity in their embedded DERs to meet their local demands. It is to be noted that a remote area/town can be supplied by several independent MGs, where

each may have a different owner (operator), and each is responsible for providing the load demand of a specific region.

In addition, smaller generators (like small islanded MGs) have economic benefits such as shorter construction times and transmission lines [9]. The policy and prospective planning achievements for rural electrification are well discussed in [10], [11]. African countries such as Uganda or Nepal or India, have their own site-specific requirements and community microgrids has been developed according to that. Pre-planned rural islanded electrification is also well discussed in [12]–[14]. The development of such rural off-grid community microgrids has been well reported by the Canadian Government [15].

The intermittency of non-dispatchable (e.g., SPV and wind based) DERs in addition to load uncertainties can lead to an imbalance between the instantaneous power generation and demand in an isolated MG. Any generation deficiency (overloading) will lead to a voltage/frequency drop. To address power imbalance problems in isolated MGs, several solutions provided by researchers and are pointed out below:

- Under frequency/voltage load-shedding [16];
- Utilisation and control of battery energy storage system (BESS) [17];
- Optimal capacity design of dispatchable DERs (e.g., diesel generators) [18];
- Interconnection of the MG to utility [19];
- Coupling of one MG to one/more neighbouring MG(s) [20].

Implementation of intelligent demand response techniques or installation of micro storage devices like battery, diesel generator or flywheel etc. can provide required power to avoid this power scarcity. However, load shedding is still necessary if there is not sufficient power in MG as well. Coupling of neighbouring isolated MGs are economical and technically more feasible for any power exchange during any contingency. So, under

this condition, a microgrid should have sufficient options to operate in grid-connected mode or in standalone mode. If the microgrid operates in standalone mode, then overloading can be managed by coupling the microgrid with the neighbouring one. MGs coupling is introduced in [20] as a solution to proliferate the number of DERs in distribution networks. Each MG may be supported by one/more of its neighbouring MG(s) during a power deficiency. This can be achieved by closing the normally open Interconnecting Static Switch (ISS) which is located between every two adjunct MGs.

Inverter parallel operation is the crucial issue of standalone Coupled Microgrids (CMG). The objective of the parallel inverter system is to realise the load sharing between inverters and keep the voltage and frequency stable under different load conditions and during load variations. Usually, a conventional droop control method is employed to control the load sharing between the inverters. In a low-voltage static microgrid, as the distribution feeder is mainly resistive, this droop method is subject to poor transient (or even poor stability) due to poor decoupling of the real and reactive power when no additional inductance is present. The intermittent nature of the DERs (SPV, wind) has also the significant effect on the accuracy of active and reactive power control during islanding mode due to which an unexpected voltage and frequency drop may occur. Due to any sudden voltage and frequency drop, the stability of the individual MG can also deteriorate. Lots of new research has been conducted to overcome these drawbacks during these uncertain circumstances. The literature review in the following sections has addressed the pros and cons of different new findings. However, more research is still necessary to propose an efficient and stable controller to couple the neighbouring MGs for available power-sharing, and this finding has helped to form the aims and objectives of present thesis.

## 1.2 Aims, objectives and research question

Maintaining generation/demand balance in a power system is a critical task for a system operator. This requires maintaining a certain level of flexibility in the system, which forms an inevitable system service requirement. Microgrid can be isolated to deliver energy to the local communities efficiently, where large power grid back-up is not economically feasible. Such rural community microgrids are most likely to experience overloading due to the intermittency of renewable energy sources and load demand. The research in monitoring and control of rural microgrids has been ongoing for the last two decades to protect and enhance the critical community infrastructure during any contingency. In this regard the coupling of isolated neighbouring microgrid is the way to enhance the power resiliency, stability and sustainability.

This thesis is mainly focused on investigating the operational challenges of two parallelly connected inverter-based islanded microgrids. In the following, the **significant challenges** for coupling the neighbouring microgrids are highlighted:

- Share the power between the neighbouring microgrids and as well as maintaining the voltage and frequency setpoints in the absence of grid power.
- Restoration of frequency and voltage to its nominal value for a stable mode of operation.
- Facilitating a seamless reconnection topology between the neighbouring MGs.
- Ensuring stability of the coupled system.

To address these challenges, the primary **research questions** this thesis seeks to answer are:

- How to share the power efficiently among the neighbouring microgrids?

- How to monitor and control the reference set point of voltage and frequency?
- How to ensure the system stability and design a seamless interconnection topology among the isolated microgrids, where the system has only static generation?

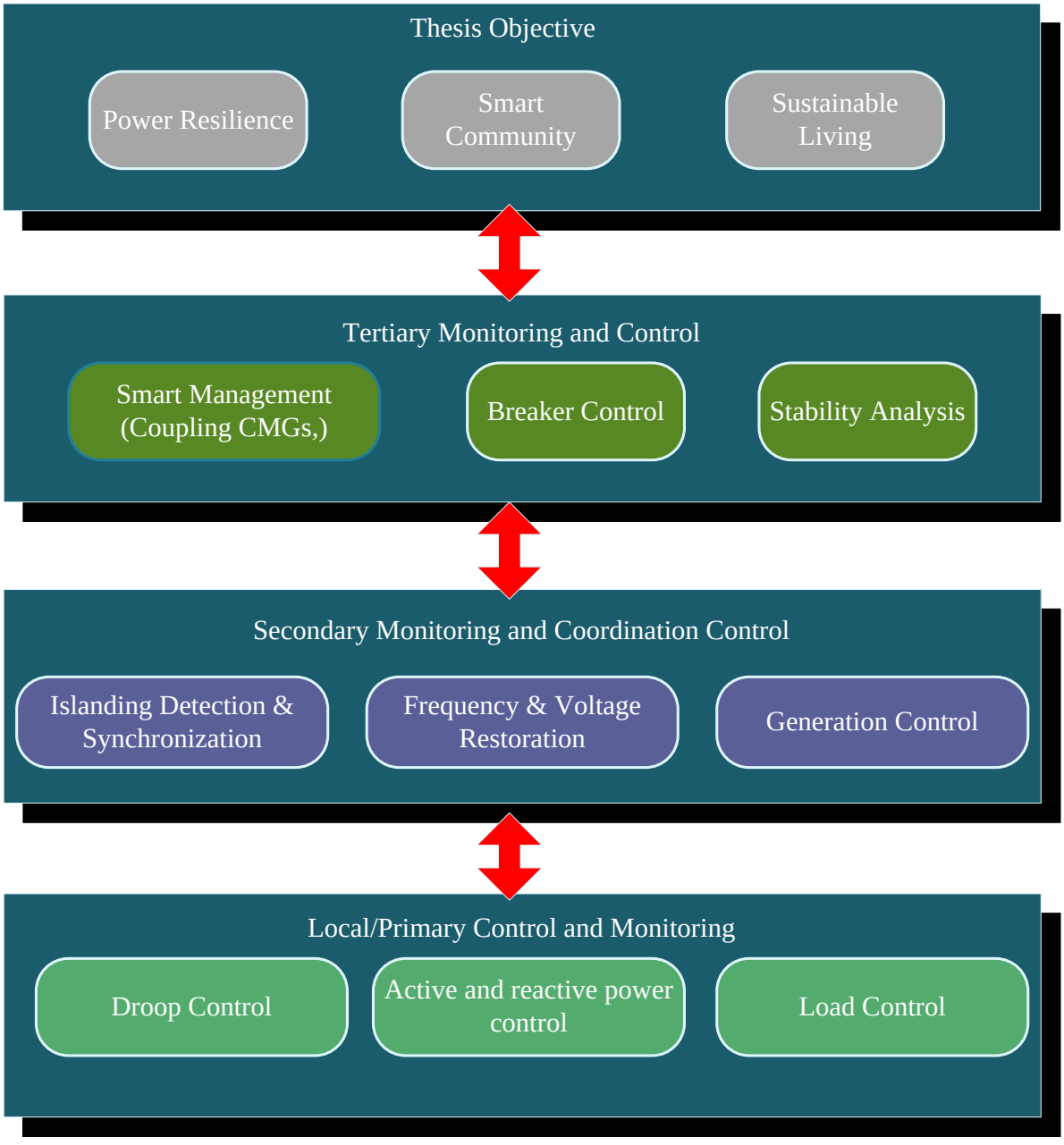


*Figure 1.1 The monitoring and control functionalities of Microgrids*

To address these research questions, the foremost **objectives** of the thesis are summarised as follows:

- To design a controller for the most efficient coupling of neighbouring MGs for available power-sharing.
- An improved droop control with frequency and voltage restoration that can be implemented to share the power among community MGs.
- A seamless reconnection mechanism among community microgrids should be established for stable mode of operation.
- A mathematical model of the coupled system has to be developed to ensure a stable mode of operation.

The monitoring and control functionalities have been summarised in Figure 1.1.

## 1.3 Thesis organization

The thesis has been organised in seven chapters. Chapter 1 presents the introduction and the motivation of the research. In Chapter 2, a relevant literature survey pertinent to the research contribution, which is presented in the subsequent chapters.

Chapter 3 introduces the details of the experimental setup of small-scale MGs in order to verify the efficacy of the proposed controller. A short description of voltage and current sensor boards and all the controllers used for the implementation is provided in this section.

In Chapter 4, a load sharing control topology among the neighbouring standalone static MGs is discussed. This chapter focuses on developing an interconnection scheme, for connecting neighbouring standalone single-phase AC MGs that have no access to a utility grid. A power management based droop control strategy is developed in order to share the power among the neighbouring MGs, keeping the voltage and frequency within acceptable limits.

In Chapter 5, a double layer advanced droop control is proposed for frequency/voltage restoration in CMG. The frequency regulation in islanded AC MGs with no/low inertia (i.e., those consisting entirely of static generation like PV) is addressed in this chapter. The proposed control architecture ensures the frequency and voltage is restored to its nominal value without compromising the power-sharing capability of the coupled system. In the proposed frequency/voltage restoration technique, double layer droop control is introduced by adjusting the droop gain according to the nominal value. It uses the d-axis component of the terminal voltage to restore the frequency or voltage. The proposed control topology also helps to de(couple) the neighbouring microgrids seamlessly. The seamless de(couple) mechanism also discussed in this chapter.

A very high gain of droop control ensures the power-sharing accuracy in resistive and weak rural networks. But it provides a negative impact on overall system stability. The drawbacks in weak and resistive networks is eliminated by introducing the double layer droop control. A mathematical model is presented to analyse the stability of the proposed controller. Frequency domain modelling and eigenvalue analysis of coupled islanded MG is presented in Chapter 6.

The general conclusion and the scope of the future work are presented in Chapter 7.

Chapter 2

# Review of Active Power-sharing and Frequency Control Strategies for Isolated Microgrids

## 2.1 Introduction

Due to very high electricity demand over the last decade, there is a dire need to espouse the alternative renewable energy resources into modern civilisation. The massive proliferation of renewable energy sources raises many technical and social issues [21]–[26], but overall, it can also be used to meet the increasing power demand. A microgrid, which incorporates the renewable energy sources is able to operate in grid-connected mode and islanded mode. The low scale microgrids are incredibly beneficial for a remote and rural area where the main power grid is not available due to some constraints like area accessibility and economic concern. But due to the very high increase in load demand and intermittent nature of renewable energy sources, microgrids become very uncertain about meeting the load demand properly. So, in order to resolve the energy balance glitches locally, some additional action has to be taken like, - intelligent load-shedding [27], [28], installation of micro storage elements [29]–[31], and coupling of neighbouring MGs [32], [33], [42], [43], [34]–[41]. The installation of micro storage elements- battery energy storage system (BESS), flywheel, diesel generator etc. can enhance some extra flexibility and reliability in these standalone rural MGs. On the other side, these storage devices are not economically feasible, and they also have some power limitations. In the case of very high load demand; however, the load shedding is required to maintain stable operation. In this situation, if possible, the

coupling of neighbouring standalone microgrids is economically and technically more feasible to meet the scarcity of power demand.

The power-sharing of neighbouring MGs can be achieved by connecting the MG inverters parallelly. The proper load sharing can be achieved by implementing different control topologies like power management based secondary control, communication less droop control etc. But among them, droop control is the most commonly used to realise load sharing. In a rural microgrid, where distribution networks are mainly resistive, droop control usually provides abysmal performances. Moreover, in the case of rural standalone static (like solar photovoltaic generation) MGs, frequency and voltage control is another crucial issue, that needs to be addressed. This thesis is focused on developing a control topology for the most efficient coupling of neighbouring MGs.

In this context, this chapter provides an extensive literature survey to understand the state of the art practice, identify the research gap and to develop the research objectives.

## 2.2 Different MG configurations

SPV, wind, diesel generators, and BESS are most commonly used in rural MGs. Among them, the installation of PV plants is significantly increased in the last 5 years [44]. The intermittent nature of SPV power generation poses a significant challenge to the widespread adoption of SPV systems in isolated microgrids. This necessitates the deployment of BESS to complement the intermittent generation of SPV units in order to maintain the power balance in islanded microgrids. In other words, battery systems mimic the role the utility grid plays in grid-connected microgrids, to supply/absorb needed/surplus energy. However, battery systems have limited power ratings, limited capacities, and restricted charging scenarios that depend on the battery state-of-charge (SoC). Therefore, the operation of the SPV and battery units must be coordinated to

consider both the intermittent SPV generation and the operating constraints of the battery units. Moreover, SPV and battery units must be able to coordinate with dispatchable units that are commonly deployed to ensure continuity of supply. But in some cases, the cost of the battery and its low life cycle (could have to be replaced 3 times in a total SPV plant life cycle) is the main obstacle for battery installation. In community-based MG where the power rating typically varies from 5-50 kW, a central storage system is eventually more effective than installing locally for each end-user.

According to the existing literature regarding the rural microgrid structure, there are a considerable number of variations in that. Usually, PV, Wind, Diesel generators, Biomass, and BESS are the most used power resources for the implementation of small scale rural MGs [29], [45]–[49]. These implemented microgrids are on the scale of 1kW-600 kW, either in single-phase or in 3-phase. Keep in mind, with the efficiency increment in solar cells, the penetration of PV installations has also increased. A significant number of MGs with only PV and BESS are also either implemented or are under construction [48], [50]–[52]. These kinds of community-based or private PV MGs either use a grid or BESS as a backup.

As discussed previously, battery units are costly, and sometimes it is not economical to deploy together with each PV units. Moreover, for a coordination strategy, to be practical, it should be able to handle multiple units of different types of microgrids in a decentralized/centralized fashion with minimum transients when switching among different control objectives/modes. Considering all these pros and cons, two community based rural, isolated PV microgrids have been considered for power-sharing during any power shortage/excess. In this circumstance, as both the microgrids are PV based static MG, frequency and voltage regulation become very crucial during power-sharing.

## 2.3 Power sharing issues in rural, isolated MGs

### *2.3.1 Mode of operation*

Until now, most MG configurations have been the AC microgrid in grid-connected mode. But nowadays the isolated mode of operation is also gaining significant attention, especially in remote areas [6], [15]. The DG units of a microgrid can be classified into grid forming (voltage-controlled) and grid-following (current-controlled) DG units. In grid-connected mode, the units are often controlled as grid-following. The most adopted control strategies for grid-following inverters are discussed in [53]. In islanding mode, the electronic converter interfaces between the loads and the micro-source act as voltage sources, which are also responsible for the power-sharing according to their ratings and availability of power from their corresponding energy sources or prime movers.

Among the different existing control strategies, integrated control strategies refer to hierarchical structures, which usually consist of primary, secondary, and tertiary control. The primary control stabilizes the voltage and frequency and offers the plug-and-play capability for DGs. The secondary control, as a centralized controller, compensates for the voltage and frequency deviations to enhance the power quality. Tertiary control considers the optimal power flowing of the whole microgrids or interaction with the main grid [54]. In addition, hierarchical control has other special functions: 1) distributed intelligent management system [55]; 2) voltage unbalance compensation for optimal power quality [56]; 3) self-healing networks [57]; 4) smart home with a cost-effective energy ecosystem [58]; and 5) generation scheduling [59]. So, the hierarchical structure of microgrids can be regarded as an intelligent, integrated, and multiagent system. Some reviews of microgrid control have been published recently in [60], [61]. Reference [60] classifies all the control strategies (e.g., decentralized control, centralized control, model

predictive control, and multiagent systems) into three levels: 1) primary; 2) secondary; and 3) tertiary based on their speed of response and infrastructure requirements. The authors also highlight future challenges and trends in microgrid control. Reference [61] discusses the control methods and objectives from the point of the voltage and frequency stability and presents the factors affecting power load sharing.

Power management strategies for PV/battery hybrid units are proposed in [62]–[67]. In a hybrid unit, the PV and battery systems are integrated and deployed as a single system in the microgrid. In this configuration, the control strategy has the advantage of accessing both the PV power measurements and the battery SoC. Therefore, the strategies in the above literature cannot be utilised for decentralised power management of separate PV and battery units in islanded microgrids. The control strategies proposed in [66], [67] are specifically designed for a single unit microgrid, which, from a control point of view, acts as a standalone power supply. Therefore, they cannot be deployed in multiple-unit microgrids without modification. A novel control strategy is developed to avoid the DC bus voltage collapse in a PV-BESS based hybrid standalone system [68], where PV and BESS both are considered as voltage sources. However, any power management strategy of the battery units is not considered. In further research [69], a multi-segment adaptive *p-f* droop control is proposed. This control strategy is applied for a single PV and a single BESS unit.

In the above section, all the individual control topologies of the isolated MGs are discussed. But in order to operate the MGs in islanded mode and to share the power among the neighbouring MGs, can be done using communication-based control or by the communication-less droop control technique. Coupling of hybrid (combination of different RESs) MGs and their coupling issues are also elaborately discussed by the

researchers in [32], [35], [36], [39], [40], [70]–[72]. The communication-based control techniques like concentrated control [73], master/slave control [74], distributed control [75] etc. have their own pros and cons and are well discussed in recent literatures [76], [77]. A dynamic multi-criteria decision-making system based overload management technique is presented in [37], [38]. However, the computational burden and communication channel is the main drawback of these proposals. These control techniques required the communication lines among the MGs, which sometimes reduce the reliability and expandability and also increase the cost of the system. However, in the droop control method, the system cost is reduced, and the reliability and the redundancy of the system also increases. Those are the apparent reasons for dropping the implementation idea of a communication-based control technique, especially in rural MGs. A complete review of droop control based clustering topology is also proposed in recent literature [78]–[80]. The next section provides a comprehensive review of different droop control techniques.

### *2.3.2 Droop Control based power-sharing*

In this section, an extensive review of different droop control techniques is presented. The conventional frequency droop control is first demonstrated. The basic power system model of two DG sources with the load in the point of common coupling is presented in Figure 2.1.

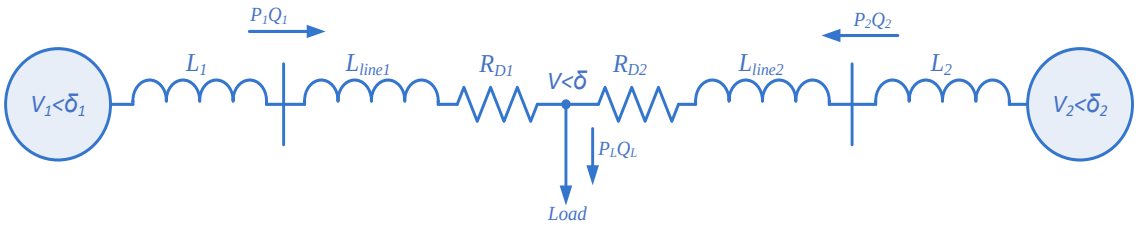


Figure 2.1 Two islanded inverters connected to load

The microgrids output voltages are denoted by $V_1\angle\delta_1$ and $V_2\angle\delta_2$ with the output

filter inductance of $L_1$ and $L_2$. $P_1$, $Q_1$, and $P_2$, $Q_2$ are the active and reactive power of the microgrids where $P_L$ and $Q_L$ are representing the active and reactive power demand by the Loads. The line resistances are denoted by $R_{D1}$ and $R_{D2}$ while $L_{Line1}$ and $L_{Line2}$ are representing the line inductance.

The conventional droop equations are given below

$$\omega = \omega_N - mP \quad (2.1)$$

$$V = V_0 - nQ \quad (2.2)$$

Where $m$ and $n$ are the droop coefficient; $\omega_N$ and $V_0$ are the nominal frequency and voltage, respectively; $P$ and $Q$ represent the active and reactive power supplied by the converter. The main objective is to control frequency and voltage by controlling the active and reactive power outputs of microgrids.

However, this conventional droop control presents several drawbacks especially

- In the islanding mode of operation, frequency, and voltage control are the most critical parameters to be controlled. By implementing the steeper droop (very high droop gain), the power-sharing accuracy can be achieved, but the voltage and frequency deviation increase a lot, and that may lead to microgrid instability [81].
- A highly resistive line typically used in rural networks, challenges the power-sharing controller efficacy. Strong coupling of active and reactive power leads to inaccurate load-frequency control. A high gain of droop co-efficient is required to ensure proper load sharing. However, a very high gain also has a negative impact on the overall stability of the system [81].

- ❖ The conventional droop control fails drastically in the presence of harmonic power as the conventional droop control is designed based on fundamental power-sharing [82].
- ❖ The intermittent nature of renewable energy sources is also the reason for the failure of conventional droop control [83].

Due to these reasons, the topic has been of active research interest to overcome these drawbacks. Lots of improved droop control (compared to the conventional droop control) have been proposed by the researchers. However, these techniques also have their own merits and demerits. Most of the proposed droop control techniques with their advantages and disadvantages are represented in tabular form in Table 2.1.

It is to be noted that each of the above techniques can only accommodate two of the symmetrical or hybrid DG units in microgrids. In most of the existing work, symmetrical droop units have been considered, although these units are the most common type in islanded microgrids to ensure the continuity of the supply. In symmetrical droop control, the inverters can share the power equally, which sometimes restricts the MGs to take the foremost advantage of coupling. Moreover, in rural MG, due to resistive coupling networks, a very high droop gain is required to achieve the accurate power sharing. The high value of droop gain can create a significant frequency deviation. So, the maintaining of frequency in rural isolated MG is another important task. The next section reviews the different frequency regulation techniques in MGs.

*Table 2.1 Summary of different droop control methods*

| Control | Variants | Advantages | Disadvantages |
|---|---|---|---|
| Conventional droop | P-ω and Q-V [84] | • Avoid critical communication link<br>• High reliability, expandability and flexibility. | ○ Slow dynamics response<br>○ Poor harmonic load sharing<br>○ Poor voltage and frequency regulation<br>○ Poor performance with renewable energy resources |
| | VPD/FQB droop control [85]–[87] | • Designed for the highly resistive line. | ○ Poor voltage and frequency regulation<br>○ Poor performance with renewable energy resources |
| | Complex line impedance [88] | • High accuracy on voltage regulation | ○ Line impedance should be known in advance |
| | Angle droop control [89], [90] | • High accuracy on frequency regulation | ○ Poor accuracy on power-sharing.<br>○ Requirement of a communication signal. |
| Virtual impedance (VI) based droop | Output impedance Control method [75], [91] | • Faster dynamics response<br>• Good power-sharing<br>• Excellent current sharing | ○ Difficult to choose the suitable coefficient for the integral-derivative term and filter gain<br>○ Poor voltage regulation |
| | Virtual frame transformation method[92], [93] | • Decoupled P/Q sharing control | ○ Requirement of a communication signal.<br>○ System parameters should be known.<br>○ Difficult to implement |
| | Enhanced VI control [94] | • Better voltage harmonic sharing<br>• Minimize harmonics circulating currents<br>• Good dynamics response | ○ System parameters should be known.<br>○ Requirement of a communication signal.<br>○ Sometimes Poor active power-sharing |
| | VI with conventional droop [95] | • Better voltage harmonic sharing<br>• Accurate reactive power-sharing | ○ Poor stability<br>○ Poor active power-sharing |
| Adaptive droop | Adaptive voltage droop control [96], [97] | • Excellent power-sharing under heavy load condition<br>• Good transient response | ○ Virtual reactance need to minimize the circulating power<br>○ System parameters should be known. |
| | Optimization-based Adaptive droop [98], [99] | • Improve power-sharing<br>• performance and system stability | ○ Complicated, difficult to implement.<br>○ Poor active power-sharing |
| Robust Droop | [100], [101] | • Modified the droop equation by subtracting RMS output voltage value to the voltage set point.<br>• Improve reactive power-sharing.<br>• Good frequency and voltage regulation. | ○ High total harmonic distortion of current components<br>○ System parameters should be known. |
| Signal Injection method | [102], [103] | • Can handle the linear and non-linear load | ○ Cause harmonic distortion of voltage. |

## 2.3 Review of frequency regulation of rural, isolated MGs

A mismatch between the supply and demand in an isolated MG creates the frequency or voltage deviation. In a RESs based static MG where generation and loads both are intermittent in nature, frequency control plays a vital role in system stability. In this section, an detailed review of the frequency regulation of isolated microgrid is presented.

In grid-connected mode, a microgrid is connected to the main grid, which usually has large system inertia; hence, the microgrid frequency is almost identical to the nominal value [104]. Thus, DG units in a microgrid typically inject the desired output power, and the electrical power mismatch between supply and demand is balanced by the main grid. However, in islanded mode, the microgrid must supply its own demand and maintain its frequency solely using DG units. There have been several studies aimed at developing control of active power and frequency for islanded microgrids. The following section arranges the literature of frequency regulation schemes in MGs into four major layouts, and those are:

- Frequency regulation based on demand response.
- Frequency regulation with different control strategies.
- Frequency regulation by installing energy storage devices and
- Frequency regulation with intelligent optimization techniques.

Based on the above layouts, a survey on frequency control in MG is presented in Table 2.2, in a very lucid manner with their respective advantages and disadvantages.

*Table 2.2 Summary on the literature of frequency regulation in MGs*

| | References | Reported Work | Limitations |
|---|---|---|---|
| Demand response (DR) based frequency regulation | [105]–[110] | 1. Provides frequency and voltage regulation.<br>2. Wind-based RESs used.<br>3. Droop based DR is also proposed | 1. Requirement of a communication channel.<br>2. System parameters should be known properly.<br>3. Transient response time is deficient due to computational burden. |
| | [111], [112] | 1. A novel quasi-oppositional selfish-herd optimisation algorithm is proposed for load-frequency control | 1. Transient response time is very low due to computational burden.<br>2. Implementation will be very complicated. |
| | [113] | 1. A demand response based secondary control is proposed for load-frequency control. | 1. Requirement of a communication channel.<br>2. Response during the intermittent nature of load/sources is not shown. |
| Frequency regulation with different control strategies | [88], [114]–[117] | 1. Traditional Load-frequency control (LFC) is proposed.<br>2. Consideration of EVs in some cases as a worst-case scenario.<br>3. Optimization/ model predictive control based LFC is also proposed. | 1. In most cases, practical implementation is not done. It can be complicated due to the complexity in control topology.<br>2. Transient response time is high.<br>3. Accuracy of power-sharing is not considered. |
| | [110], [113], [114], [118]–[124] | 1. A secondary loop is proposed for frequency control<br>2. Sliding mode control/ Liapunov based robust control is also proposed<br>3. Communication delay is also considered in some cases.<br>4. Shipboard/ EV is also introduced for validating the efficacy of the proposed controller. | 1. Requirement of a communication channel.<br>2. Accuracy of power-sharing is not considered.<br>3. Challenging to implement due to complexity in control topology.<br>4. Transient response time is high due to the secondary loop. |
| | [125], [126] | 1. A reliability-based model is proposed for frequency control.<br>2. A small-signal stability based approach is considered for frequency regulation | 1. Power-sharing accuracy is not considered.<br>2. System parameters should be known in advance for analysis. |
| Frequency regulation with the installation of energy storage devices | [119], [120], [127]–[130] | 1. Energy storage devices like BESS, flywheel, supercapacitor, diesel generator are introduced for frequency control. | 1. Installation cost is very high<br>2. May have to replace 2/3 times in a whole MG life cycle. |

| | | | |
|---|---|---|---|
| Optimization based approach for frequency control | [115], [118], [122], [123], [131]–[136] | 1. Different optimization techniques has been adopted for frequency regulation in LFC control, droop control, secondary loop of frequency control etc. | 1. Due to high computational time, the transient response is low.<br>2. Processing delay in performance due to communication delay.<br>3. With the aid of central MG controller, an extra layer for the optimization technique should be implemented.<br>4. In case of large no of constraints presence in MGs, the formulation of objective function become complex. |

## 2.4 Identification of research gap & proposed solution

It is to be noted that most of the proposed control methods as discussed above for frequency regulation/restoration is for a single unit of the micro-generation system. These researchers are mainly focused on the negative effect of low inertia on inadequate dynamic response following significant disturbances when the transient frequency dip can become unacceptable. The frequency regulation in inertia less microgrid gained attentions to the researchers [137]–[139] as the inertia less PV installation is increased in the last decade. The load frequency control in these kinds of inertia less system can be achieved by sharing the active power with neighbouring microgrids. An asymmetrical droop control should be proposed to take the coupling advantages of an isolated microgrid. The asymmetrical droop control will not restrict the MG inverters, to share the power equally. The MGs will be able to share the power according to their power availability. Problems may arise if the frequency deviation is significant, in case of choosing high droop gain. Under these circumstances, this will impose too great a burden on the frequency control units. Hence, it is desirable that the active power should be "re-shared" among DG units after the primary droop control action, so that proper load

sharing may occur.

Eventually, the *f-P* droop loop regulates the phase angle of the MG inverter and generates the control signal via an integral controller for the other control blocks. So, restoration in frequency is theoretically in conflict with the idea of active power-sharing as the active power production is sensitive to the phase angle. This distinguishable phenomenon of frequency restoration can bring significant inaccuracy in active power-sharing. Very few researchers [140], [141] have mentioned this particular issue, though their provided solutions were not promising as that creates a stability related issue in the network.

Additionally, in the worst-case scenario, when the load demand is too high, and the available RESs (in coupled MGs) are unable to supply the load demand, the MGs should be decoupled in order to maintain the system stability. In some cases, intelligent load shedding or a demand response technique can be introduced to maintain the system stability. In this condition, a seamless connection/reconnection topology is required for the smooth operation of power-sharing among the neighbouring MGs.

In a rural network, with a very highly resistive line (with a ratio of $R/X > 3.5$) [142], the power-sharing efficiency between the inverters reduce. A very high value to droop gain is required for proper load sharing, which reduce the system stability. Many researchers have explored the stability analysis for standalone MG, and the review of the existing literature is presented in [143], [144]. Stability analysis, considering the communication delay, is also presented in [145]. Stability analysis in a droop controlled MG is also presented in [146], [147]. In the droop control method, the absence of communications between the distributed energy resources and its flexibility are some of its advantages. So, a mathematical model has to be developed to examine the stability of

the proposed controllers of the coupled microgrid.

## 2.5 Novel contributions of the thesis

So, in this context, the main contributions of the thesis are as follows:

- A Power Management (PM)-based droop control is proposed for available power sharing between the rural neighbouring MGs. In this research, the PM strategy is developed to maintain the power set-point of the autonomous MG. An improper selection of power set point in autonomous MG can raise the DC link voltage to an unmanageable value and can cause an inadvertent shutdown of MG. The active power-sharing between the MGs is achieved by monitoring the power reference set point in droop control. The proposed controller is able to share the power asymmetrically, which means it does not restrict the inverters for equal power-sharing.
- An improved double layer droop control method is proposed for load sharing among the autonomous static MGs to either restore the frequency or voltage to its nominal value. Based on the proposed strategy, the frequency or voltage is regulated by controlling the d-axis component of the terminal voltage of the standalone system.
- In this research, a seamless connection/reconnection scheme among the neighbouring MGs is developed. In rural, isolated microgrids (where large grid power is not available), setting a common reference voltage or frequency after the coupling and decoupling can be a challenging issue. A (de)coupling controller has been proposed based on double-layer improved droop control for seamless reconnection of neighbouring MGs for available power exchange.

- A linear model with the proposed droop controlled microgrid is also presented to investigate the stability of the coupled MG. Using this linear model, the influence of proposed frequency control on the whole connected system has been studied. The effect of line impedance and dynamic load change is also studied.

The detail modelling and the efficacy of the proposed controller has been analysed in the subsequent chapters.

Chapter 3

# Building A Laboratory Scale Microgrid

## 3.1 Introduction

An investigation on efficient power-sharing topology among the neighbouring isolated MGs has been done in this research. A power management-based droop control is proposed for effective asymmetric power-sharing among the neighbouring MGs. On top of that, a double layer droop control is proposed for frequency restoration in standalone MGs. Also, a seamless reconnection topology between the neighbouring MGs has been developed. The efficiency of the proposed controllers has been tested using the real time simulators (OPAL-RT and PLEXIM) by using a Power Hardware in Loop (PHIL) simulation and finally, by implementing a small laboratory scale MG. The proposed implementation techniques follows strictly the IEEE standard [148] for verification of the proposed MG controllers.

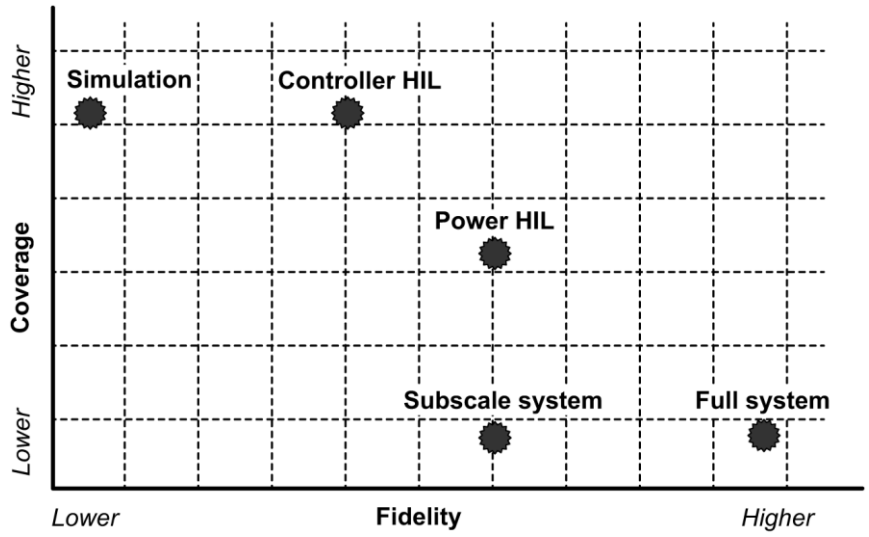


*Figure 3.1 Recommended laboratory test for the microgrid controller* [148]

Figure 3.1 shows the IEEE recommended laboratory tests for the microgrid controllers. This chapter presents the design and implementation procedure of two

inverter-based small-scale MGs. A compact description of each component and controllers used for implementation is provided in the following sections. A LabView based sbRIO controller has been used for practical implementation. Along with this OPAL-RT, Plexim real-time simulator and Texas Instrument based F28335 controller also used for PHIL experiment.

## 3.2 Overview of experiment setup

The schematic circuit diagram of the small-scale laboratory-based microgrid is presented in Figure 3.2. In each of the MG, a PV simulator has been used as a primary source of energy, and they are connected to local loads through a single-phase inverter. A manual switch has been used in order to couple both the inverter-based MG to realise the power-sharing.

In the proposed experimental setup, three 1 kW PV simulator have been used as a primary DC source. The schematic diagram of the proposed system consists of two parallel inverters is also implemented. Mitsubishi PM25CL1A120 intelligent 3 phase power modules have been used for the inverter. However, only two phases were used to configure the single-phase inverter. The output of each inverter is connected to the local load in standalone mode through an LC filter. Voltage and the current signals at the point of common coupling of each inverter are measured using LEM (LV 25 and LA 55) sensors. The switch SW1 is used to couple both the MGs for power-sharing. The power management-based droop control algorithm is implemented in a LabView based sbRIO controller. All the detailed control topology and practical implementation results will be discussed in Chapter 4. The picture of the developed experimental setup is given in Figure 3.3.

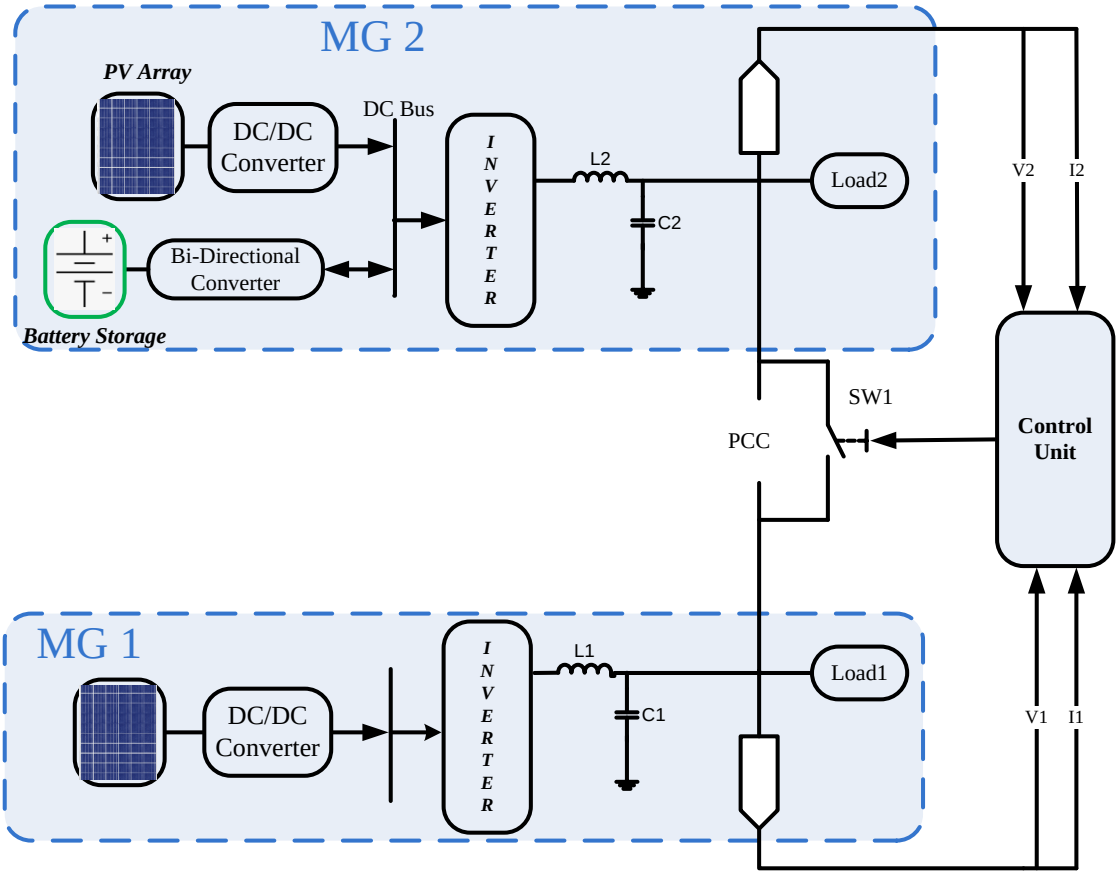


*Figure 3.2 Schematic diagram of the laboratory setup, connecting two neighbouring MG for power-sharing*

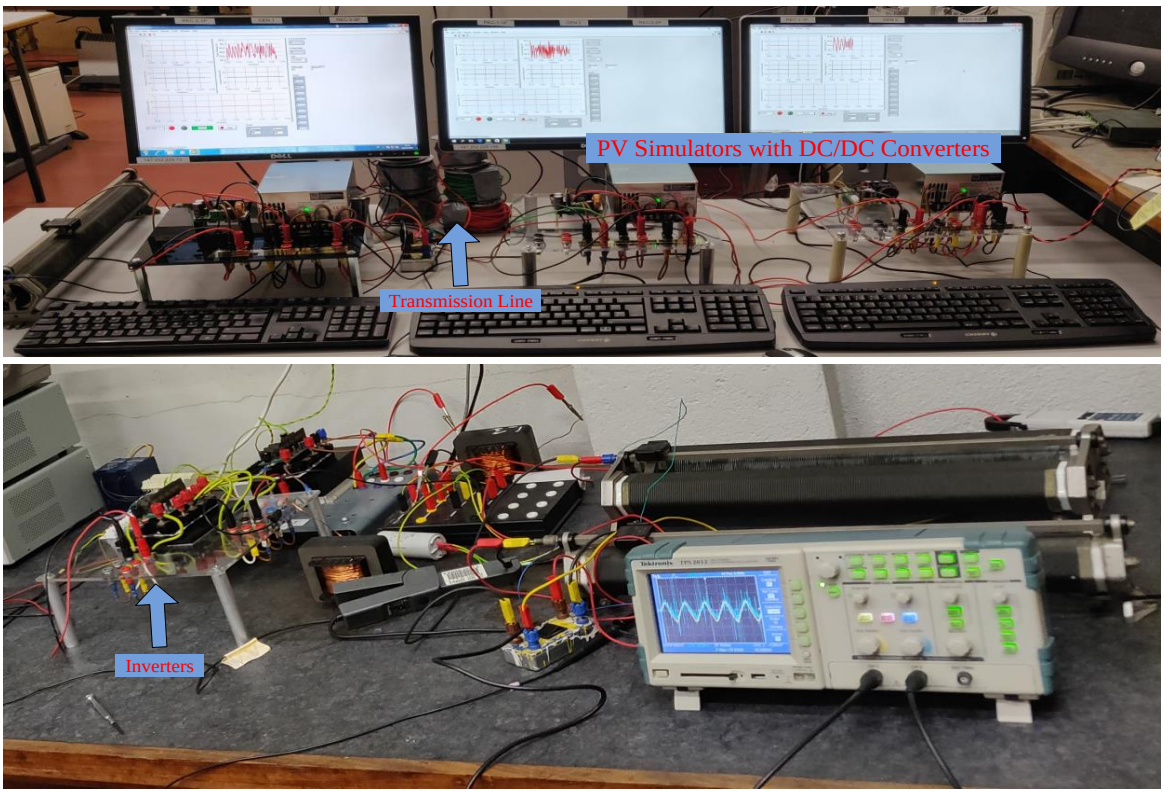


*Figure 3.3 Proposed system experimental setup*

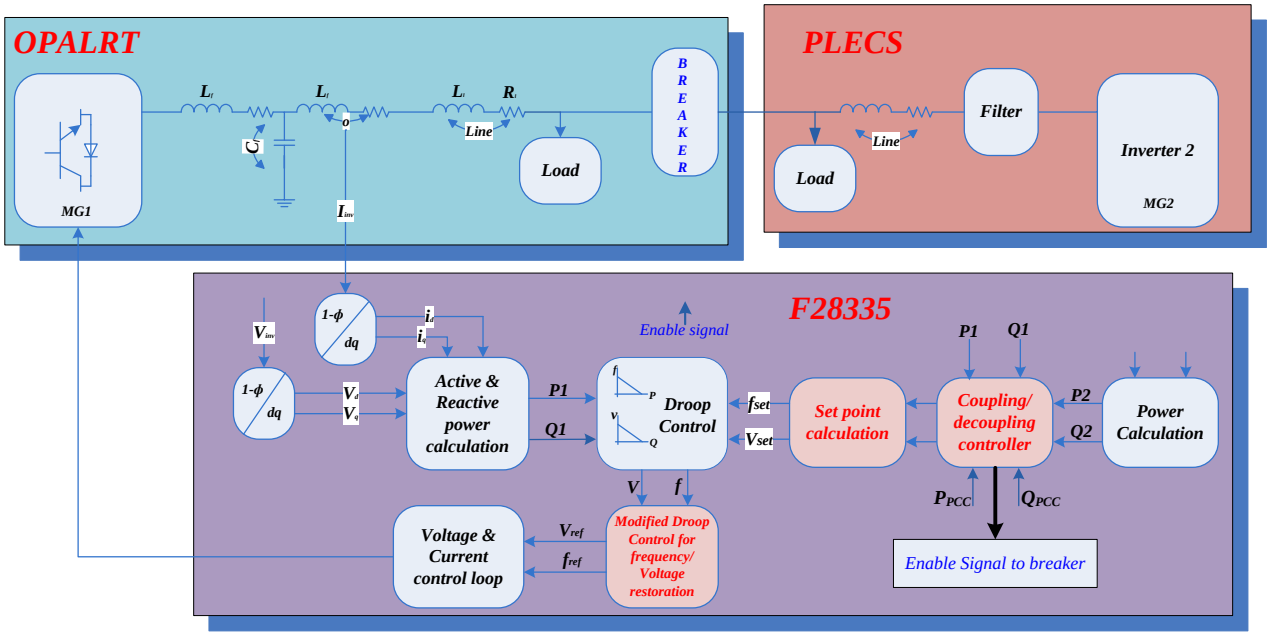


*Figure 3.4 Layout of chapter 5 experimental work.*

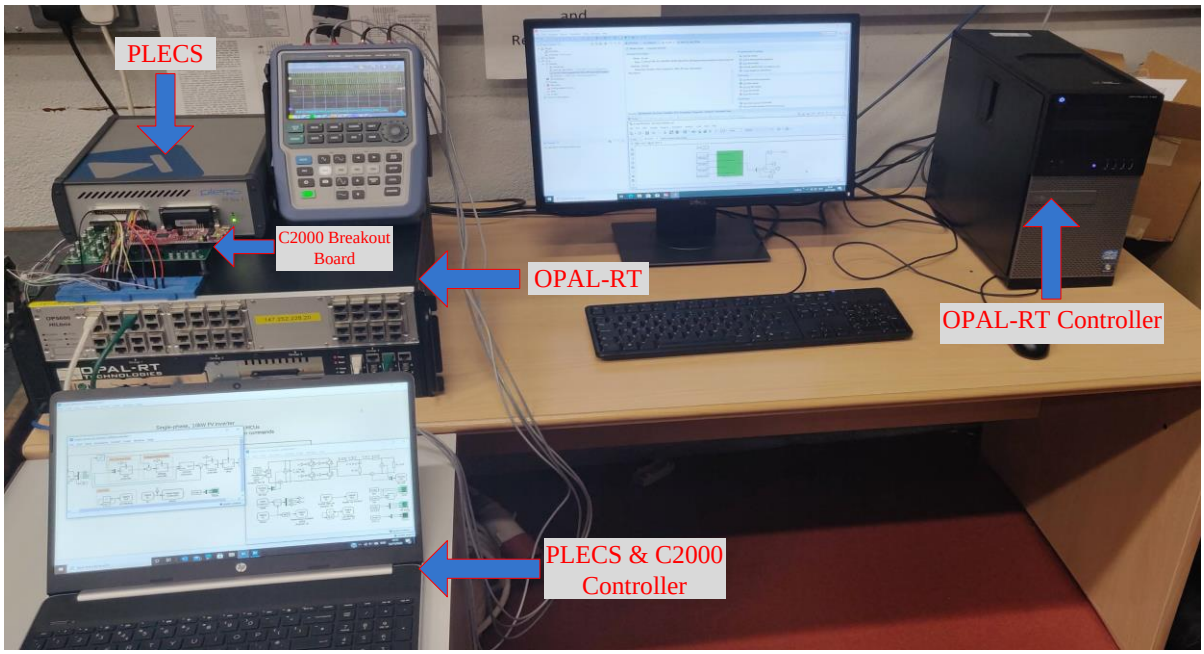


*Figure 3.5 Experimental setup for the PHIL test*

Moreover, a double layer droop control-based frequency restoration and seamless reconnection topology for neighbouring MGs have been developed. To assess the efficacy of the proposed controller, a PHIL setup also has been developed. The layout of the proposed system is depicted in Figure 3.4. The physical system of MG1 has been developed in OPAL-RT real-time simulator, and physical system of MG2 has been developed in PLEXIM real-time simulator. The control topology for frequency

restoration and seamless reconnection has been developed in Texas Instrument based F28335 controller. The detail experimental system and control topology as shown in Figure 3.5 will be discussed in Chapter 5.

## 3.3 IGBT module with gate driver

The Mitsubishi L series Intelligent Power Module (IPM) PM25CL1A120 [149] is used for implementing both the inverters. The power module is designed mainly for 3 phase applications, but in this research work, only two phases are used to implement the single-phase inverter. Figure 3.6 shows the internal block diagram of the IPM, and Figure 3.7 shows the picture of it. The IPM consists of 6 IGBT switches with freewheeling diodes with inbuilt temperature sensor, current sensor and protection logics. All the essential specification of the IPM is provided in Table3.1.

*Table 3.1 Specification of PM25CL1A120 module*

| Parameter | Module Rating |
|---|---|
| Supply Voltage | 1200 V |
| IGBT Breakdown Voltage | 1200 V |
| Maximum DC-Link Voltage | 900 V |
| Peak current limit | 50 A |
| DC link trip voltage | 915 V |

An external gate driver BP7B [150] is required for interfacing the gate signals. The BP7B is a complete isolated interface circuit for this Mitsubishi L-Series IPMs. This circuit features the VLA606-01R opto-interface IC for isolation of control signals and isolated power supplies for the IPM's built-in gate drive and protection circuits. The isolated interface helps to simplify prototype development and minimize design time by allowing direct connection of the IPM to logic level control circuits. Figure 3.8 shows

the picture of BP7B gate driver.

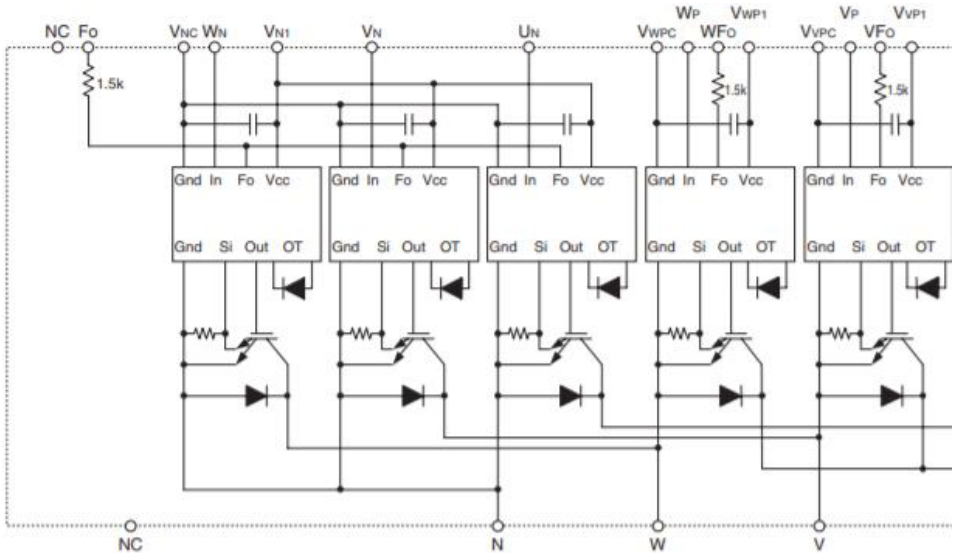


*Figure 3.6 Internal circuit diagram of PM25CL1A120* [149]

*Figure 3.7 PM25CL1A120 module*

*Figure 3.8 BP7B gate driver for IPM* [150]

## 3.4 Voltage and current measurements

Capacitor voltage and inductor current should be measured and appropriately captured in order to design the closed-loop system. LV 25P and LA 55P have been used to measure the voltage and current, respectively.

### *3.4.1 Voltage Measurement*

The voltage transducer LV 25 P is used to measure the capacitor voltage. The LV 25 sensor can measure a minimum 10 V to maximum 500V. The conversion ratio of the sensor is 2500:1000. The internal circuit diagram and connection points are shown in Figure 3.9.

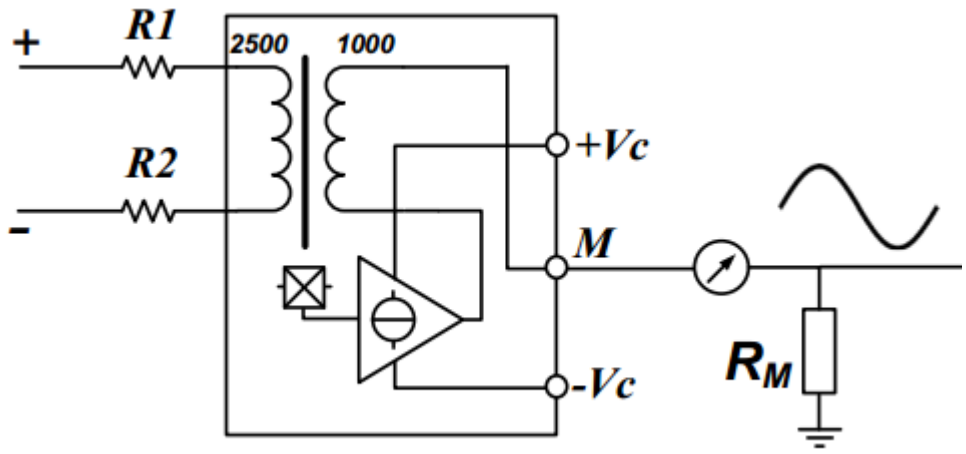


*Figure 3.9 Internal configuration of LV 25 P* [151]

### *3.4.2 Current Measurement*

The inductor current is measured by using the LA 55A transducer. The transducer can measure up to 50 A with a conversion ratio of 1:2000. The internal configuration of the LA 55P is shown in Figure 3.10. As the output of LA 55P is a current signal, in order to capture that as a voltage signal, a measuring resistor ($R_m$) is connected. All the essential values are provided with the datasheet [152].

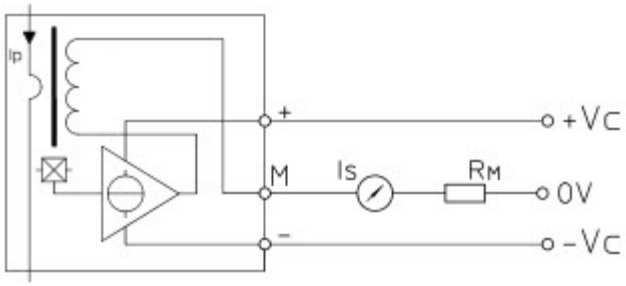


*Figure 3.10 Internal configuration of LA 55P* [152]

During the experimental procedure, it is undeniable that these transducers are very sensitive to high-frequency noise, and it reflects at the output. As the developed laboratory scale MG is a very low rating, the signal to noise ratio is also shallow. Therefore, an active low pass filter is required to mitigate the noise.

### *3.4.3 Filter Design*

A low pass filter is designed with a cut-off frequency of 1 kHz to eliminate the high-frequency noise. The performance of the filter was satisfactory. The experimental result with a comparison of with and without the filter is shown in Figure 3.11. It can be observed from the captured figure that the extra EMI noise produced in the field can be reduced using this low pass filter. The complete circuit diagram of the voltage and current measurement with filter circuit is provided in Figure 3.12. Any phase shift introduced by the filter circuit and LEM can be adjusted by tuning the 10k rheostat, placed just after the filter circuit. The phase shift can also be reduced by the internal circuit, designed in Labview.

*Figure 3.11 Performance of low pass filter in the current sensor board*

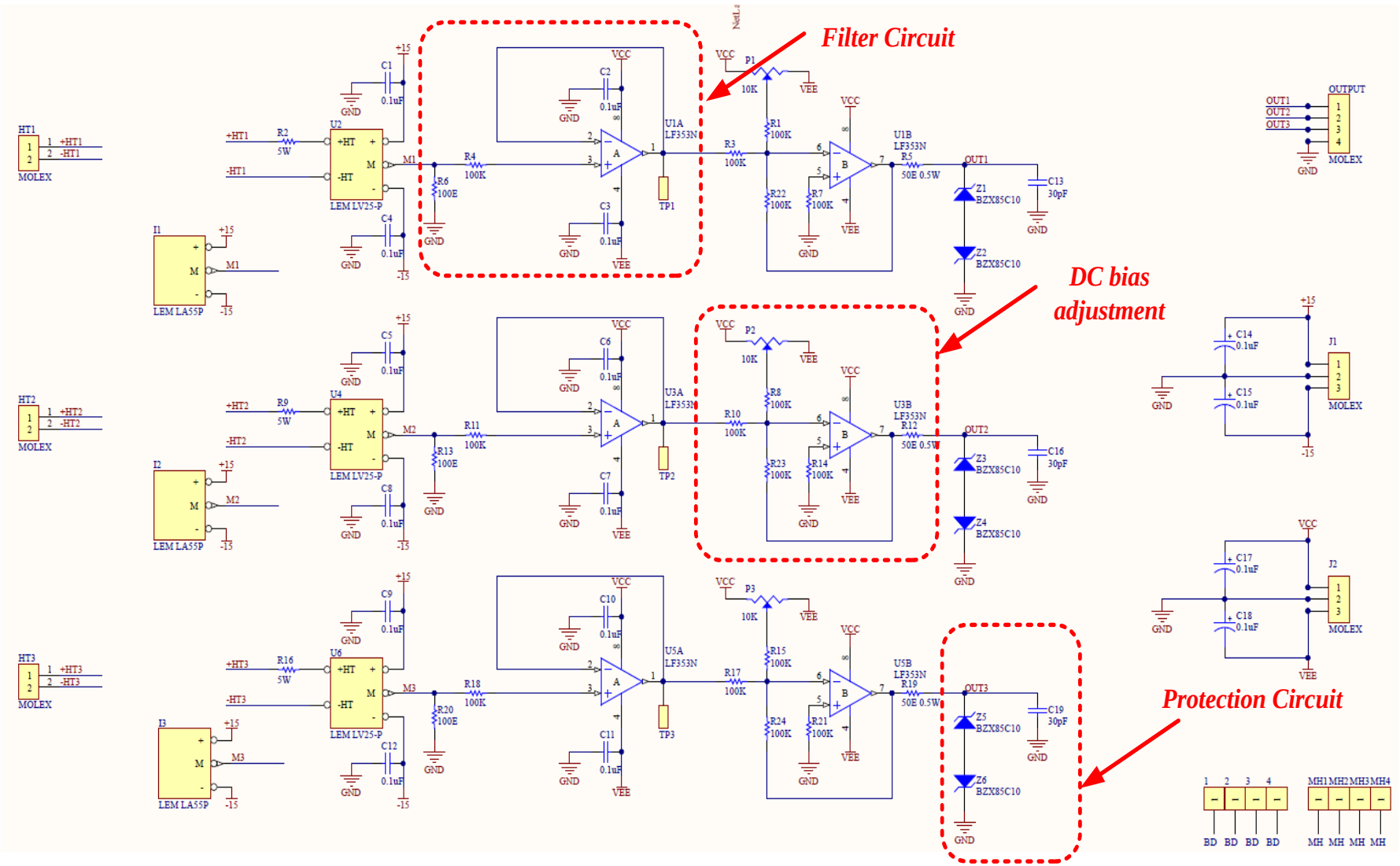


*Figure 3.12 Schematic diagram of PCB for voltage and current sensor board*

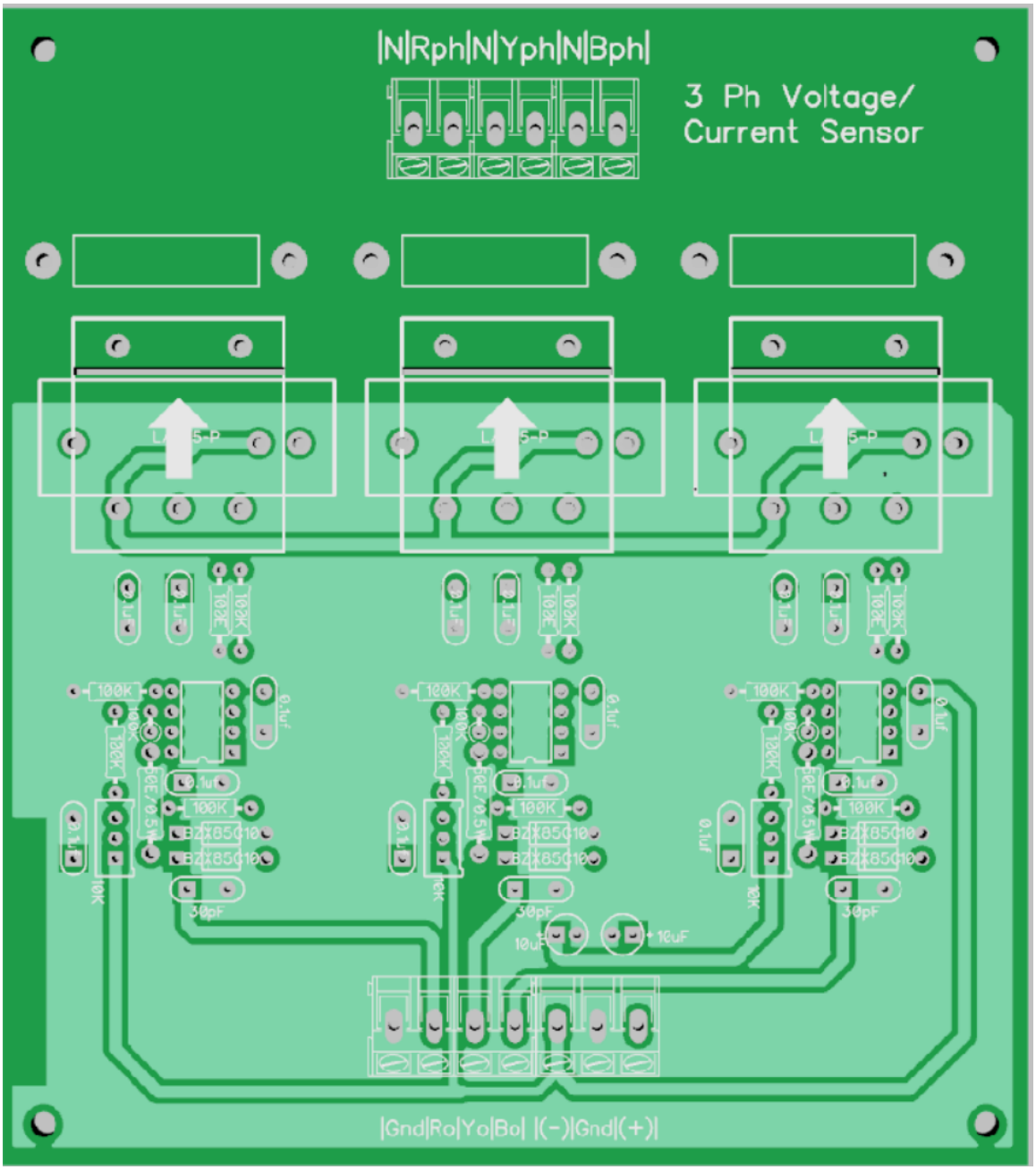


*Figure 3.13 Designed PCB for voltage and current sensor board*

### *3.4.4 DC bias adjustment and protection circuit*

The DC bias adjustment and protection circuit are also required to capture the voltage and current effectively. The designed circuit for dc bias adjustment and protection requirement is highlighted in Figure 3.12. Two back-to-back BZX85C10 Zener diode has been added to protect the controller under any kind of faulty condition.

A view of the final assembled PCB for voltage and current sensor board is shown in

Figure 3.13. The board can be used either as a voltage sensor or as a current sensor or combination of voltage and current sensor as well.

## 3.5 Controllers

In this section, all the necessary details are provided regarding all the controllers used for experimental validation purposes.

### *3.5.1 NI sbRIO 9606 controller Platform*

National Instrument based sbRIO 9606 [153] is an FPGA based platform, mainly used in this research work for controller design. LabView is a block diagram based graphical user interface, which can generate and compile automatic VHDL code. Each graphical block can be converted to VHDL codes automatically using the Xilinx code generation tools, which is inbuilt with LabView. The converter codes can be compiled and synthesized over the FPGA platform, and the functionality of the implemented controller can be tested easily. The user-friendly graphical interface helps the researcher in prototyping and testing of controllers in a very smooth and easy way as automatic VHDL generation features reduce the task of writing tedious code. In Figure 3.14, there is a view of sbRIO-9606, which is compatible with LabView software and used in this thesis as the main core of the control unit.

*Figure 3.14 FPGA based National Instrument sbRIO 9606* [153]

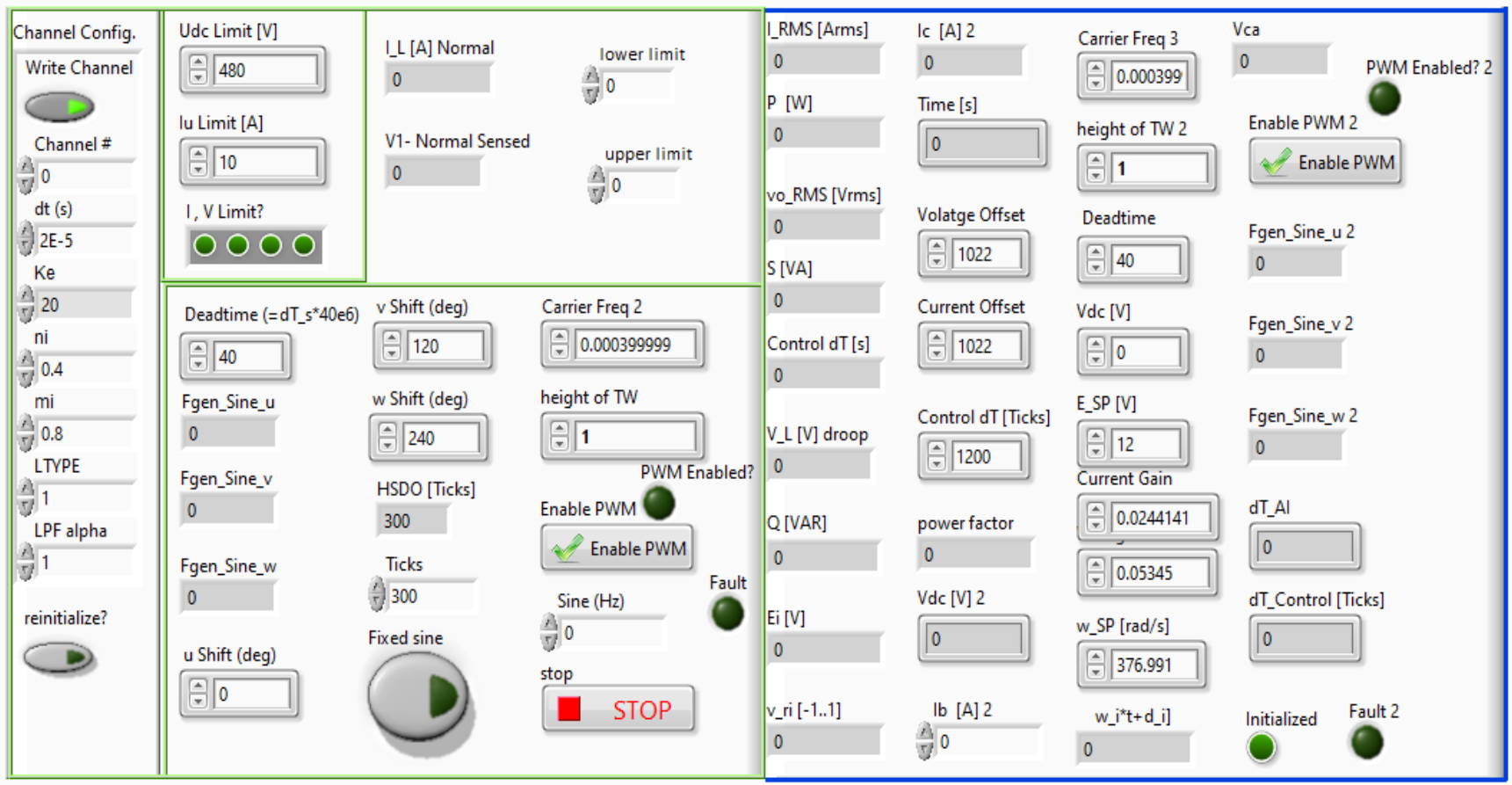


*Figure 3.15 Graphical interface of the proposed controller in LabView platform*

The other nice feature of LabView is enabling the users to track any signal and feedback graphically. This is a very critical feature which enormously helps the users to minimize the timing spent for debugging or tuning their controllers and devices. Also, users can capture any signal they want, and they can show them instantly or buffer them for future usage. Figure 3.15 shows the graphical user interface of the LabView environment for the proposed controller.

### *3.5.2 General Purpose Inverter Controller- NI GPIC 9683*

In order to control the inverters with sbRIO 9606, an add-on input/output interface card, which is commonly known as General Purpose Inverter Controller (or technically NI GPIC 9683 mezzanine card) is required. This NI GPIC 9683 mezzanine card [154] receives/sends analog/digital signals to establish a proper and safe connection between the controller and inverter. The inbuilt safety feature helps the controller to operate safely during any faulty condition in the inverter side.

The NI 9683 mezzanine card provides connections for 16 simultaneous analog input channels with isolated ground reference; all with ±30 V overvoltage protection. 28 simultaneously sampled sourcing digital input channels; 14 push-pull half-bridge digital output channels; 24 sinking digital output channels; four relay control digital output channels; and 32 LVTTL digital I/O channels are also inbuilt with this mezzanine card. The connection diagram of 9683 mezzanine card is shown in Figure 3.16. Figure 3.17 provides a picture of a sbRIO 9606 along with interfacing 9683 GPIC card.

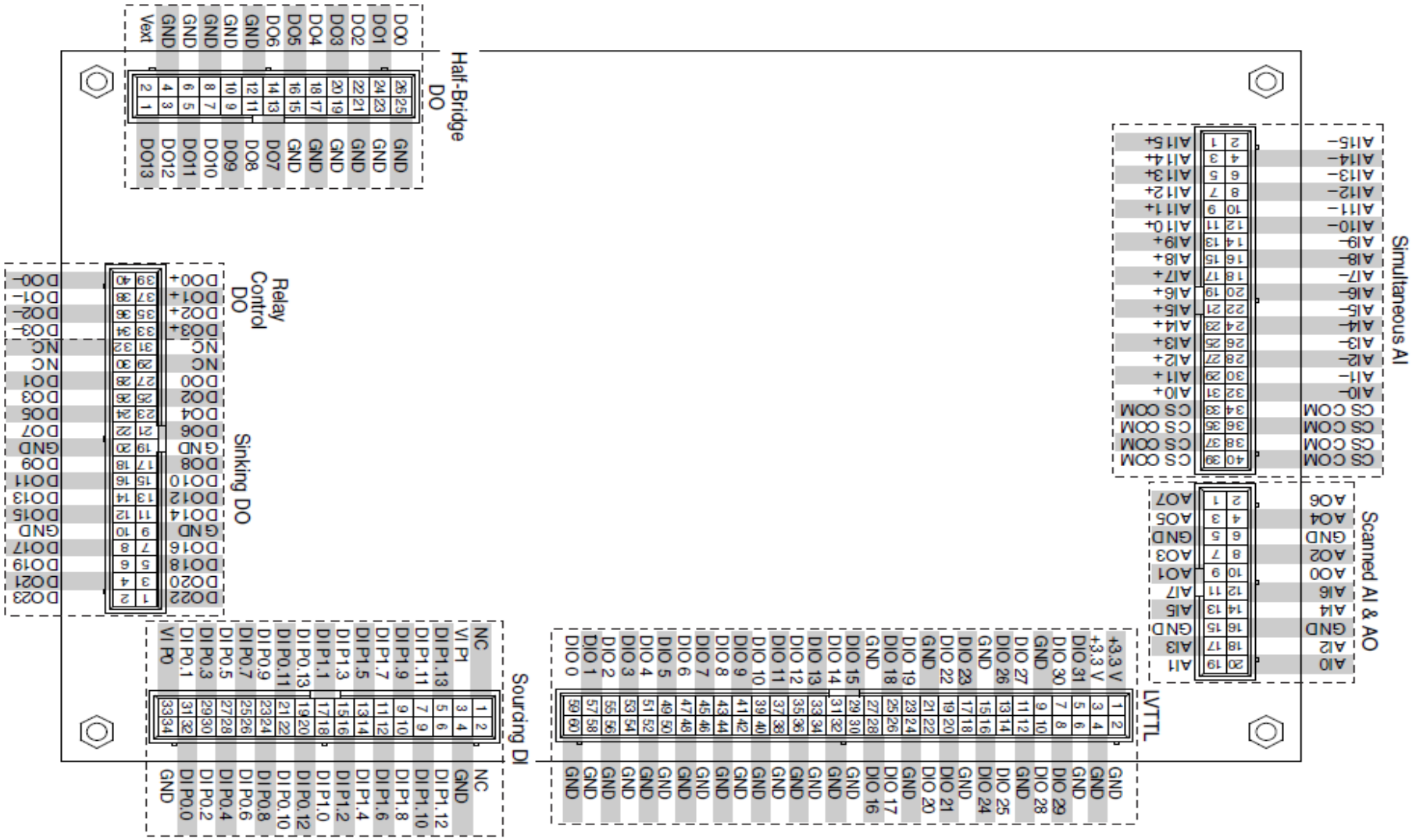


*Figure 3.16 NI 9683 pinout* [154]

*Figure 3.17 Stacked sbRIO 9606 on GPIC 9683 mezzanine card*

### *3.5.2 TMS320 F28335 controller Platform*

The TMS320F28335 [155] is a 32-bit microcontroller that specializes in control applications such as robotics, industrial automation, mass storage devices, lighting, optical networking, power supplies, and other power electronics control applications needing a single processor to solve a high-performance application. The TMS320 F28335 evaluation board controller kit is shown in Figure 3.18. In this research the TMS320F28335 is used for PHIL application.

The architecture of TMS320F28335 DSP is given in Figure 3.18. Enhanced PWM, enhanced CAP, and enhanced QEP are the upgraded peripherals in F28335, compare to other controllers in this family. And the floating-point unit is the primary source of its performance. The use of the floating-point unit, Enhanced Pulse Width Modulation (epwm) module, inbuilt dead-band generation module, and most importantly, the easy interface with Matlab and other power electronics software (like PLECS) make this controller a handy and efficient unit for implementation purpose.

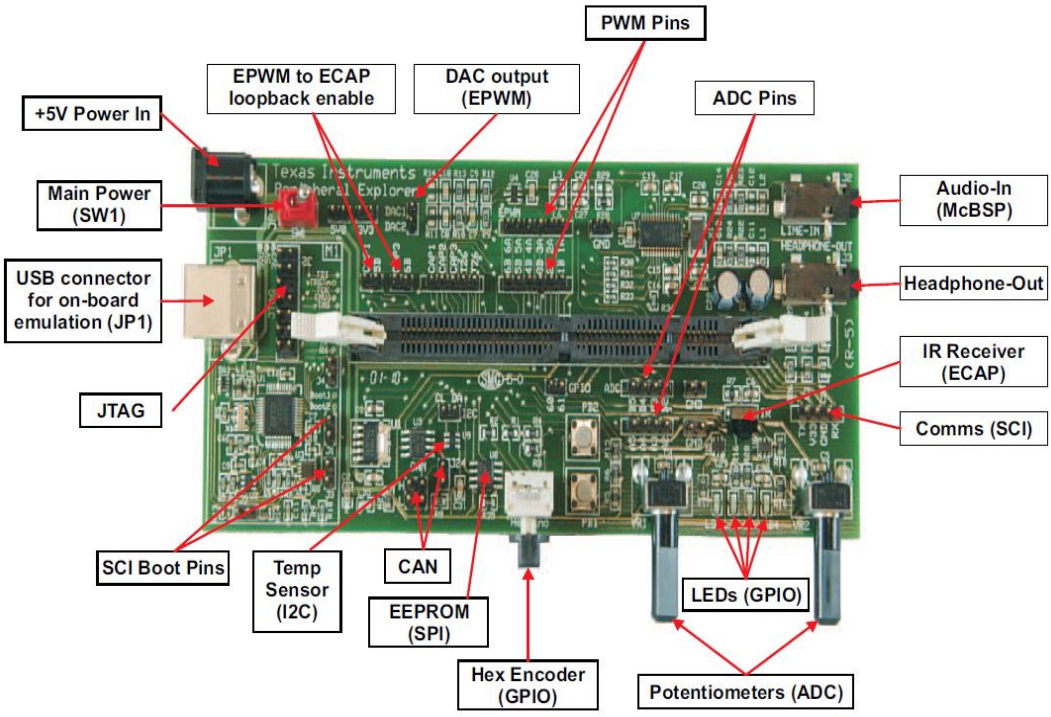


*Figure 3.18 Evaluation board of F28335 controller* [155]

## 3.6 Real-time simulators

### *3.6.1 OPAL-RT*

OPAL-RT TECHNOLOGIES is the leading developer of Real-Time Digital Simulators and Hardware-in-the-Loop testing equipment for electrical, electro-mechanical and power electronic systems. The OPAL-RT simulator consists of a chassis called the OP5600 simulator with many digital and analog input and output connection ports and FPGA based controller inside. The interfacing software called RT-Lab helps to provide a link between the OP5700 simulator and Matlab.

The OP5600 family [156] are adding advanced monitoring capabilities with scalable I/O and power calculation to OPAL-RT's product line of the real-time digital simulator. The OP5600 modular and flexible design can be fully customized to meet specific I/O requirements and can be easily expanded as needed. Different inbuilt software configuration like eFPGAsim, eMEGAsim, Hypersim or ePHASORsim are completely

configured for OP5600 chassis, which enables implementation of several real-time simulation applications, including HIL testing, rapid control prototyping, and FPGA development projects. Complex power grids, micro-grids, wind farms, hybrid vehicles, more electrical aircraft, electrical ships and power electronic systems can be simulated in real-time with time step as low as 10 microseconds or less than 250 nanoseconds for some subsystem to achieve the best simulation accuracy. Several power electronic manufacturers are now using OPAL-RT real-time digital simulators instead of expensive and less flexible analog test benches.

Additional signal conditioning modules are also available to cover a wide range of applications. One OP5600 chassis can then accommodate up to 256 digital or 128 analog I/O. Several OP5607 (OP5600 I/O expansion chassis using Virtex7 FPGA) can be interconnected through a PCI Express expansion chassis to increase the number of the channel up to 2048 fast digital signals or 1024 analog signal or a mix or analog and digital I/O. The total round-trip transfer time of all 2048 channels from OP5600 system to the target processor memory is less than 25 microseconds. Signal interface equipment and accessories such as fault insertion unit, breakout and signal mapping boxes and amplifiers are also available to interface actual electronic controllers to perform HIL tests. Figure 3.19 shows a front panel of OP5600 simulator.

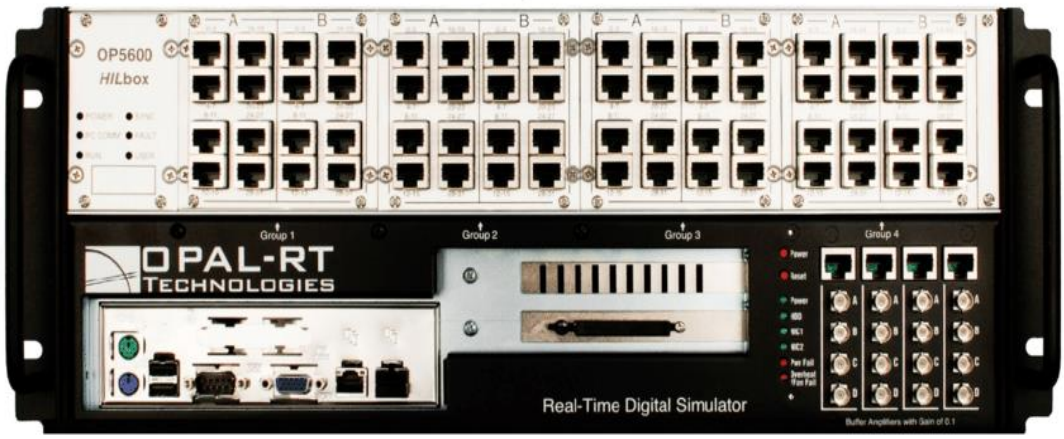


*Figure 3.19 Front panel of OP5600 simulator* [156]

### *3.6.2 PLECS RT Box*

The PLECS RT box [157] is a real-time simulator built by PLEXIM Inc. It has 1 GHz dual-core central processing unit (CPU) along with provision for 32 analog inputs and outputs, and 64 digital inputs and outputs. This simulator can be used for HIL applications and rapid controller prototyping. In HIL applications, the PLECS-RT Box emulates the power stage of a power electronic system. The power stage could be as simple as a buck converter or as complex as a motor drive system. In the HIL setup, The Device Under Test (DUT) is the controller connected to the PLECS RT Box. Fig. 3.20 shows the PLECS-RT box along with the controller. This module has three hardware blocks

- PLECS RT Box which emulates the power stage of a converter system.
- Controller, which is the DUT. The controller used for the smart inverter design is a Texas Instrument DSP, TMS320F28335.
- Breakout board, which acts as the interface between the controller and PLECS RT box.

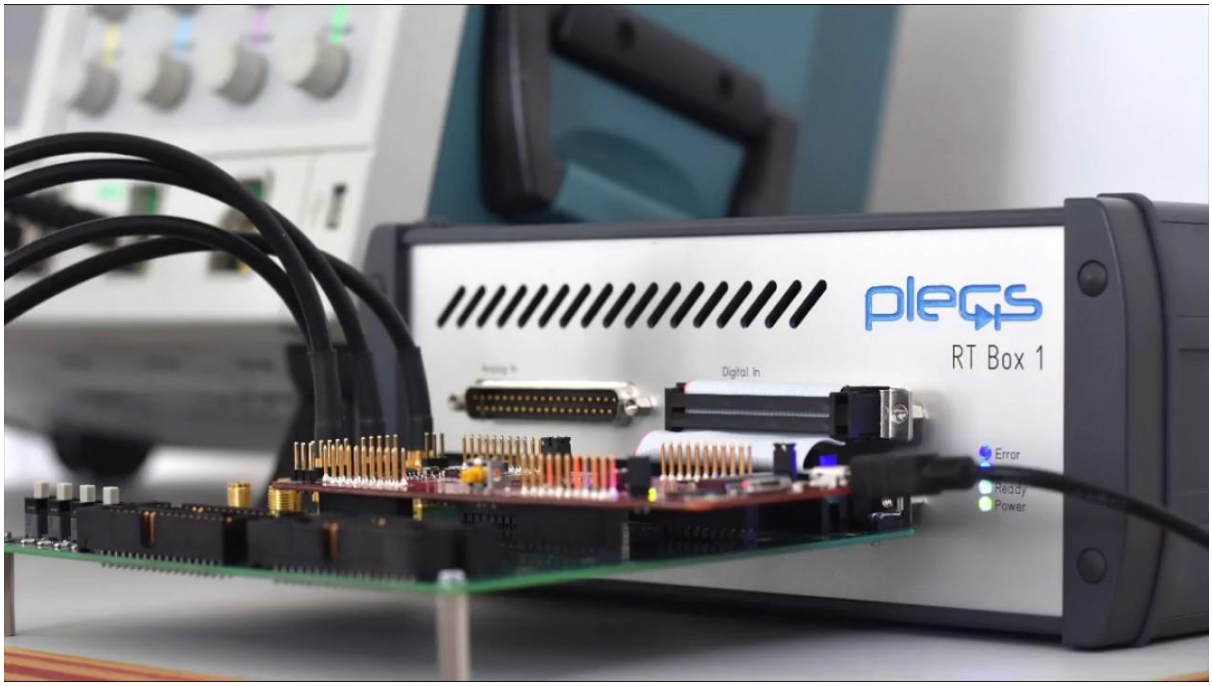


*Figure 3.20 PLECS RT box with controller and I/O card* [157]

The PLECS-RT box can receive analog and digital inputs and can also transmit analog and digital outputs. The analog inputs can be in the form of voltage, current, or position sensor output. The analog inputs can be differential or single-ended. The analog outputs can be also in the form of measured parameters in the PLECS software, which are scaled and then offset to ensure the output voltage from PLECS is within limits. The PLECS RT box has 16 analog inputs and 16 analog outputs. The digital inputs can be in the form of pulses generated from a controller. The digital outputs can be in the form of pulses generated from the PLECS-RT Box as well. The RT box has 32 digital inputs and 21 digital outputs.

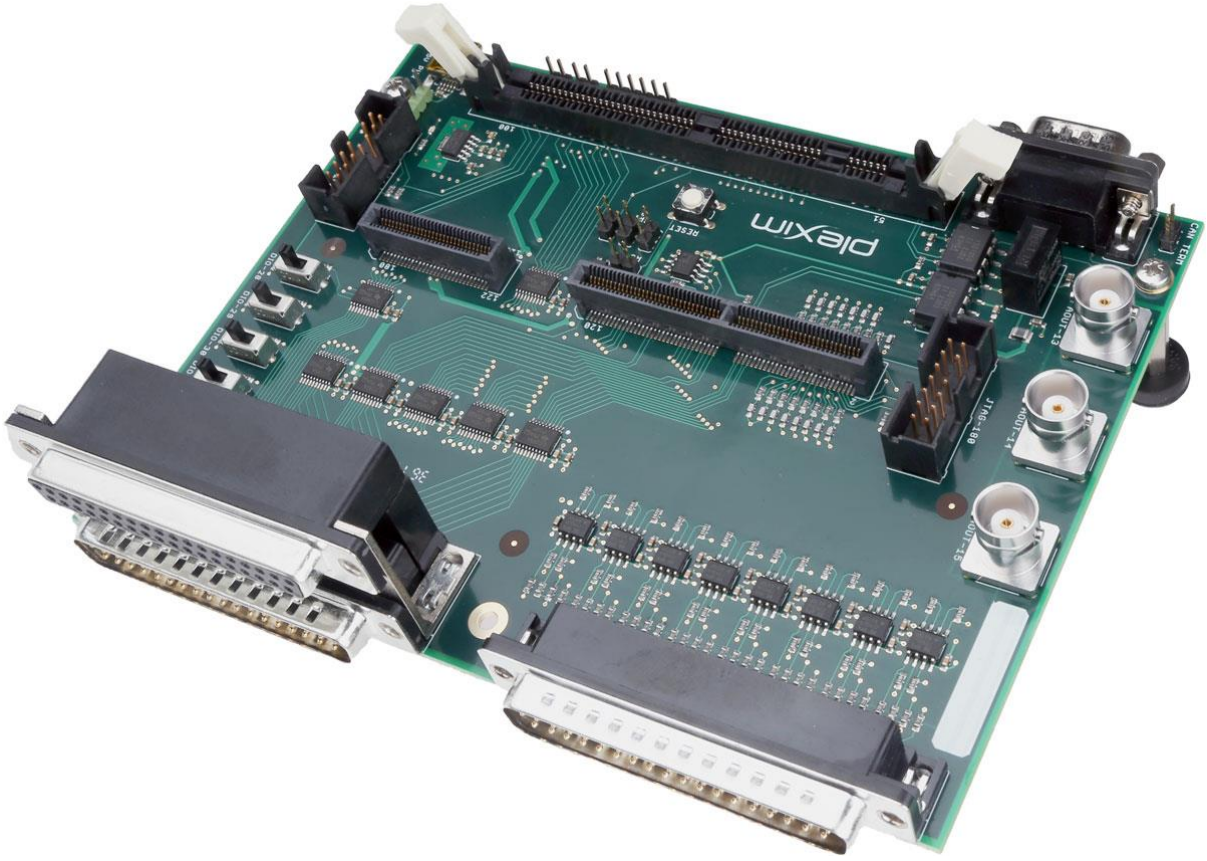


*Figure 3.21 PLECS C2000 Launchpad development kit*

Texas Instruments DSP Delfino TMS320F28335 is used for designing the controller stage of the inverter. This DSP is a single CPU core 32-bit fixed-point processor with a

clock frequency of 200 MHz belonging to the C-2000 family of processors. The DSP comes with twelve channels for EPWM and six channels for High-Resolution Pulse Width Modulation (HRWPM). The DSP also comes with 16 channels of ADC, with the resolution configurable to 16-bit or 12-bit. Three channels of ADC can also act as DAC in 12-bit resolution. Figure 3.21 shows the PLECS breakout board designed for the C2000 Launchpad development kit.

## 3.7 Summary

This chapter has presented the instruments, controllers, real time simulators, used for the development of laboratory-scale experimental setup for validating and testing the proposed controllers. A PHIL experimental setup and finally two low laboratory scale microgrid is developed to check the efficacy of the power sharing accuracy of the proposed controller. The detail experimental setup using these peripheral components will be presented in the subsequent chapter.

Chapter 4

# Interconnection of Standalone Neighbouring Microgrids for Power-sharing

## 4.1 Introduction

The high penetration of renewable energy sources (RES) in rural microgrid energy communities (EC) are the backbone of European Strategy (2018/2001/EU, RED II)[158] towards a clean and low carbon society. EC are the modern recognition of the smart communities, where energy policymaker, customers- everyone plays an important role to achieve a sustainable living for society. Maintaining generation demand balance in an EC is a critical task for a system/community operator. This requires maintaining a certain level of flexibility in the system, which forms an inevitable system service requirement. The intermittent nature of distributed energy sources and the load uncertainties can create a power mismatch and can cause unintended frequency and voltage deviation in these isolated community MGs (CMG). This research work, aims to develop a smart virtual energy-community (EC) microgrid (MG) to enhance power resiliency and sustainable living for the rural community-microgrids. Remote area isolated ECMGs are likely to experience overloading or power scarcity during any natural disaster like catastrophic events such as earthquakes, thunderstorms, hurricanes etc. Critical community infrastructures have to be connected with the power supply for the sustainable development of the community during any contingency. This proposed scheme combines autonomous ECMGs for power exchange using a power management (PM)-based droop control. It not only supports the local load, but can also support the neighbouring EC

loads if there is any excess power requirement in the neighbouring EC. During the grid-connected mode, the droop control may have different power setpoints of each EC microgrid, but during the standalone mode of operation, the power setpoint should be defined according to their power rating and availability. In this research work, a power management (PM) strategy is developed to maintain the power setpoint of the autonomous ECMG. An improper selection of power setpoint in autonomous ECMG can raise the DC link voltage to an unmanageable value and can cause inadvertent shutdown of ECMG. The active power sharing between the ECMGs is achieved by monitoring the power reference setpoint in droop control.

The majority of the implemented techniques as discussed extensively in the literature review section of Chapter 2, can only accommodate two of the symmetrical or hybrid distributed generation (DG) units in a MG. In most of the published literature, symmetrical droop units have been considered, where equal power sharing have been achieved. But in practical cases, due to the intermittency of DG sources and different power rating of neighbouring MGs, equal power sharing can restrict proper utilization of coupling advantages. During an asymmetric power sharing, inappropriate selection of droop gain can lead the standalone MG to an unstable condition and can deviate the system voltage and frequency considerably. To reckon with the above issues, this research work has considered the following enhanced features:

- A well-defined control strategy where symmetric and asymmetric (if required) power sharing can be achieved through a PM-based droop control in order to couple the neighbouring MGs more efficiently. The proposed PM strategy defines the reference power set point for the conventional droop control.

- An improved frequency regulation scheme without implementing any secondary controller for this purpose. The power flow between the MGs are controlled keeping the frequency within an allowable range. As the considered system is static and standalone, the proposed PM-based droop control helps to maintain the system frequency in an acceptable range.
- A validated test of the proposed controller by developing laboratory scale MGs.

## 4.3 Power management based droop control strategy

In the proposed system configuration, as shown in Figure 4.1, two static microgrids with a standalone PV system has been considered. The intermittent nature of PV power generation poses a significant challenge to the widespread adoption of PV systems in islanded microgrids in the absence of MS devices. Also, frequency regulation is a great challenge in this kind of complete static generation.

In order to maintain a power balance in islanded microgrids, the deployment of BESS is necessary to compensate for the intermittent nature of PV units. However, battery systems have limited power ratings, limited capacities, and restricted charging scenarios that depend on the battery SoC. Therefore, the operation of the PV and battery units must be coordinated for effective and efficient energy generation. Installation of BESS incorporation with PV is not economical sometimes due to the low lifecycle of BESS (compare to PV, could have to replace 3 times in an entire PV plant life cycle) and high installation cost [159]. Considering the above-stated issues, two microgrids are considered for coupling; in the first one, there is SPV generations connected to local loads, and in the other one, there are SPV systems with BESS and local load. Both the MGs are inverter-based MG and operated only in islanded mode. The SPV systems are

connected to the main MG inverter through DC/DC converters. In this scenario, droop control is considered for required power-sharing. The conventional voltage and frequency droop control equations for each inverter of MGs are-

$$\omega = \omega^* - k_\omega(P - P^*) \quad (4.1)$$

$$V = V^* - k_V(Q - Q^*) \quad (4.2)$$

Where $k_\omega$ and $k_V$ are the frequency and voltage control droop co-efficient; $\omega$* and $V$* are the nominal value of frequency and voltage, respectively.

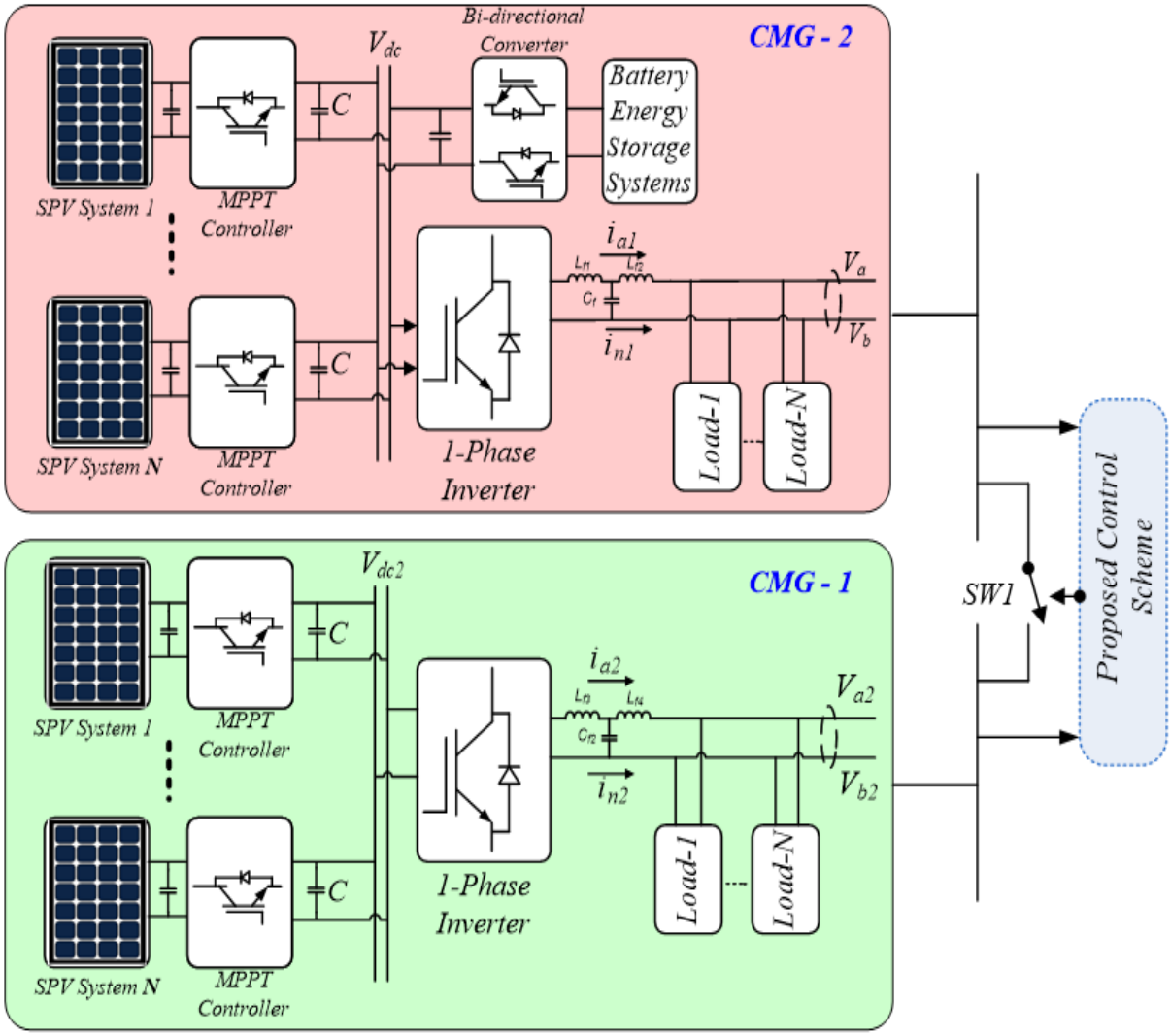


*Figure 4.1 Proposed system configuration*

Usually, in the case of grid-connected mode, the grid provides the rigid voltage and frequency support, and it specifies the active and reactive power setpoints for the

microgrids. If there is any significant deviation from the setpoint value, the MG controller needs to disconnect/connect some load/sources. But in the case of a standalone mode of operation, the voltage and frequency are set to its nominal value, and the power setpoints play an essential role in order to maintain the voltage and frequency. In the proposed droop control, a power management topology is adopted in order to maintain the frequency and voltage within an acceptable range. The droop slopes are calculated accordingly to maintain the stable mode of operation during coupling.

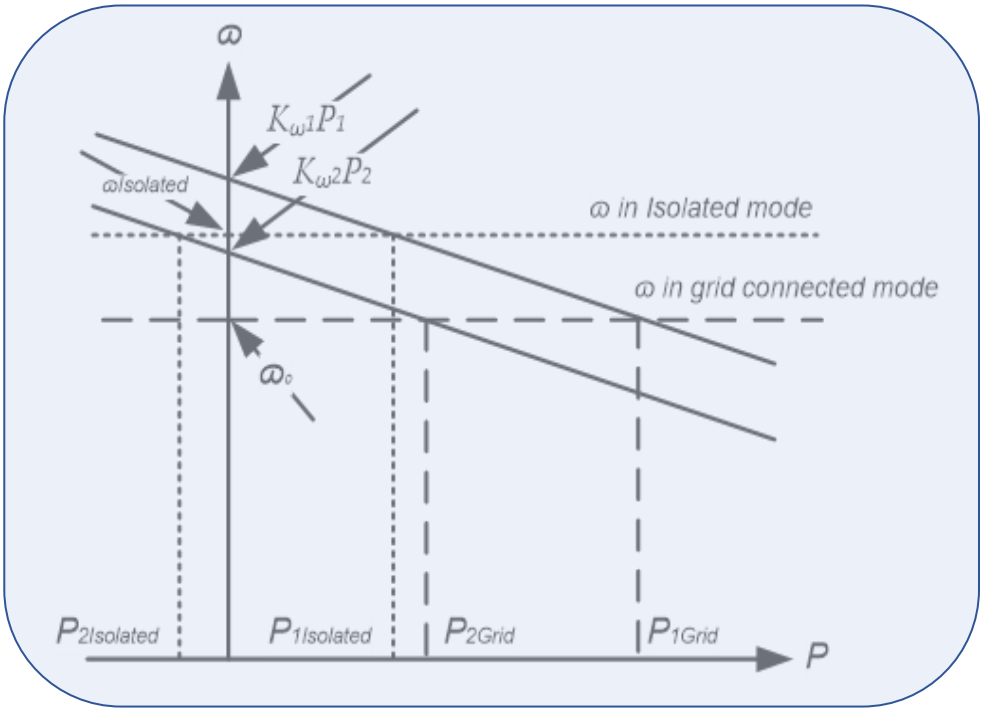


*Figure 4.2 Proposed droop control*

The droop control topology, as shown in Figure 4.2, consists of two inverters for the grid-connected and standalone mode of operation. In grid-connected mode, as the frequency is controlled by the stiff grid, the two inverters generate different power ($P_{1Grid}$ & $P_{2Grid}$) in the same frequency. But in the islanded mode of operation, the frequency of the system starts to diverge from the nominal value. In this situation, it is crucial to define an acceptable frequency region for a stable mode of operation. For the standalone mode of operation, the acceptable frequency range is 50 Hz ± 2 Hz [160], [161]. After reaching

a stable frequency ($\omega_{island}$), both the inverters produce $P_{1Islanded}$ and $P_{2Islanded}$ for the same droop coefficient. Now, the steady-state standalone frequency can be calculated as-

$$\omega_{island} = \omega^* - k_{\omega 1}P_1 + k_{\omega 1}P_1^* = \omega^* - k_{\omega 2}P_2 + k_{\omega 2}P_2^* \quad (4.3)$$

As the droop coefficients ($k_{\omega 1}$=$k_{\omega 2}$) are the same so,

$$P_1 = P_1^* + P_2 - P_2^* \quad (4.4)$$

As the total load power ($P_L$) is supplied by the two inverters ($P_L$=$P_1$+$P_2$), further the steady-state islanded frequency can be calculated as:

$$\omega_{island} = \omega^* - \frac{k_\omega}{2}(P_L - P_1^* - P_2^*) \quad (4.5)$$

So, it can be noted that the islanded frequency depends on the total load connected to the system and the power set point for the droop control. For equal power-sharing from both the inverter, the power setpoints ($P_1$* & $P_2$*) should be equal.

In this steady-state islanded frequency, the generated power from both the inverter can be calculated as:

$$P_1 = \frac{1}{2}(P_L + P_1^* - P_2^*) \quad (4.6)$$

$$P_2 = \frac{1}{2}(P_L + P_2^* - P_1^*) \quad (4.7)$$

A critical case study where power transfer from one CMG to another has been illustrated in Figure 4.2. When the total load demand is less than the difference between two power set points of the inverters, i.e., $P_L < |P_1^* - P_2^*|$ , the power can be drawn from one CMG to another. In this condition, one of the inverters will import the power (in Figure 4.2, the connecting inverter of CMG2 is importing power). The imported power will cause to upsurge in the DC link bus voltage. So, extra power can be utilized to fulfil the load demand in another CMG to maintain a stable mode of operation. The BESS will further supply/import the power in case of any critical power balance situation.

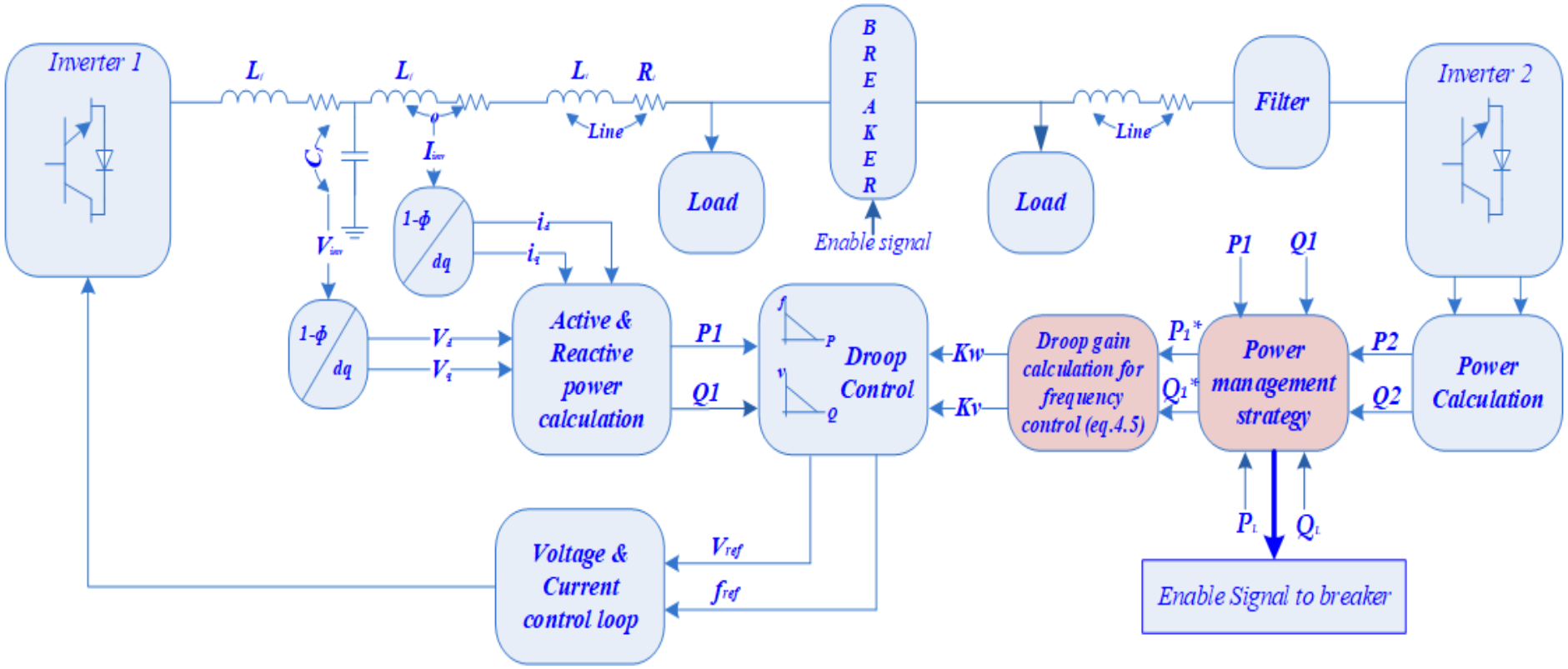


*Figure 4.3 Inverter control topology*

## 4.4 The proposed control topology

The proposed system configuration with two static power generation sources, i.e., SPV power generation is shown in Figure 4.1. Each MG consists of a primary source of energy (SPV), DC/DC converters, voltage source inverter, LCL filter, and local loads. In one of the MG, the PV unit is interconnected with BESS through a bi-directional converter. Both the MGs are coupled through a switch during any contingency.

The power rating and the system parameters for both the microgrids are shown in Table 4.1.

*Table 4.1 MG Parameters*

| System Parameters | |
|---|---|
| Dc Link Capacitor | 2000 µF |
| Filter Inductor (L1) | 6.8mH |
| Filter Inductor (L2) | 6.8 mH |
| Filter Capacitor | 30 µF |
| Power Rating for Inverter 1 | 10 kW |
| Power Rating for Inverter 2 | 10 KW |
| BESS Capacity | 10 kWh |
| Frequency drooping gain | 0.05 rad/s/W |
| Voltage drooping gain | 0.01 V/Var |
| Nominal MG Voltage | 230 V |
| Nominal MG Frequency | 50 Hz |

To make the system configuration more realistic for rural area connection, a conventional standalone single-phase system is considered. The implemented inverter control technique is shown in Figure 4.3, where one side of the inverter control is shown elaborately, and on the other side, also the same control technique is adopted. For power-sharing purposes, a droop control technique is also implemented where a power

management technique is adopted for frequency control, i.e., to keep the frequency in the allowable range. The power setpoints ($P_1$* & $P_2$*) are defined from the frequency management block. Further, the voltage and frequency droop co-efficient are calculated in such a way that the voltage and frequency always remain in the allowable range.

## 4.5 Working principle

The working principle for the proposed coupled MGs shown in Figure 4.2 is discussed in this section.

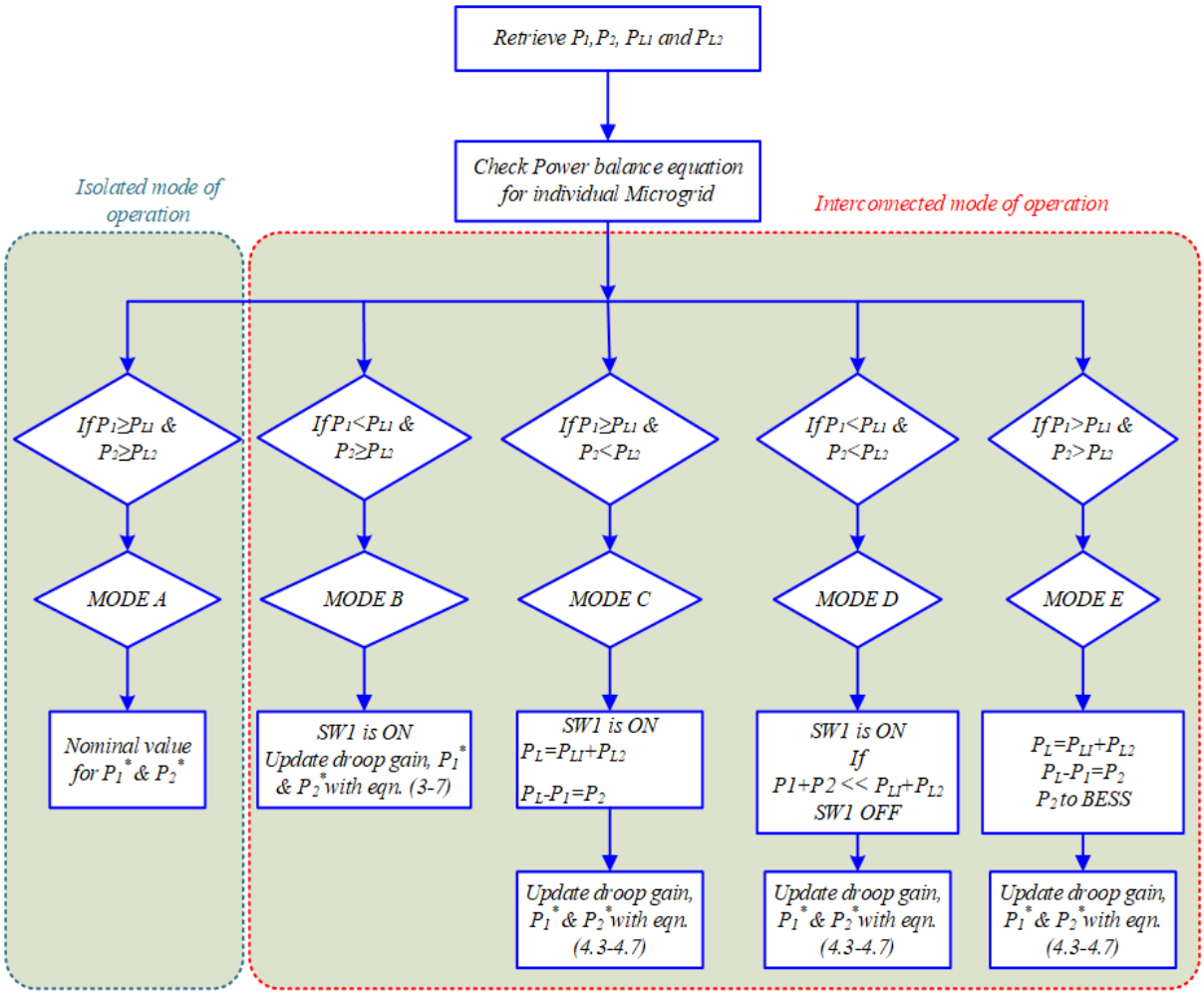


*Figure 4.4 Flow chart to calculate power setpoints in different modes of operation*

SW1 is the breaker switch that is used to connect the neighbouring MGs. The detailed control topology is shown in Figure 4.3, where a power management strategy is

implemented to define the power setpoint of the droop control, and the frequency of the proposed controller is maintained by adjusting the droop gain accordingly. The power flow chart of the power management system is given in Figure 4.4. The working principle and the power flow diagram during different working modes are also discussed in detail.

### *4.5.1 Normal Operation*

In this mode of operation, both the microgrids are supplying the required local loads by maintaining the desired frequency. As shown in Figure 4.5, both the MGs are operating separately, and the breaker switch S1 remains in 'off' condition.

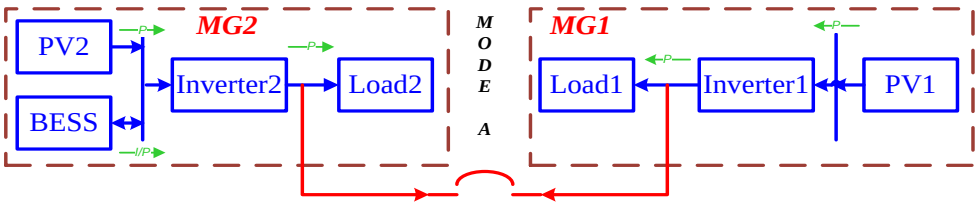


*Figure 4.5 Power flow for operation mode A*

### *4.5.2 Microgrid 1 is overloaded*

In this mode of operation, the shortage of power in MG1 can be exported from MG2 if there is any excess power in MG2 by triggering on the breaker switch. The power calculation can be done in the power management block and to maintain the stable allowable frequency, the power setpoint and the droop gain values should be updated accordingly. The power flow diagram in this condition is shown in Figure 4.6.

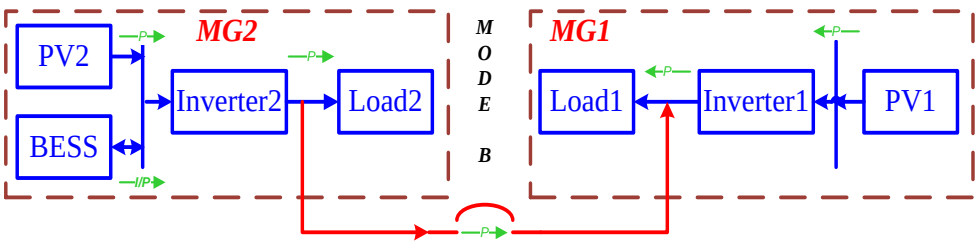


*Figure 4.6 Power flow for operation mode B*

### *4.5.3 Microgrid 2 is overloaded*

In this case, as shown in Figure 4.7, power can be drawn from the BESS to meet the

local load demand; otherwise, the power can be drawn from the MG1 (if there is any excess power) to utilise the renewable energy generation in MG1 fully. In the proposed power calculation algorithm, as shown in Figure 4.7, any excess power in MG1 is imported in MG2, and the further deficiency (if any) is fulfilled from the BESS.

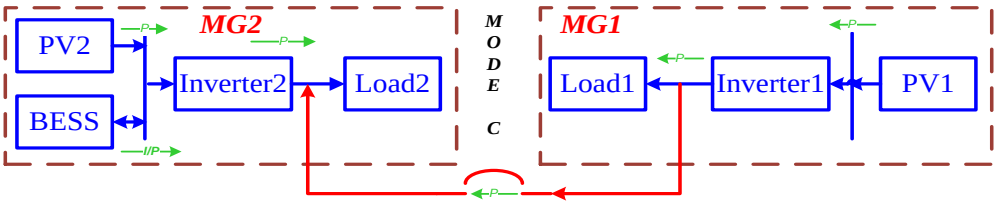


*Figure 4.7 Power flow for operation mode C*

### *4.5.4 Both Microgrids are overloaded*

In this condition, BESS is used to meet the total load demand. The power flow diagram is shown in Figure 4.8. In the worst-case scenario, when BESS and both the PV plants are unable to supply the local loads, the MG coupling connection can be revoked, and the load shedding technique can be adapted to maintain the system stability. It is to be noted that the load shedding techniques are beyond the scope of the current research topic of the thesis.

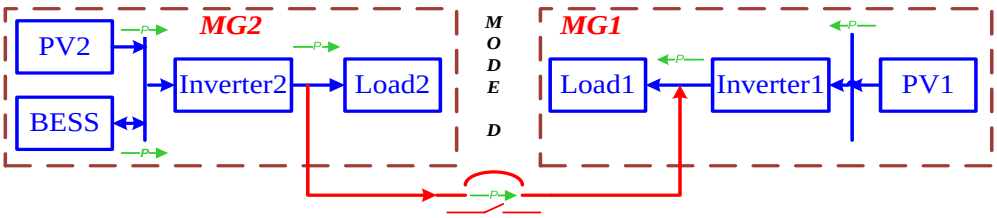


*Figure 4.8 Power flow for operation mode D*

### *4.5.5 Both the MGs are underloaded*

In this condition, both the MGs can be used to recharge the BESS. In this condition, the complexity in the control topology can be increased. So, in order to keep it simple, the full produced power is utilised to meet the local load demand in MG1 and MG2. The power produced in MG2 is utilised to recharge the BESS and to meet the remaining load power demand. The power flow diagram is shown in Figure 4.9.

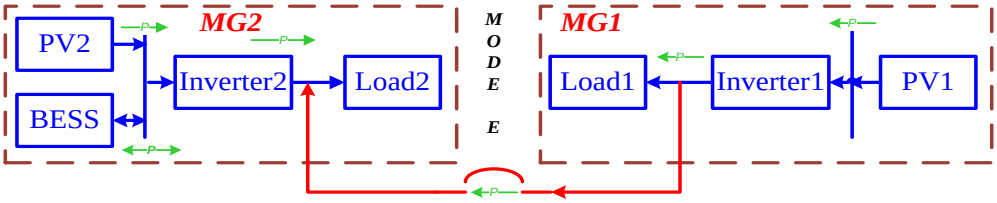


*Figure 4.9 Power flow for operation mode E*

## 4.6 Simulation studies

To prove the efficacy of the proposed system, two PV based single-phase microgrids are developed, and previously discussed five different modes of operations are considered. Both inverters are interfaced with the local load through an LCL filter. All the system parameters are provided in Table 4.1. Matlab SimPowerSystem is used to develop the detailed model of the MGs.

### *4.6.1 Normal Operation:*

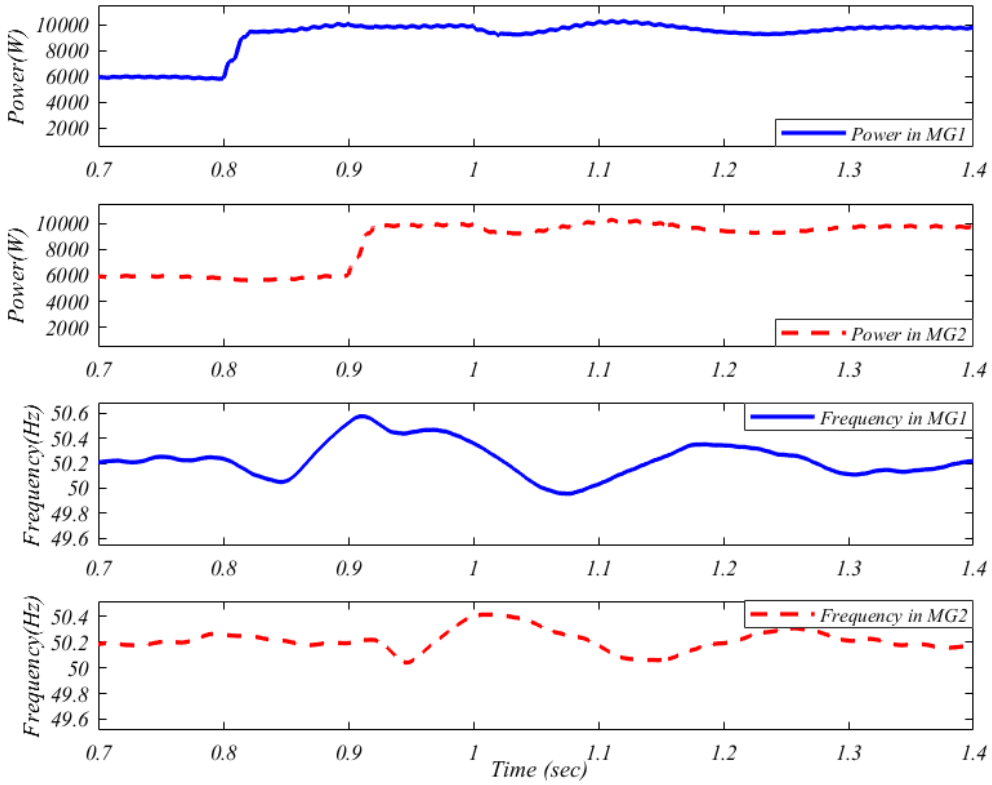


*Figure 4.10 System parameters for case study A*

Regular operation of power-sharing between two MGs is considered in this case study. The total load demand in MG 1 and MG 2 is 6 kW, respectively. The load power

and the frequency in both the MGs are shown in Figure 4.10. Now in this situation, suddenly, the load demand in both the MGs are increased by 4 kW at time instant 0.8sec in MG1 and at 0.9 sec in MG2. It can be observed from Figure 4.10 that the frequency is maintained within the allowable range as the power set point of the MGs are modified to maintain the frequency. It is also notable that as both the systems are not connected together, so MG 1 will not be affected by any change in MG2. It can be observed that both the system have two different frequency profile as they are not connected.

### *4.6.2 MG 1 is overloaded*

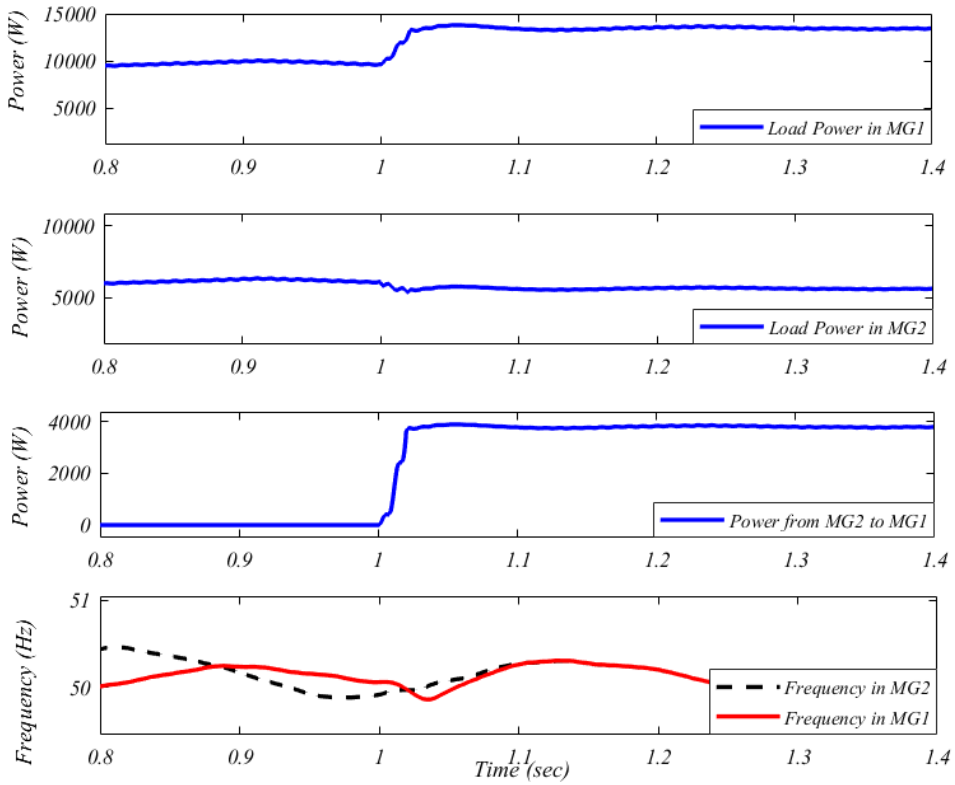


*Figure 4.11 Illustration of MG 1 overloading*

In steady-state operation, if the power demand increases in MG 1 and exceeds the total power rating of the MG 1, then according to the proposed configuration, power can be drawn from the MG 2, if there is any excess power available. In this situation, the load consumption in MG 2 is always constant. In this case study initially, a 10-kW load is attached to MG 1, and 6-kW load is attached to MG 2 so that there is excess available

power in MG 2. Now the load demand is increased by 4 kW in MG1 at the simulation time instant 1sec. It can be observed from Figure 4.11 that the excess power is supplied in MG 1 from MG 2. The frequency response also is shown in Figure 4.11, which is also within the allowable range. In this case study, a symmetric droop control is applied for equal power-sharing during the coupling condition.

### *4.6.3 MG 2 is overloaded*

In this case study, the load consumption in MG 1 is constant, and load demand in MG 2 is increased and exceeds the PV power generation rating of the MG 2. In this situation there are two possibilities to supply the excess load demand; one is from BESS which is already installed in MG 2, and the other one is if there is any excess power in MG 1 that can be transferred to MG2 to meet the requirement.

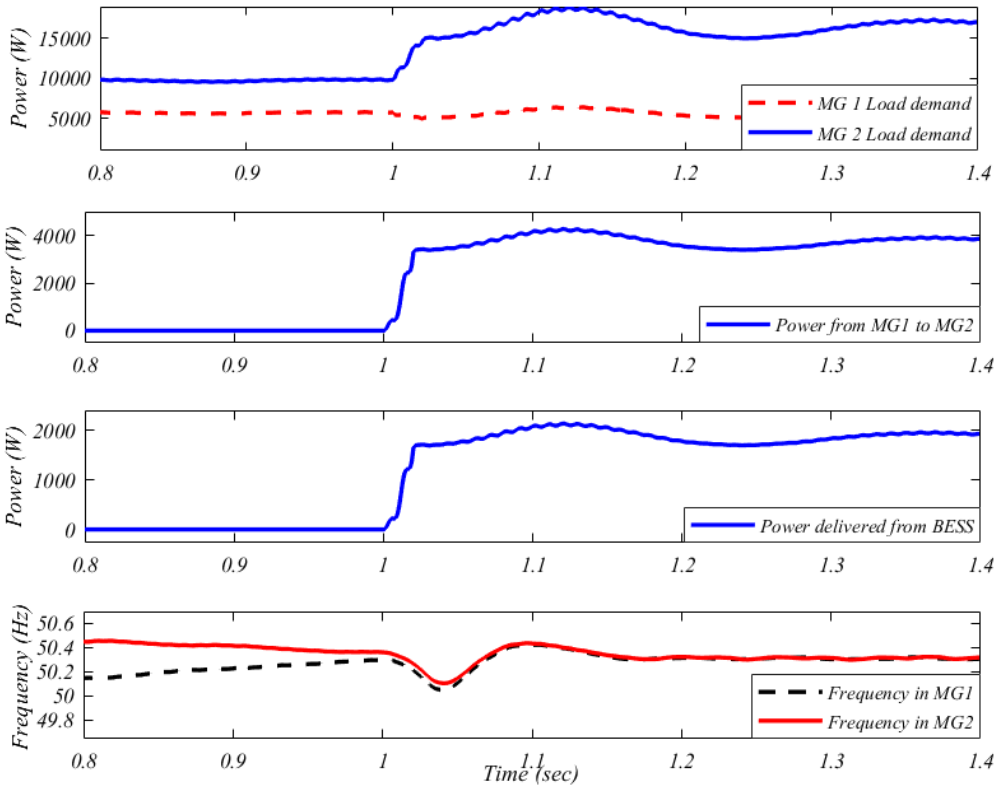


*Figure 4.12 Illustration of MG 2 overloading*

Here, in this case, study 6 kW load is added to MG 1 so that there is some excess power to transfer to MG 2 and initially in MG 2, the load demand is 10 kW. At the

simulation time, 1 sec the total load demand in MG 2 is increased to 16 kW and in this situation according to the flow chart the excess power in MG 1 (4 kW) is transferred to MG2 and the remaining power demand (2kW) is supplied by the BESS in MG2. An asymmetric power-sharing has been achieved in this case study by adjusting the power set point and droop gain properly. It can also be observed from Figure 4.12 that initially when power demand was supplied individually, both the MGs had different frequency, and after coupling, both the MGs have the almost same stable frequency.

### *4.6.4 MG1 & MG2 both are overloaded*

When Both MGs are overloaded, then the excess load demand can be supplied from the BESS. But it can be noted that this BESS also has some limitation. The load demand should not be increased beyond the rating of BESS, and MGs should not be overloaded for a long time.

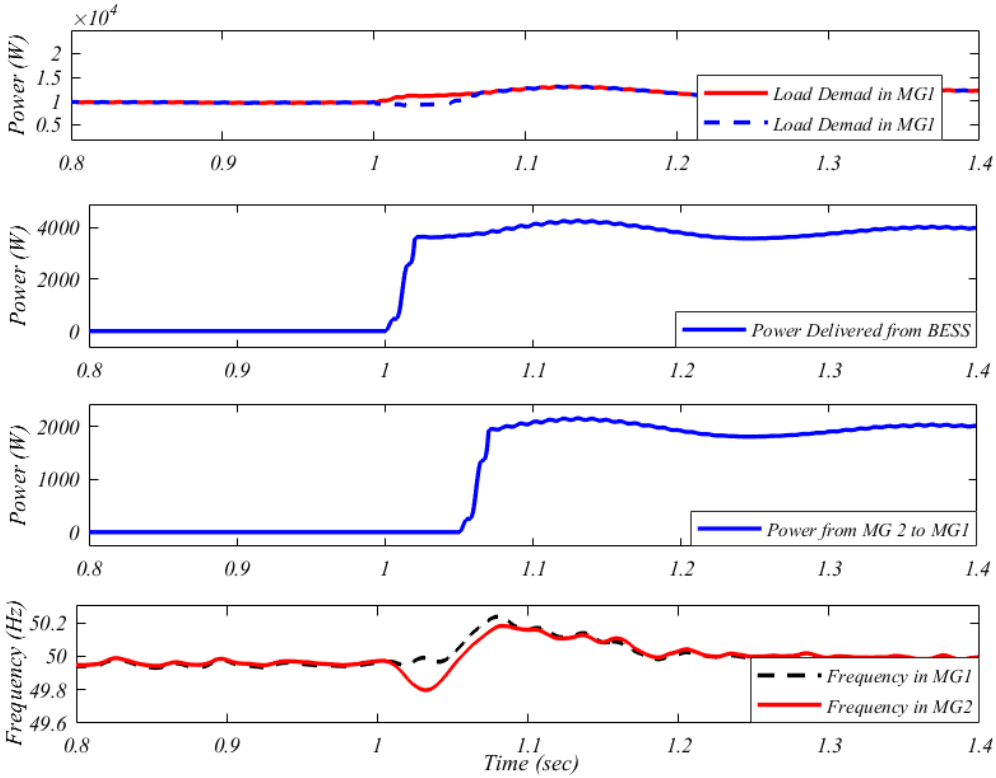


*Figure 4.13 Illustration of MG 1 & MG 2 both are overloaded*

In this case study initially, the load demand is 10 kW individually in both the MGs. At simulation time instant 1sec the load demand in both the MGs are increased to 12 kW,

which exceeds the inverter power rating for both the MGs. Figure 4.13 illustrates that the 4 kW excess power is supplied from the BESS and 2 kW power is transferred from MG 2 to MG1. In this case study also an asymmetric power-sharing and a stable mode of operation are achieved.

### *4.6.5 MG 1 & MG 2 both are under loaded*

When both MGs are underloaded, in this situation, the excess power can be utilised to charge the BESS. In this case study, it is considered that both the MGs are having 8 kW load. In this situation according to the power management algorithm (given in Figure 4.4), the available excess power (2 kW) in MG 1 can be transferred to meet the load demand and the internal excess power of MG 2 can also be utilised to recharge the BESS.

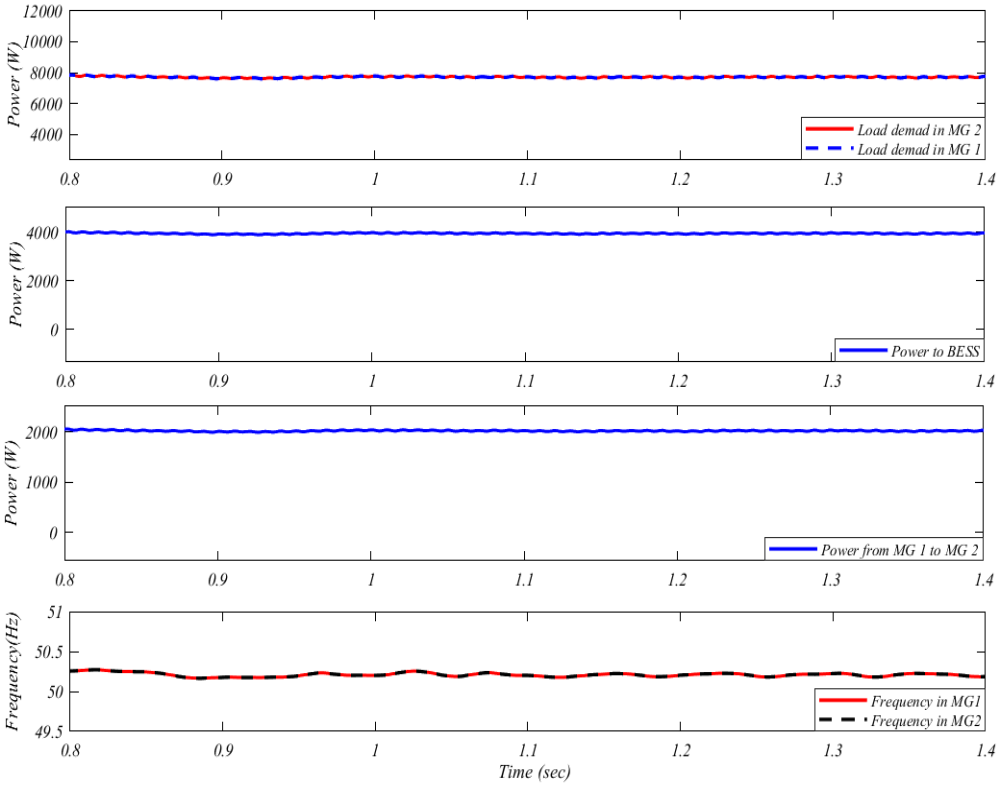


*Figure 4.14 Illustration of BESS charging situation*

It can be observed from Figure 4.14, that the excess 2 kW power is transferred from the MG1 to MG 2 and 4kW internal power of MG 2 is utilised to recharge the BESS. As both the system is interconnected, they are having the same system frequency.

## 4.7 Experimental results

The different elements used in the experimental test rig has been shown in Figure 4.15. Three 1 kW SPV simulators with DC/DC converters has been implemented to use as a primary source of energy for each MG. The SPV system is connected to the main microgrid inverter. The Mitsubishi L series Intelligent Power Module (IPM) PM25CL1A120 is used for implementing the single-phase inverters of the MGs. The proposed control schemes as shown in Figure 4.3 is implemented using the National Instrument based sbRIO-9683 controller.

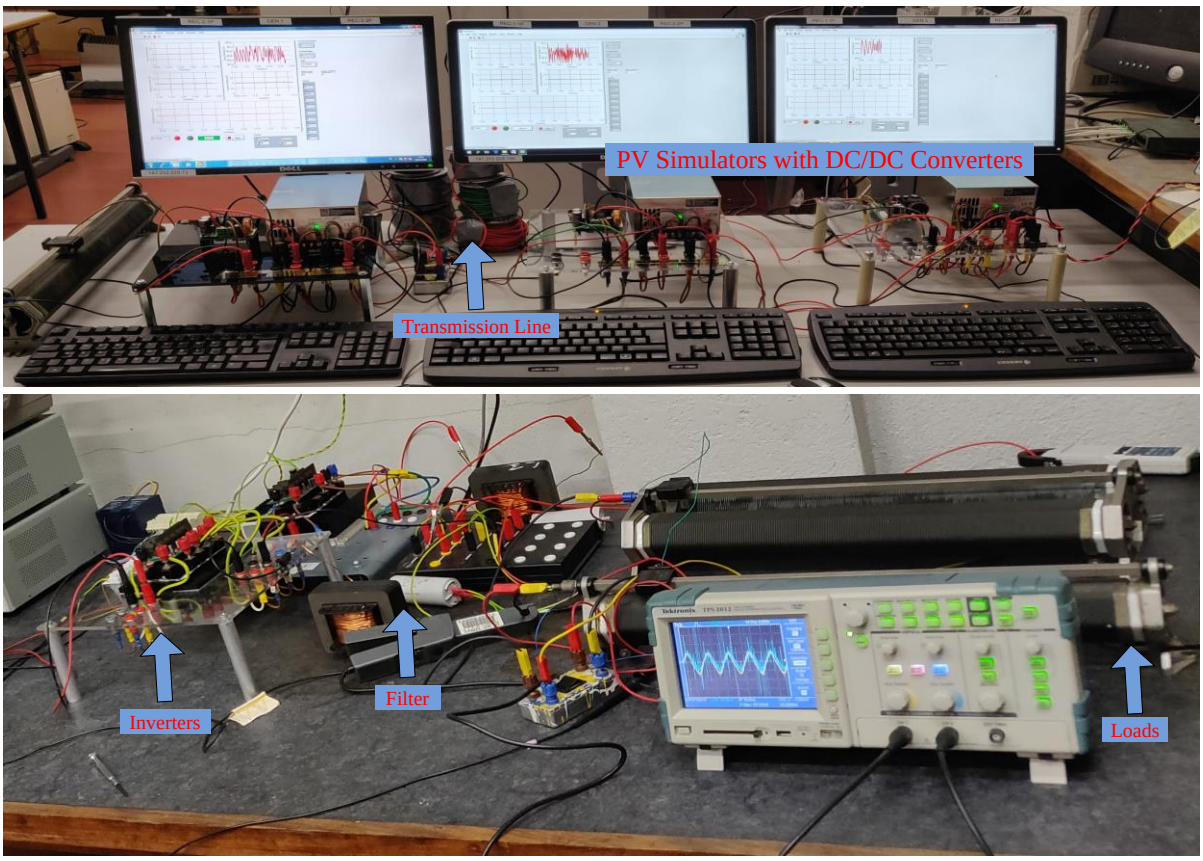


*Figure 4.15 Experimental prototype of the proposed system*

### *4.7.1 Case1: MGs are operated independently and sudden load change:*

In this case study, both the MGs are operated separately and supplying the local load individually, as shown in Figure 4.16 (a). The implemented controller is able to maintain the desired voltage and frequency and also able to provide the required load demand.

Initially, in case study 1 (Figure 4.16 (a)), 10 A (~ 1.2 kW) and 5A (~ 0.6 kW) load was connected to MG1 and MG 2 individually. In the second case study in this section, as shown in Figure 4.16, (b) a transient load change condition is considered to check the efficacy of the proposed controller. In this section, initially, 10A (~ 1.2 kW) load was connected in MG 1, and MG 2 was in no-load condition, and suddenly 5A (~ 0.6 kW) load was added in MG 2. It can be seen that voltage was remained unchanged during this load change. This scenario provides satisfactory testing of the MG controllers in the standalone mode of operation.

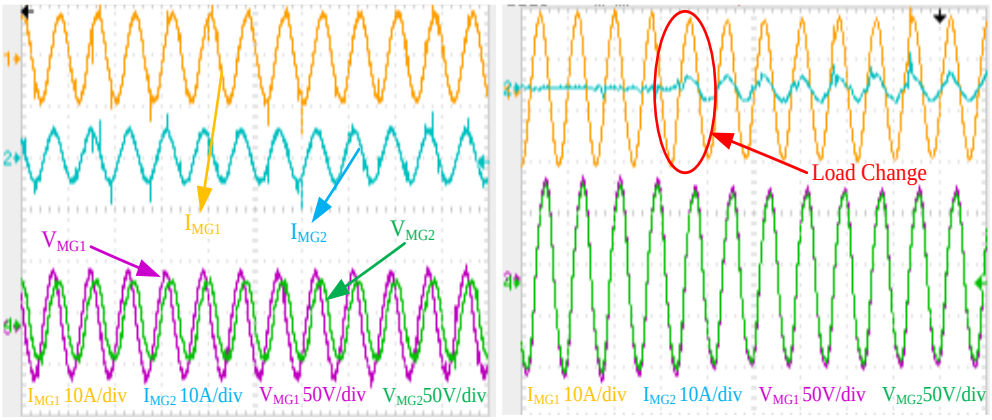


(a) (b)

*Figure 4.16 MGs operating condition- (a) in decoupled mode and (b) effect of a sudden load change*

### *4.7.2 Case 2: Symmetric and asymmetric power-sharing*

One of the most important contributions of this research work is to share the power according to the power set point of the inverter, calculated from a power management strategy. According to the power management strategy, as shown in Figure 4.17, the power set-points are defined by the power availability of the MGs and load connected to the MGs. As the distributed energy sources are intermittent in nature and low voltage MGs have some limited capacity to fulfil the load demand, in case of coupling neighbouring MGs, the power should be shared according to the limitation and requirement, and that can be symmetric or asymmetric. In this case study, as shown in Figure 4.17 (a) a symmetrical/equal power-sharing has been illustrated. Initially, 10A (~

1.2 kW) and 6A (~ 0.8 kW) load was connected in MG1 and MG2 respectively, and in this condition, MGs are coupled to share the total load. The power management strategy has been implemented and can be seen from Figure 4.17 (a), the loads are shared symmetrically, and the frequency is also in the allowable range. On the other hand, as shown in Figure 4.17 (b) a asymmetrical power-sharing has been illustrated. In this case study, during the coupled condition, an asymmetrical power-sharing has been achieved, where MG 1 is supplying 4A (~ 0.5 kW) of loads and MG2 is supplying 8A (~ 1 kW) of loads.

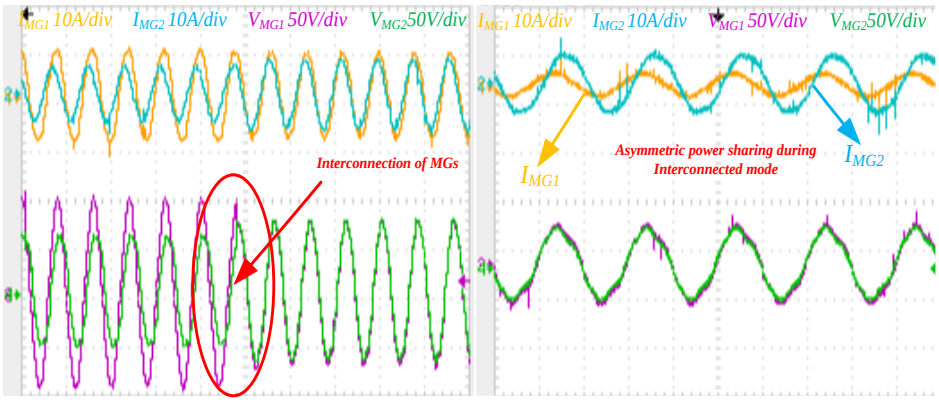


(a) (b)

*Figure 4.17 MGs power-sharing - (a) symmetric and (b) asymmetric power-sharing*

### *4.7.3 Case 3: Power transfer between the microgrids*

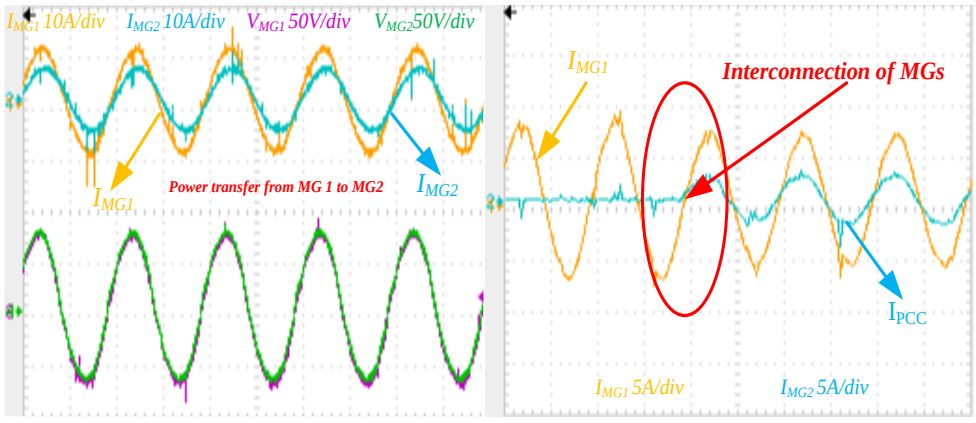


(a) (b)

*Figure 4.18 Power transfer between the MGs (a) power from MG1 to MG2 (b) Power from MG2 to 1. IPCC*

In this section, finally, power transfers between the MGs have been achieved. As shown in Figure 4.18, both the MGs are in the coupled condition. In Figure 4.18 (a) MG

1 generated current was 18A (~ 2.1 kW) , and MG 2 generated current was 14A (~ 1.7 kW) . PCC current at the time of coupling has been measured and is given in Figure 4.18 (b). It can be clearly seen from Figure 4.18 (b) that power has been transferred from MG1 to MG2 to share the load demand.

## 4.8 Conclusions

In this chapter, an improved droop control method is proposed to enhance the power-sharing accuracy in a standalone coupled microgrid. Two PV based static MGs were considered to verify the power management-based droop control. The Matlab based simulation and experimental validation results conclude the following:

- An efficient coupling scheme for available power-sharing among the neighbouring microgrid is developed. The proposed scheme is able to support neighbouring MG during any kind of contingency.
- The power management-based setpoint calculation for the droop control provides an accurate power-sharing between the MGs. The proposed topology is able to share the power among the MGs in asymmetric way as-well, which does not restrict the inverters for equal power-sharing. This is one of the novelties of this research-work.
- This proposed topology is also able to keep the system frequency in acceptable allowable range (50 Hz ± 1). A wide range of case studies has been considered, and the efficacy of the proposed controller for frequency regulation is verified.
- It should be noted that the proposed technique also has some limitation; if the power demand exceeds the limit of BESS; in that situation, load shedding is the only option to maintain a stable operation.

As stated clearly, the proposed coupling topology have some limitation in case of very

high load demand; if the installed BESS is unable to supply the total load, the MGs has to be decoupled. So, a seamless coupling and decoupling topology have to be developed to maintain the stability of the system. The next chapter proposes a robust frequency restoration technique, which will help to develop a seamless coupling and decoupling techniques.

Chapter 5

# Frequency Restoration and Seamless Reconnection of Neighbouring MGs for Power-sharing

## 5.1 Introduction

In the previous chapter, the available resource sharing has been shown among the neighbouring microgrids to meet the load demand. Coupling the neighbouring MGs could be an excellent solution for increasing load demand. Besides, it is to be noted that all the MGs have their own power ratings and some limitations, and it cannot be overloaded for a long time (depends on the BESS capacity). So, a proper connection and reconnection topology has to be developed for available power-sharing and stable mode of operation.

In an isolated rural microgrid where X/R ratio is very low, the conventional droop control interrelates a cross-coupling between Q-V and P-f droop control, which have a drastic effect on the power-sharing performance. Conventionally, virtual impedance or virtual damping based controller [162], [163] is introduced by researchers in order to resolve this issue. Sometimes that results in a significant voltage drop from its nominal value. The voltage drop over the high resistive rural coupling network can cause inaccurate reactive power-sharing, that can introduce a circulating current among the coupled MGs [164]. Traditionally, a secondary controller has been employed by the researchers in order to chop off this power quality issue related to voltage drop. Another major concern and the main focus of this thesis for this networked rural MGs is related to P-f droop control. In order to improve the active power sharing performance of the

droop controller, a very high droop gain is required, which leads to a significant frequency droop in the system [165].

Eventually, a secondary controller is introduced by the Microgrid Central Controller (MGCC) to restore the frequency to its nominal value. All the recently proposed frequency restoration methods can be divided into three main categories- centralised, decentralised and consensus control topologies [166]–[169]. The communication channel based secondary controller usually suffers from a single-point-of-failure, and the extra computational burden (due to massive data handling) can lead to poor dynamic performance [170]. An improved droop controller can resolve the communication channel-related issues and also provide a greater redundancy to the system. Adaptive droop controller [171], virtual impedance-based adaptive droop controller [172], and optimised adaptive droop controller [173] can provide an accurate active power sharing performance, faster dynamic response and a significant stability margin to the system. However, the performance deviates in the presence of a low impedance network and with critical loads (like constant power loads). It is difficult to choose the suitable co-efficient for the integral-derivative term and droop filter gain, which imposes power quality problems to the system. The signal injection-based frequency/voltage restoration method [162], [174] has been recently introduced by researchers, which estimate the MG frequency/voltage based on the injected signal. If the estimated voltage/frequency deviates from its nominal value, then the MGCC adjusts the droop gain, in order to restore the nominal value. But these methods can introduce a power quality problem in the system. The recently introduced synchronverter concept [175], [176] is also adopted by the researcher in order to maintain the frequency of the system, and this method also provides higher stability. However, this introduces a prolonged dynamic response due to the computational burden as the operating frequency is determined by solving a

complicated swing equation. The extensive literatures survey discussed in chapter 2, suggest a robust frequency restoration technique is still required for maintain the system stability [140], [141] and without affecting the power sharing accuracy.

Further, in order to maintain the stability and frequency of the system, there should be sufficient active power to execute the frequency restoration controller. The load-frequency control in photovoltaic generation based inertia-less system can be achieved by sharing the active power with neighbouring community microgrids. The frequency deviation will be significant when the load demand is too high, and the available RESs (in coupled MGs) are unable to supply the load demand. Under these circumstances, this will impose too much burden on the frequency control units. Hence, it is desirable that the active power should be 're-shared' among DG units after the primary droop control action, so that proper load sharing may occur [177].

On the other hand, the MGs should be decoupled in order to maintain system stability. In this condition, a seamless connection/recommission is required for the smooth operation of power-sharing among the neighbouring MGs. Lots of research has been conducted for seamless transfer [178]–[181] of operation modes between grid and islanded microgrid. But a seamless (re)connection between the neighbouring islanded microgrids has not been addressed till date. In a grid-connected system, the reconnection mainly depends on the grid forming and grid following inverter modes [182], [183] and need to control the voltage only as the stiff grid governs the frequency. But, in the inertialess isolated microgrids, frequency regulation plays an essential role in seamless reconnection. In this research work, an improved double layer droop control strategy is proposed for frequency/voltage control to address this issue. Further, a (dis)connection topology is developed based on that, in order to (de)couple the MGs seamlessly. The

proposed controller is robust, and it does not have any effect on the power-sharing accuracy between the microgrids. The Matlab based simulation and real-time simulator-based HIL experimental results provide the accuracy of the proposed controller.

## 5.2 Proposed methodology for frequency/voltage regulation

The state of the art of the proposed research area, indicates that the frequency/voltage of any isolated microgrid primary controller with the droop function will deviate from its nominal value as long as the total nominal power output is different from the consumption of real power. Further, to connect the isolated neighbouring community microgrids, a proper connection and disconnection topology has to be designed. Thus, a secondary controller is required to restore the frequency/voltage and to achieve a seamless connection/disconnection. In order to summarise this, the control objectives of this research work are:

1) Restore the frequency to its nominal value i.e.,

$$lim_{t\to\infty}\omega_i(t) = \omega_0, \forall i \in N \tag{6.1}$$

And for ensure the real power-sharing accuracy, i.e.,

$$\frac{P_{MGi}}{P_{MGk}} = \frac{k_{\omega i}}{k_{\omega k}}, \forall i, k \in N \tag{6.2}$$

where $k_{\omega i}$ and $k_{\omega k}$ are the active power droop gain of the $i^{th}$ and $k^{th}$ CMG inverter. That value can be chosen according to the DG rating. In primary control, the frequency droop gain is usually chosen as the inverse proportion of power rating.

2) Design a seamless connection/disconnection between the isolated CMGs

A distributed secondary controller has been proposed in this research work. The proposed secondary controller restores the system frequency to its nominal value and

helps for the seamless reconnection of the CMGs and the available active power sharing. The secondary controller generates the frequency and voltage control inputs for the primary controller.

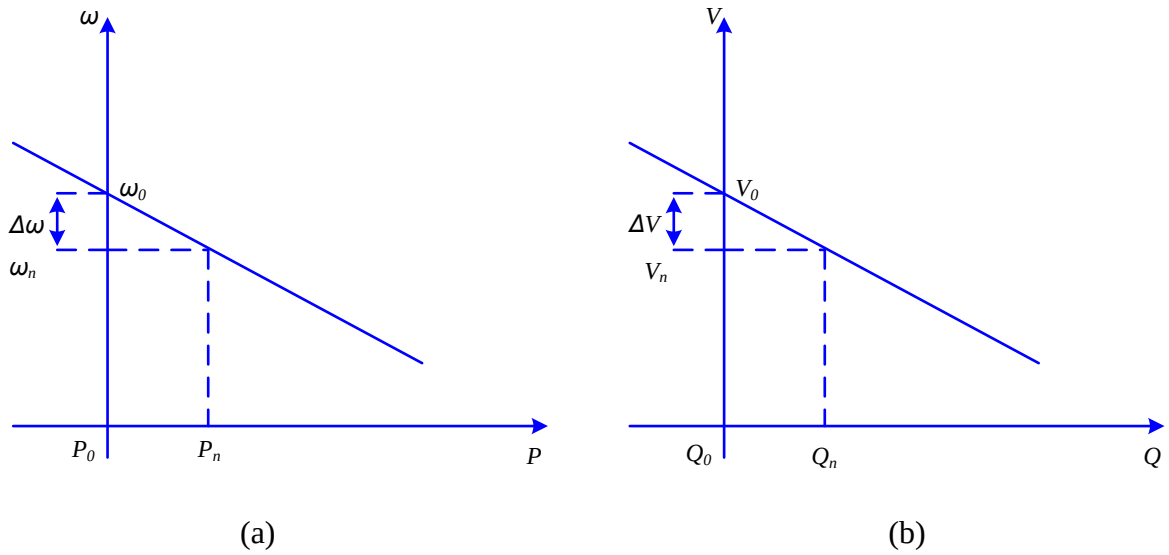


(a) (b)

*Figure 5.1 Conventional droop control (a) p-f droop control (b) V-Q droop control*

The main focus of this thesis work of the secondary controller is to restore the frequency to its nominal value and to improve the active power sharing accuracy. Though in the similar way the secondary controller could be designed for voltage restoration in rural isolated microgrid. The conventional frequency droop control (*f-P*), as shown in equation 5.3 and illustrated in Figure 5.1, is a very well-known and established technique for power-sharing. A disadvantage of this technique is the nominal value of frequency and voltage changes if output active and reactive power is a deviation from its nominal value ($P_0$). If the ratio of active/reactive power varies, the voltage and frequency fluctuate, and that can cause improper power-sharing between CMGs. This is the most important trade-off between transient responsiveness and stability: deciding how much gain to use, which was the objective of the previous chapter.

In order to solve this problem, improved droop control is proposed, as shown in

Figure. 5.2. The deviation of active power from its nominal value can be compensated on its own by shifting the *f-P* droop line to restore the system frequency. By shifting this, the system frequency can be controlled to its rated value individually in each CMG. To eliminate the frequency deviation, a correction factor is added to the frequency droop equation in terms of a time-varying filter of the frequency error ($\Delta\omega$).

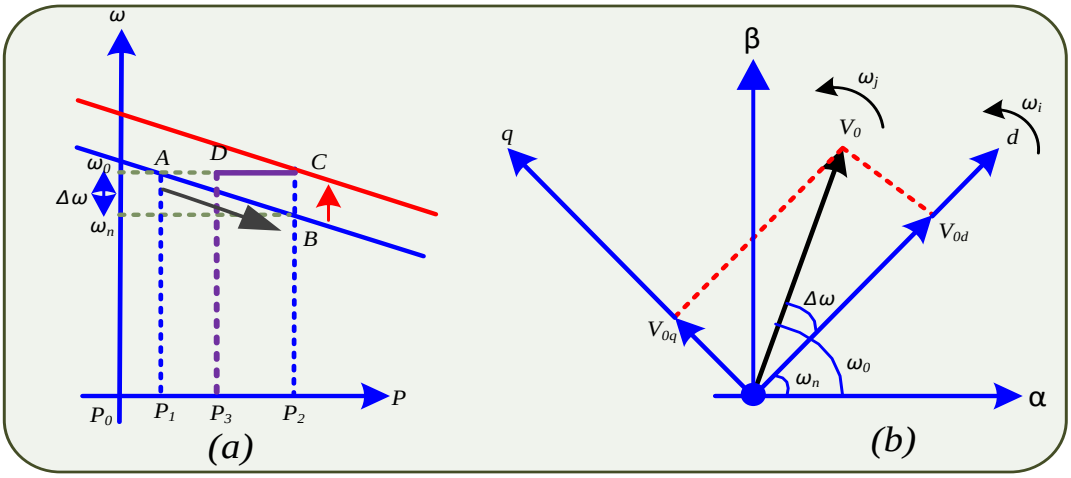


*Figure 5.2 Proposed improved double layered droop control*

Figure 5.2 has shown the droop control frequency restoration example of the participating inverter of the CMG. Initially, when the inverter operates in standalone mode, at point *A*, with frequency $\omega_0$, provides the active power $P_1$. Due to the change of any load demand, the frequency drifts to $\omega_n$ (Point *B*). At that moment the power supplied by the inverter is $P_2$. After activating the frequency restoration control, the frequency droop gain is adjusted (to the *C* point) such that the system frequency returns to its nominal value, preserving the inverter's power output. The same topology is adopted for both the synchronising isolated inverter of the CMGs. This frequency restoration feature eventually reduces the phase angle error between the participating inverters. This acts as a natural 'pre-synchronization' step, without requiring any additional control action for that. The droop line may be changed to point *D* once the seamless coupling controller is

engaged to achieve precise power-sharing as per common demand.

In conventional droop control for the $i^{th}$ inverter:

For *f-P* droop control,

$$\omega_n - \omega_0 = -k\omega(P_n - P_o) \tag{6.3}$$

$$\omega_n - \omega_0 = -k_\omega \Delta P \Rightarrow \Delta\omega = -k_\omega \Delta P \tag{6.4}$$

where, $k_\omega$ is the *f-P* droop coefficient and when the active power is $P_n$, the frequency is $\omega_{n,}$.

Further the instantaneous power of the $i^{th}$ CMG inverter ($P_i$) can be calculated as:

$$P_i = \frac{\omega_c}{s+\omega_c}\left(V_{oid} I_{0id} + V_{oiq} I_{oiq}\right) \tag{6.5}$$

or can be written as

$$P_i = \frac{\omega_c}{s+\omega_c} P_i(s) \tag{6.6}$$

where *s* is the Laplace operator, $P_i(s)$ is the instantaneous value of the community microgrid power and $\omega_c$ is the cut-off frequency for the power calculation filter. $V_{oid}$, $V_{oiq}$, $I_{oid}$, $I_{oiq}$ are the *d* and *q* axis component of the $i^{th}$ inverter output voltage and current respectively.

In order to restore the frequency ($\omega_{01}$) a corrective term ($\Delta\omega$) has to be added with the differed value. To represent this mathematically,

$$\omega_{01} = \omega_n + \Delta\omega \tag{6.7}$$

where $\Delta\omega = -k_\omega \Delta P_i = -k_\omega V_{oid}\, \Delta I_{oid}$ (6.8)

For the control requirement, in order to maintain unity power factor, as the $I_{0iq}$

reference is zero, the change in active power ($\Delta P_i$), could be represented as the change in *d* axis component of the current ($\Delta I_{oid}$), if the void is kept constant, which is the case in the present scenario.

Now assuming, $K_p = -k_\omega V_{oid}$ so that,

$$\Delta\omega = K_p(t)\Delta I_{oid} \tag{6.9}$$

Finally, $\omega_{01} = \omega_n + K_p \Delta I_{oid}$ (6.10)

Further in Laplace domain, the equation 7 and 4 can be written as,

$$\omega_{01}(s) = \omega_0(s) - k_\omega \frac{\omega_c}{s+\omega_c}\Delta P_i(s) + \Delta\omega \tag{6.11}$$

Equation (11) can be written as-

$$\omega_{01}(s) = \omega_0(s) - k_\omega \frac{\omega_c}{s+\omega_c} P_i(s) + \frac{K_g\omega_s}{s+\omega_s}\left(\omega_0(s) - \omega_{01}(s)\right) \tag{6.12}$$

where $\omega_s$ is the additional filter cut-off frequency and $K_g$ is its time varying gain. It is interesting to further expand this equation-

$$\omega_{01}(s) = \omega_0(s) - k_x(s) \frac{\omega_c}{s+\omega_c} P_i(s) \tag{6.13}$$

Where $k_x(s) = k_\omega \frac{s+\omega_s}{s+(1+K_g)\omega_s}$

The block diagram of the proposed control topology for each inverter in MGs is presented in Figure 5.3.

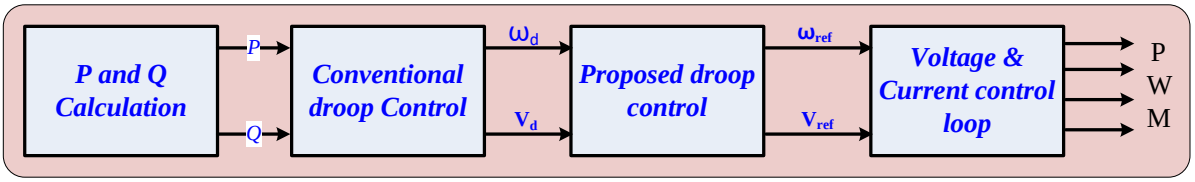


*Figure 5.3 Block diagram of the proposed control topology.*

## 5.3 System structure

The overall schematic diagram for two neighbouring isolated MGs are presented in Figure 5.4. It is assumed that both the MGs are PV based MGs and as a backup power supply, in both the MGs BESS is installed. Both the microgrids have their own local loads. It can be observed from equation 5.11 and 5.12, that the restoration of voltage and frequency is based on the d-axis component of the terminal voltage. So, it is to be assumed that the MG should have sufficient power to execute the proposed controller and in order to do that, both the MGs are connected with the BESS.

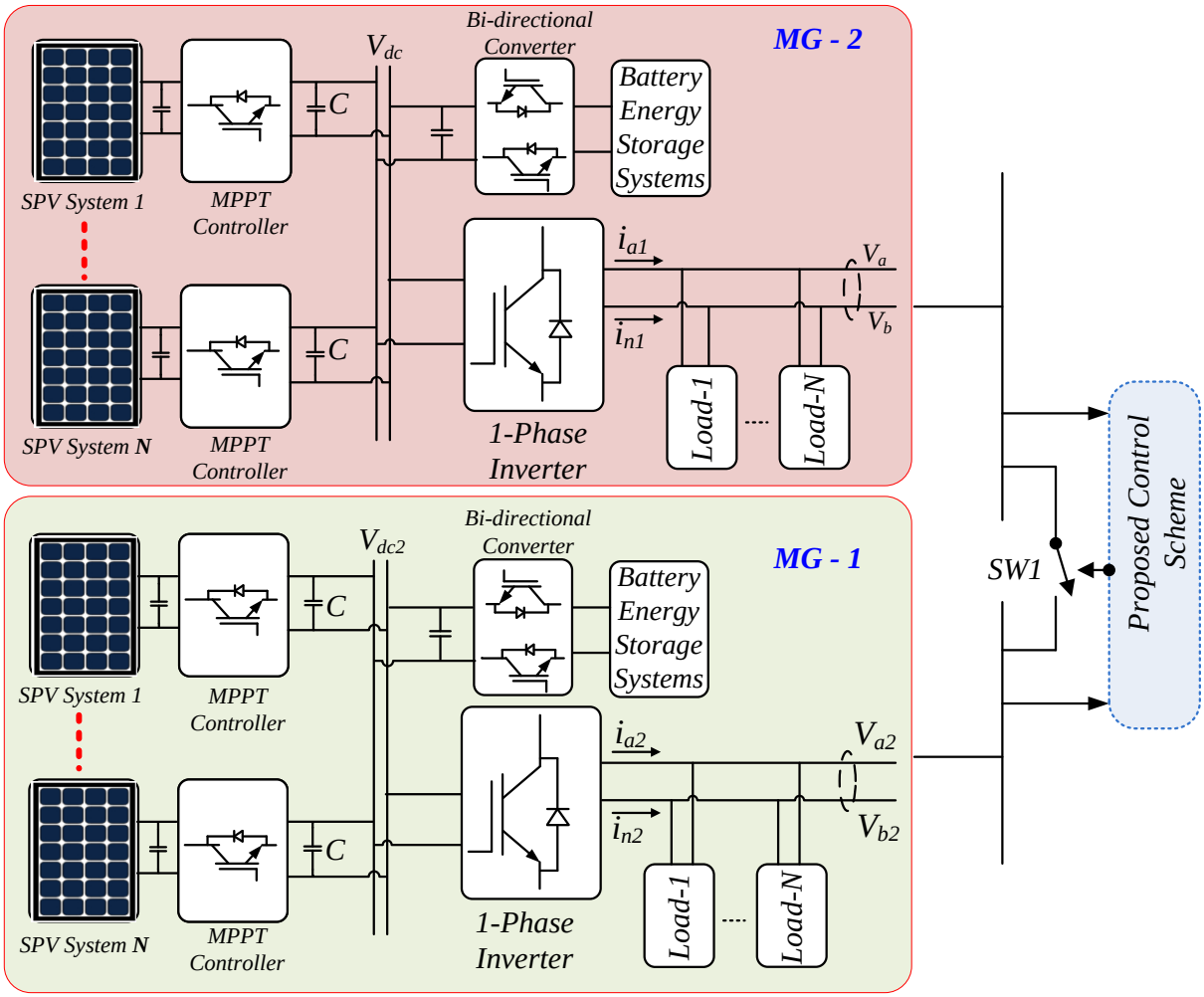


*Figure 5.4 Structures of MGs understudy*

## 5.4 Control topology for seamless (de)coupling of neighbouring MGs

In this section, a comprehensive discussion has been presented for control topology of the seamless connection of the neighbouring MGs for available power-sharing. In the previous section 5.2, we have seen if the voltage and frequency setpoints are varied then droop curve is shifted vertically upwards or downwards to arrive at the desired output values. In this proposed research, MGs can be operated in two modes, -either in standalone (only supplying its own load demand) or in interconnected mode with neighbouring MGs. In the case of operating in standalone mode, the proposed control layout (as shown in Figure 5.3) defines the operating frequency and voltage as per the nominal value of the setpoints. But in inter-connection mode, a secondary control topology must be adopted. The proposed control layout for the voltage and frequency setpoint calculation with the proposed secondary control is presented in Figure 5.5.

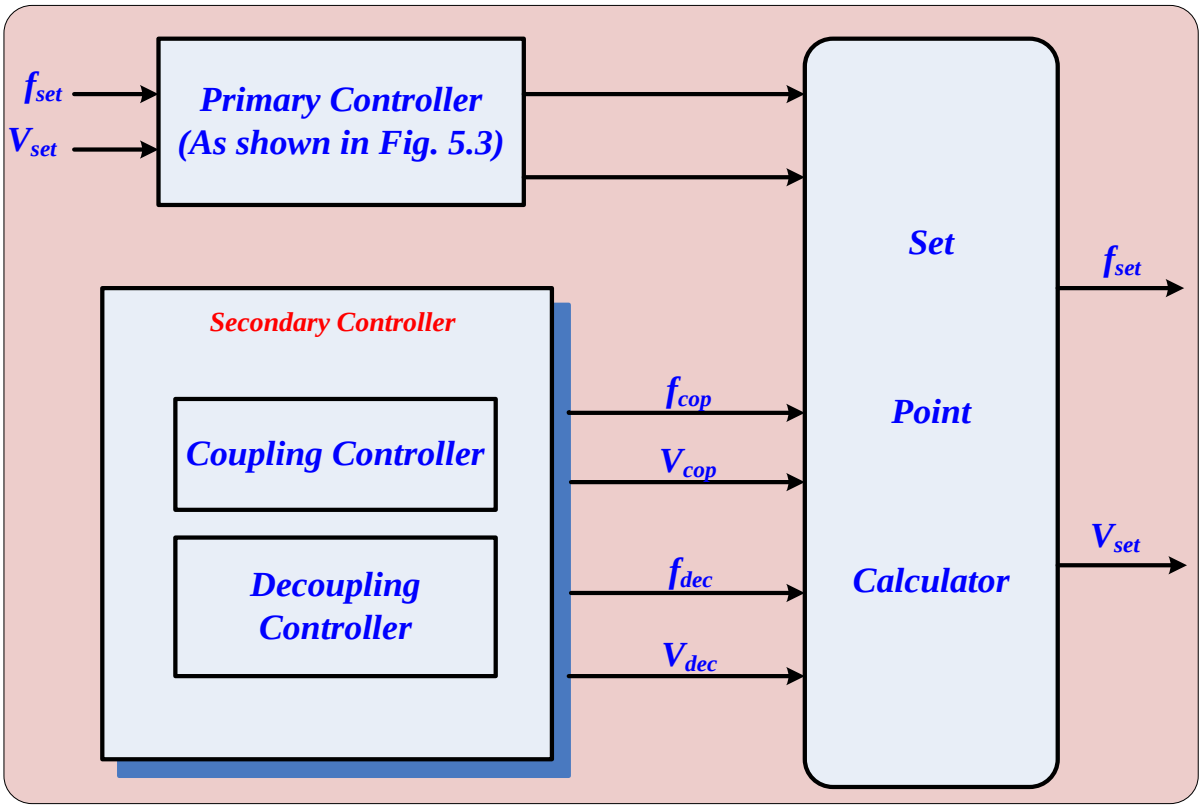


*Figure 5.5 Proposed frequency-voltage controller for seamless connection*

For a smooth transition between standalone mode to interconnected mode, a connection and disconnection strategy is presented. This secondary scheme produces necessary frequency and voltage deviation for a smooth transition between standalone mode to interconnected mode. This voltage and frequency deviations ($V_{cop}$, $f_{cop}$, $V_{dec}$, $f_{dec}$) contribute to defining the new setpoints of the primary controller's voltage and frequency.

### *5.4.1 Coupling Controller*

The foremost function of the coupling controller is to ensure a smooth transition between standalone mode to interconnected mode, without affecting the performance of each individual MG. In standalone mode, the voltage and the frequency setpoints are governed by the proposed controller, and for the interconnection, the parameters of both the MGs must be adapted to match all the values before actual closure of the contactor switch. To eliminate any abnormal transient behaviour and instability in transition, a synchronization principle is devised. The difference in voltage magnitude, frequency and phase of the voltage of two microgrids is reduced to the very low limit for the seamless transition of modes. The magnitude of the error value is reduced by creating an additional frequency. The layout of the algorithm is presented in Figure 5.6. As shown in Figure 5.6, the coupling controller consists of a voltage error and frequency error controller. Coupling of two systems with a large voltage magnitude difference can cause a voltage drop in the coupled system. In order to match the voltage of two microgrids, the voltage difference between the two microgrids is fed to the PI controller. The PI controller tries to minimize this error and bring voltages of the two systems as close as possible. The selected signal is passed through a first-order filter to generate the final voltage deviation, $V_{cop}$. Similarly, the frequency error signal of both the microgrids is passed through a PI controller to minimise the error, and finally, $f_{cop}$ is generated to create the final frequency

deviation. Another criteria for coupling is to reduce phase angle difference. The integral of frequency difference over time produce the relative phase angle. So, practically minimizing the frequency deviation, actually minimises the phase error as well.

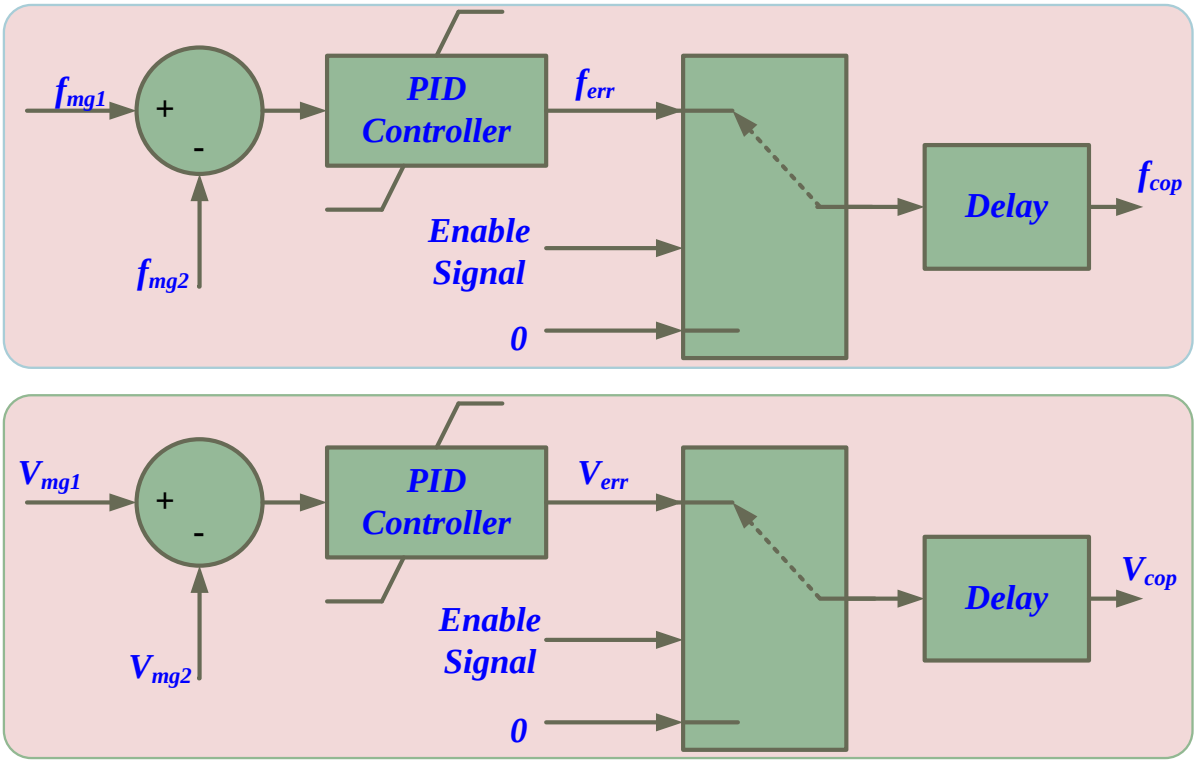


*Figure 5.6 Layout of the coupling controller*

Once all the error signals are within acceptable limits for a minimum period of 10 cycles (~ 0.2 sec), the enable signal is triggered, and seamless coupling of neighbouring microgrids are established. Figure 5.7 shows the considered maximum error limits for voltage, frequency and phase.

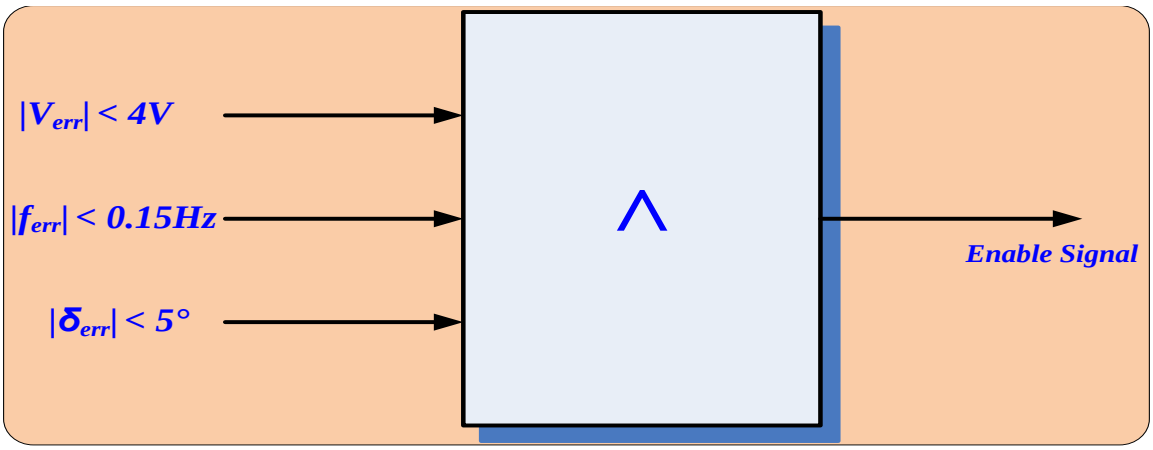


*Figure 5.7 Connection criteria*

### *5.4.2 Decoupling Controller*

The de-coupling controller confirms a smooth and seamless transition from interconnected mode to standalone mode and also ensures the associated disturbances in the interconnected systems are minimal. These standalone systems also have some limitations like they cannot be overloaded for an indefinitely long time and if the local load demand increases beyond the capacity of coupled MG, then it is advised to bring back the coupled MG to a standalone mode for individual load shedding purposes. Figure 5.8 shows the layout of the decoupling controller. The active and reactive power at the coupling point are measured and compared with zero, and the error signal is passed through a PI controller to generate the voltage and frequency deviation $V_{dec}$ and $f_{dec}$.

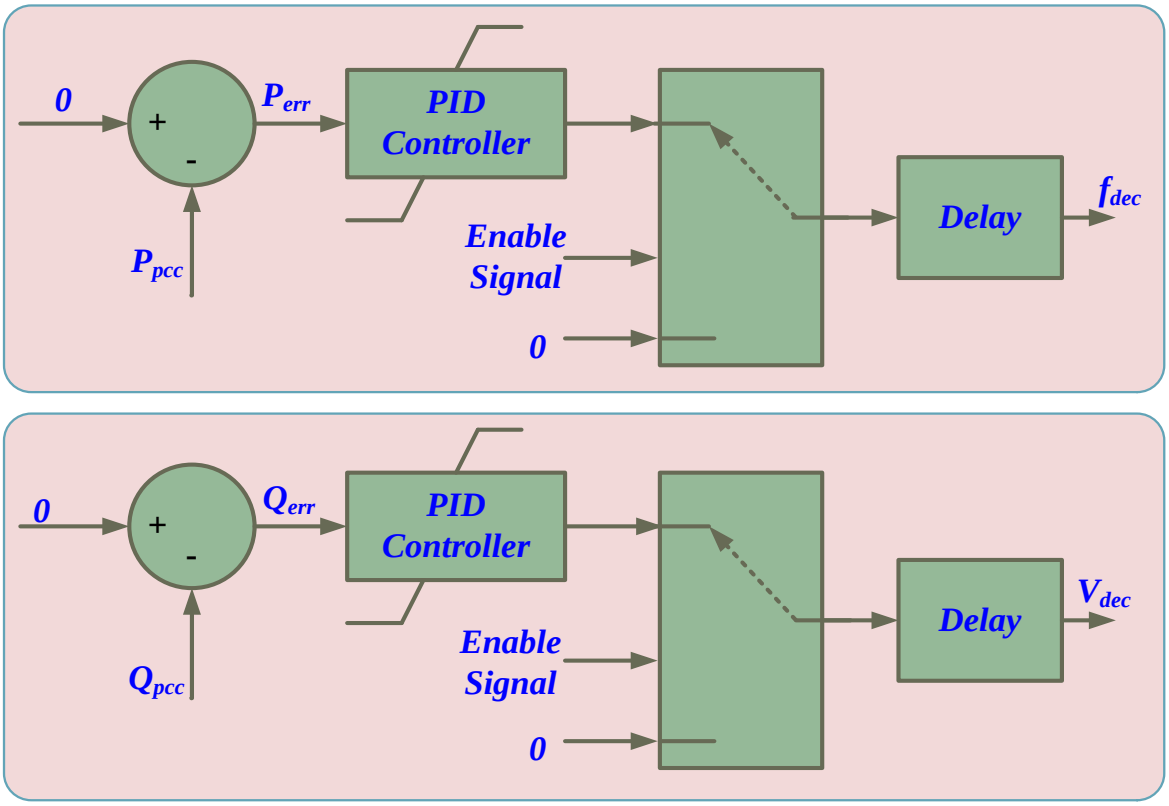


*Figure 5.8 Layout of the decoupling controller*

The controller prepares for the system disconnection when $P_{err}$ and $Q_{err}$ fall below 0.001 pu or the power of MG1 and MG2 exceed their rated values. Figure 5.9 shows the disconnection criteria for the decoupling controller.

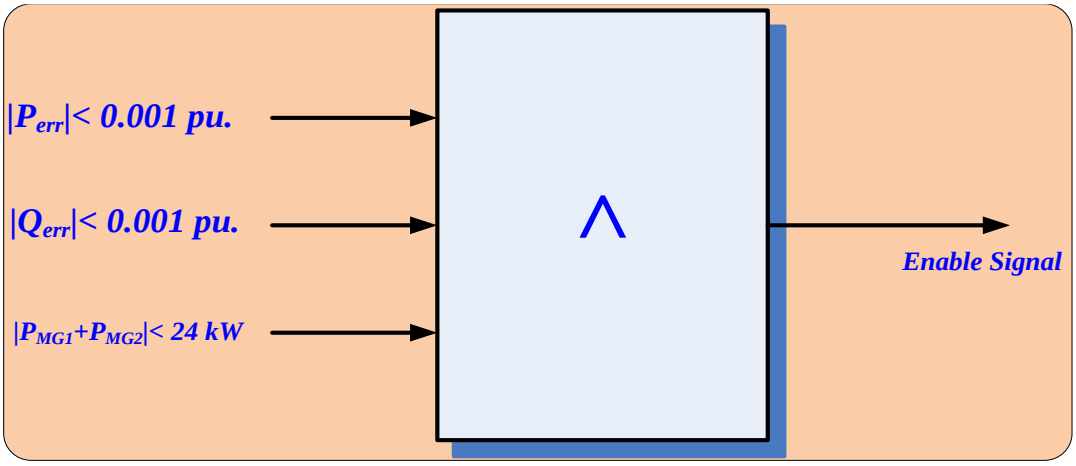


*Figure 5.9 Disconnection criteria*

### *5.4.3 Setpoint calculation for the primary controller*

As the MGs are capable of working in standalone modes, the voltage and frequency setpoints are defined by the local controllers. Figure 5.10 shows the final set point calculation for each MG. When the enable signals are high in the coupling, and de-coupling controller, the frequency and voltage deviation are produced and are added to the nominal value of voltage and frequency to define the final setpoint value of the primary controller.

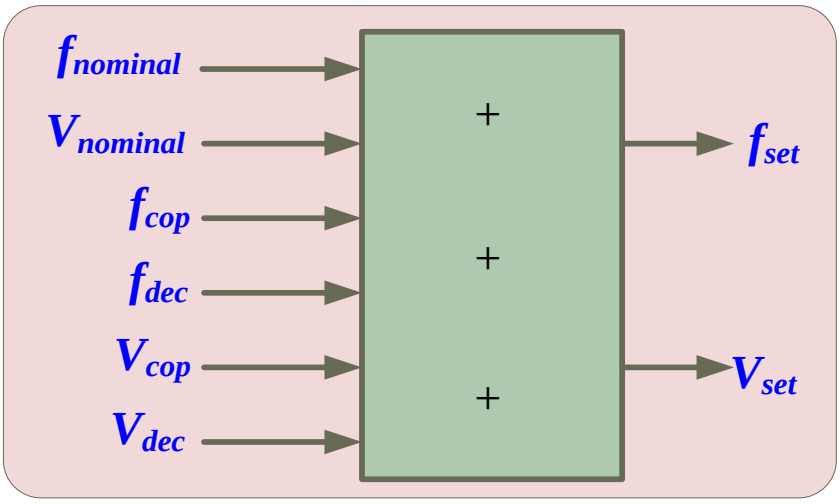


*Figure 5.10 Final setpoint calculation*

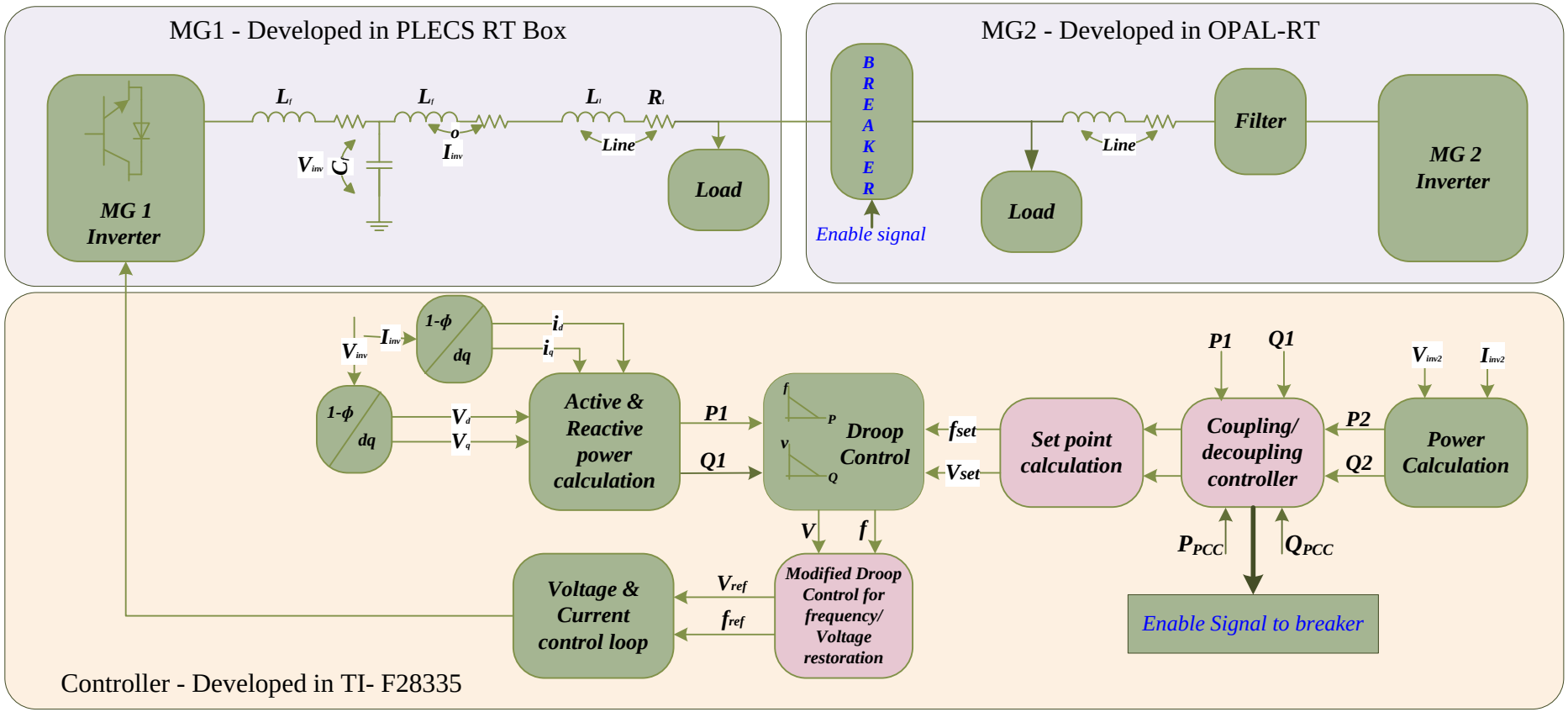


*Figure 5.11 Integration technique of the controllers*

## 5.5 Working principle

The integration technique of the proposed double-layer droop control with the secondary coupling and de-coupling controller is presented in Figure 5.11. The precise control topology of MG 1 is shown in Figure 5.11. The setpoints of voltage and frequency from the secondary controller is given to the primary droop controller to set the operating frequency and voltage of the microgrid. In case of standalone mode both the microgrids operates on its own and delivers the power to the local load but in interconnected mode both the microgrids delivers the total load connected to it and the power is shared according to the droop controller.

## 5.6 Simulation results

The proposed control strategies for frequency and voltage regulation, seamless (de)coupling between the MGs, as described in this chapter, are assessed and verified in this section. All the system parameters for the Matlab based simulation study are provided in Table 5.1.

*Table 5.1 Assumed System parameters*

| System Parameters | |
|---|---|
| Dc Link Capacitor | 2000 µF |
| Filter Inductor (L1) | 1350 µH |
| Filter Inductor (L2) | 300 µH |
| Filter Capacitor | 240 µF |
| Power Rating for MG1 Inverter | 10 kW |
| Power Rating for MG2 Inverter | 10 kW |
| BESS Capacity in MG1 | 5 kWh |
| BESS Capacity in MG 2 | 5 kWh |
| Frequency drooping gain | 0.05 rad/s/W |
| Voltage drooping gain | 0.01/W |

### *5.6.1 Frequency Restoration*

To prove the efficacy of the proposed improved frequency and voltage droop

controller, two different situations have been considered. In the first one both the microgrids are connected with 4 kW load individually. At the simulation time, instant 1 sec both the loads are increased to 5 kW, and the effectiveness of the proposed controller is analysed. Voltage and current profile of the MG1 are shown in Figure 5.12. It can be observed that both voltage and current are in phase and voltage amplitude remains stable after load change. Figure 5.13 shows the power and frequency profile of the MG1. A comparison is shown in the frequency profile with the proposed double-layer droop control and conventional droop control. It can be observed from the simulation results, the frequency profile is much smoother in proposed droop control compared to conventional droop control, though both the frequencies are within the acceptable limit.

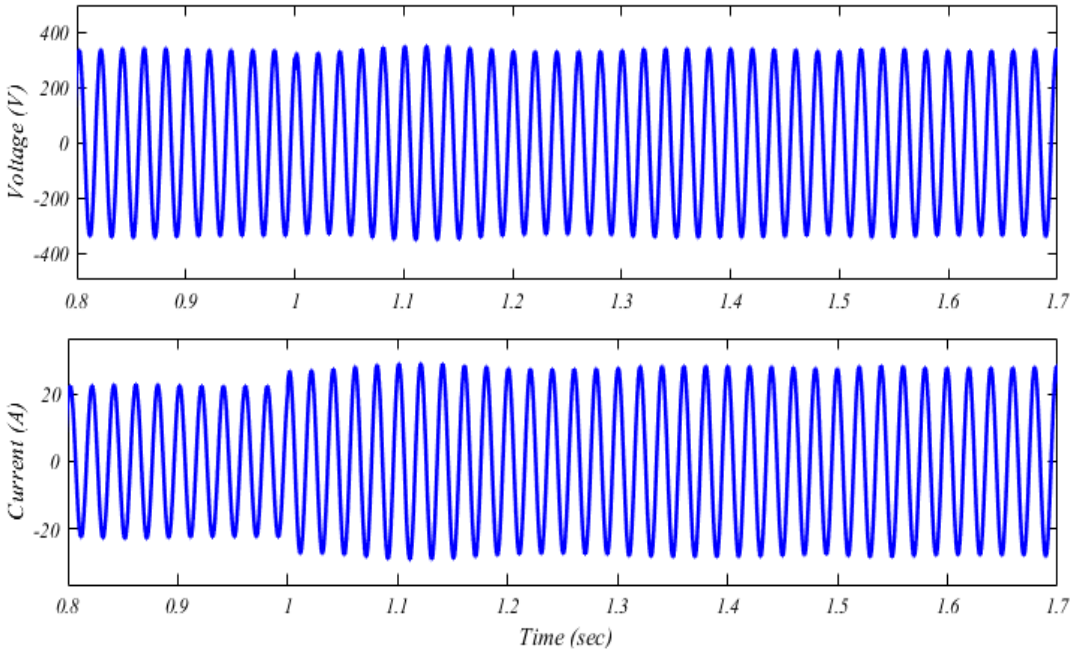


Figure 5.12 Voltage and current profile of MG1

In the second situation, both the microgrids are connected to 7 kW load and at the simulation time, instant 1 sec both the loads are increased to 11 kW. The power and frequency profile of MG2 is shown in Figure 5.14. Similar to the previous case study, the stability of frequency profile is higher in proposed droop control compared to the conventional droop control as in conventional droop control, the frequency is oscillating

in nature during any transient.

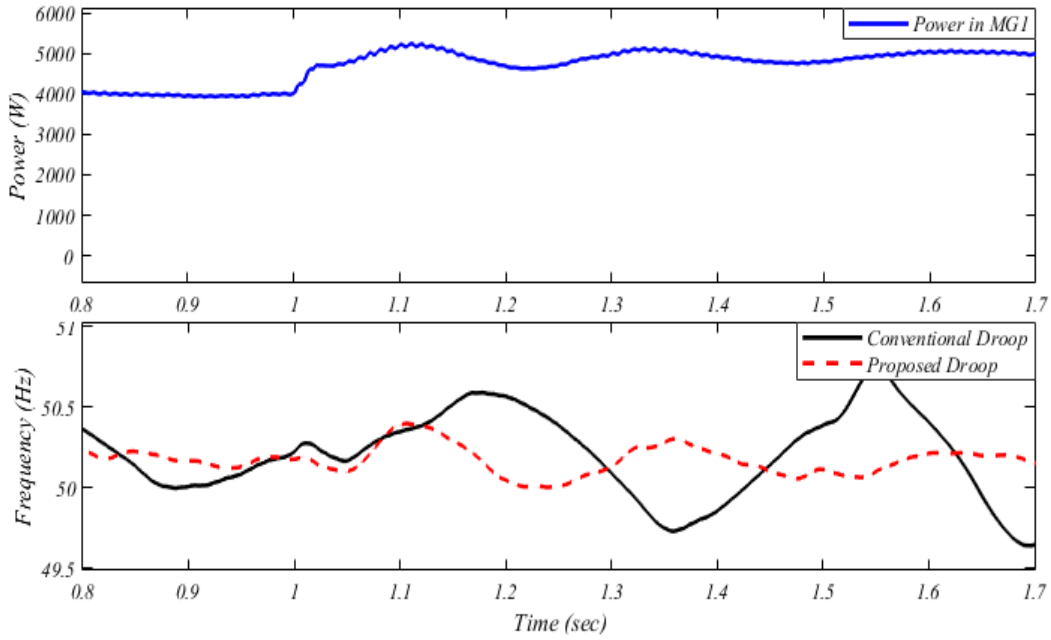


Figure 5.13 Microgrid 1 load demand and frequency profile

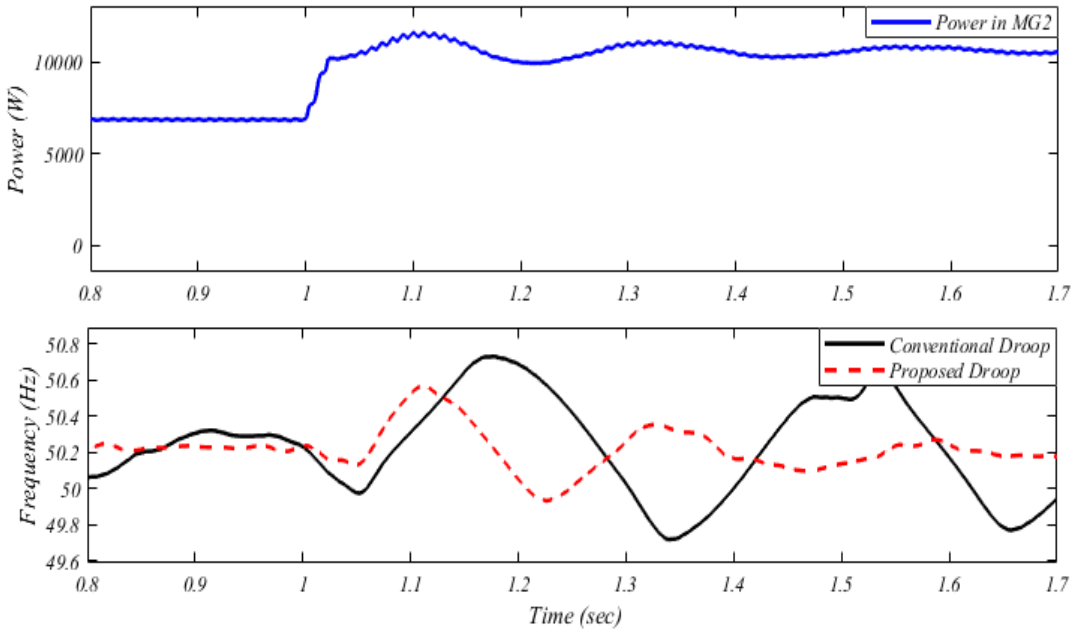


Figure 5.14 Microgrid 1 load demand and frequency profile

### *5.6.2 Seamless interconnection of Microgrids*

To establish a smooth seamless transition from standalone mode to interconnected mode, a control topology is developed as discussed in section 5.4. When enable signal of the coupling controller is triggered, the controller generates the frequency and voltage

deviation, which contribute to define the final setpoint value of the MGs. After checking the required connection criteria as shown in Figure 5.7, the breaker connecting to the network and both the MGs come to coupled condition. To check the efficiency of the proposed controller, both the MGs are connected to 6 kW load and at the simulation time, 1 sec the coupling controller enable signal is triggered. As shown in Figure 5.15, both the MGs are delivering 6kW load demand, and they have their own different frequency profile, but after getting coupled at 1 sec both have the same frequency profile. As we can see from the frequency profile, the coupled system takes only 0.05 sec to stabilize.

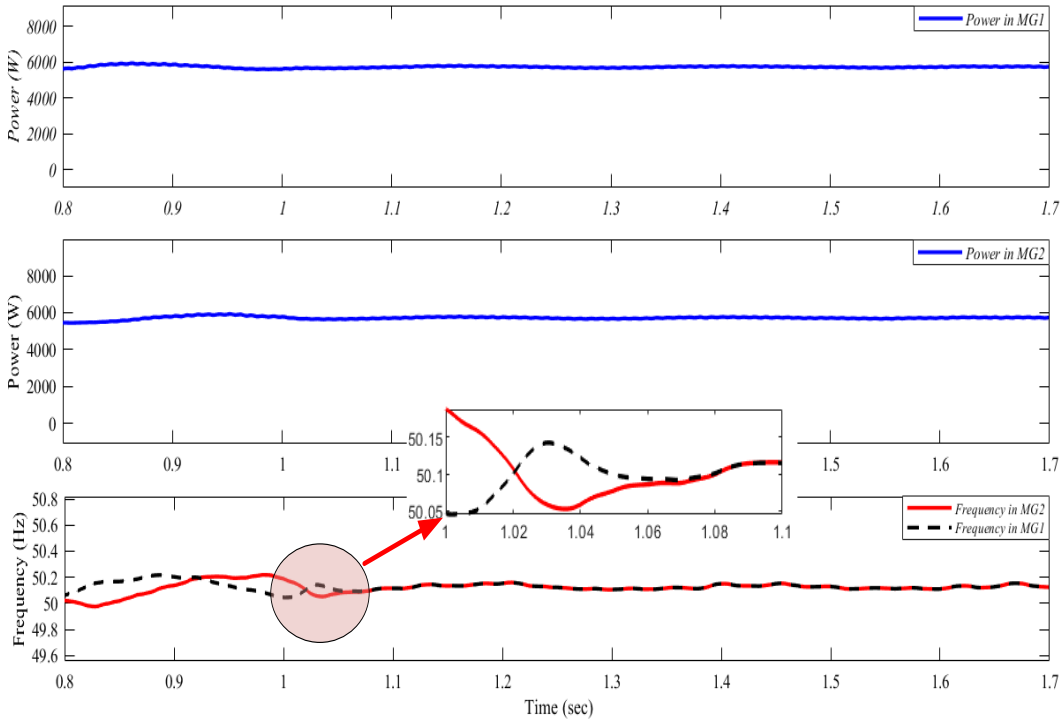


Figure 5.15 Illustration of the seamless interconnection of MGs

### *5.6.3 Power sharing performance in an inter-connected mode*

The power-sharing performance of the proposed improved droop control is discussed in this section. To examine the power-sharing performance of the proposed controller, MG 1 is connected to 8 kW load, and MG 2 is connected to 6 kW load. They are supplying their own load demand up to 1 sec of the simulation time. At this time, the

enable signal of the coupling controller is triggered. After coupling both the MGs share the total load demand and as a result, both the MGs contribute 7 kW each (as the total load demand is 14 kW) to the total load demand. The power-sharing performance of the MGs are illustrated in Figure 5.16.

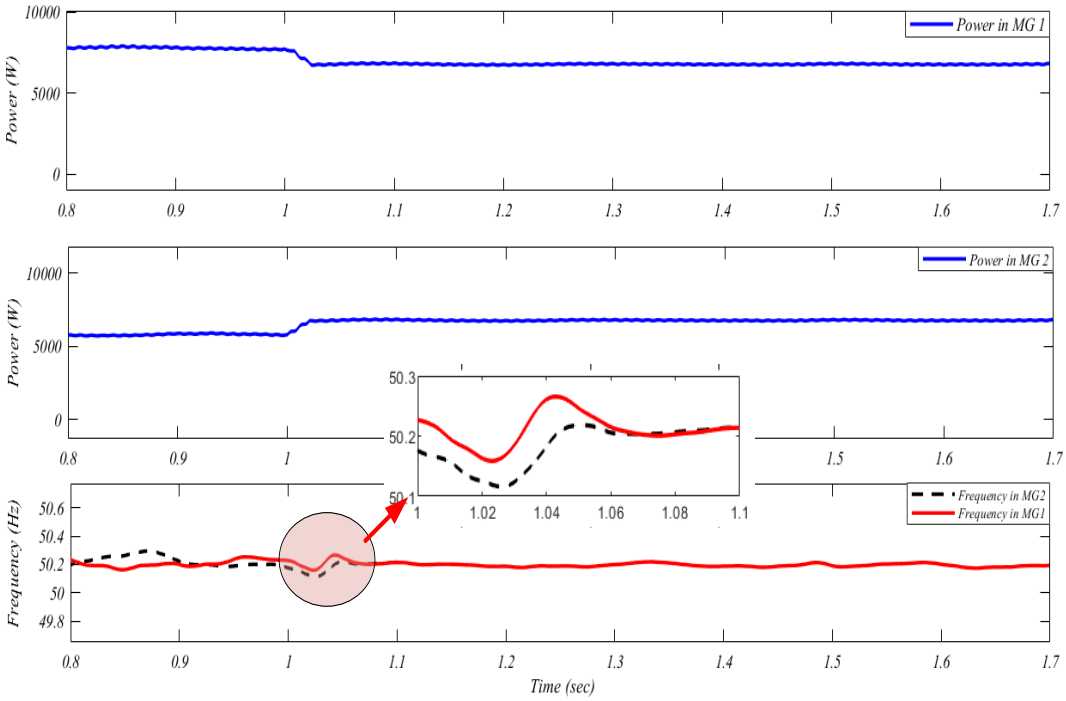


Figure 5.16 Power sharing performance in interconnected mode.

### *5.6.4 Seamless de-coupling of the MGs*

The main objective of the decoupling controller is a seamless transfer of a coupled MG to a standalone MG without affecting the system stability. In this case study initially, both the MGs have 12 kW load demand. In this condition, another 2 kW load demand is increased in MG1 then; the decoupling controller enables signal is triggered automatically. After satisfying all the disconnection criteria, the breaker operates, and both the MGs become isolated. As shown in Figure 5.17 both the MGs are supplying 16 kW load demand initially, and at 1 sec simulation time when the MG 1 load demand is increased by 2 kW, the disconnection controller operates and without affecting the system stability, a seamless disconnection occurs.

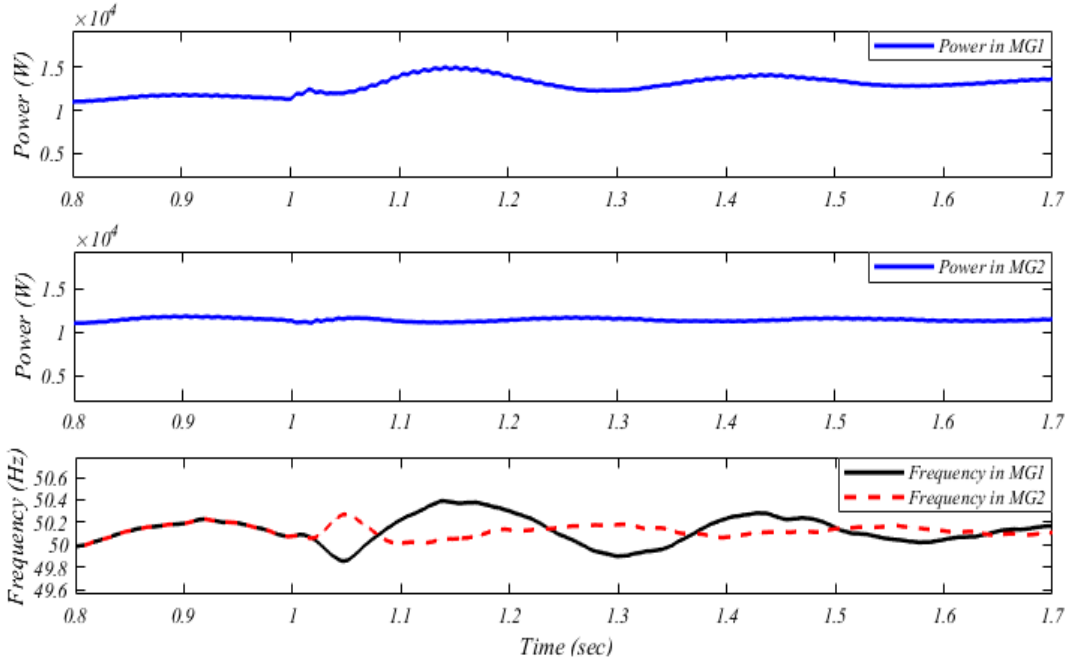


Figure 5.17 Illustration of seamless decoupling

### *5.6.5 Reconnection after decoupling*

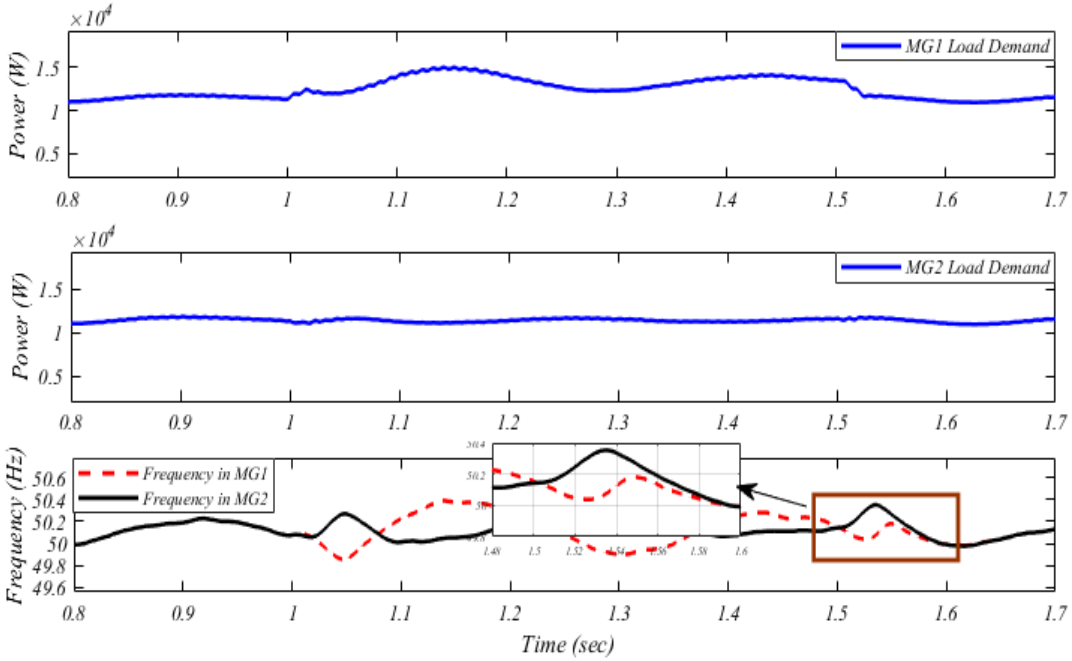


Figure 5.18 Reconnection of MGs after decoupling

In this case study, a reconnection is attempted immediately after a disconnection occurs; to check the efficacy of all the proposed controllers. Like the previous case study initially, the load demand of both the MGs is 12 kW, and at the simulation time, 1 sec, 2

kW load demand in MG 1 is increased. In this situation, the decoupling controller operates and decouples the MGs. Immediately after that at simulation time 1.5 sec, the excess 2 kW load demand is reduced, and again the coupling enable signal is triggered. As shown in Figure 5.18, throughout the simulation, the frequency remains in the allowable range, which enables a seamless reconnection again.

## 5.7 Experimental validation

The implementation of MGs with the controller hardware in loop design is done with PLECS RT box with F28335 breakout board controller and OPAL-RT simulator. In HIL application power stage of MG 1 is emulated in the PLECS RT box, and the power stage of breaker with MG 2 is implemented in OPAL-RT simulator. The digital signal processor F28335 connected to the PLECS RT box with breakout board acts as a controller of the system. The details specifications of the OPAL-RT, PLECS RT box and F28335 controller is given in Chapter 3. In order to summarize this, the hardware module has 3 main blocks, as shown in Figure 5.11.

- PLECS RT box which emulates the power stage of Microgrid 1.
- OPAL RT simulator which emulates the power stage of Microgrid 2 with the breaker.
- Breakout board with F28335 controller connected to PLECS RT box acts as a controller.

The results shown in the next subsection proves the efficacy of the proposed controller.

### *5.7.1 Normal operation with frequency restoration:*

The Hardware in Loop experimental result, as shown in Figure 5.19, provides a normal operating condition of isolated MGs, where both the MGs are supplying their individual loads, respectively. In this scenario, MG1 and MG2 both are supplying 35A

(~ 10 kW) and 25A (~ 8 kW) of load current individually while the frequency is maintained within the acceptable limit.

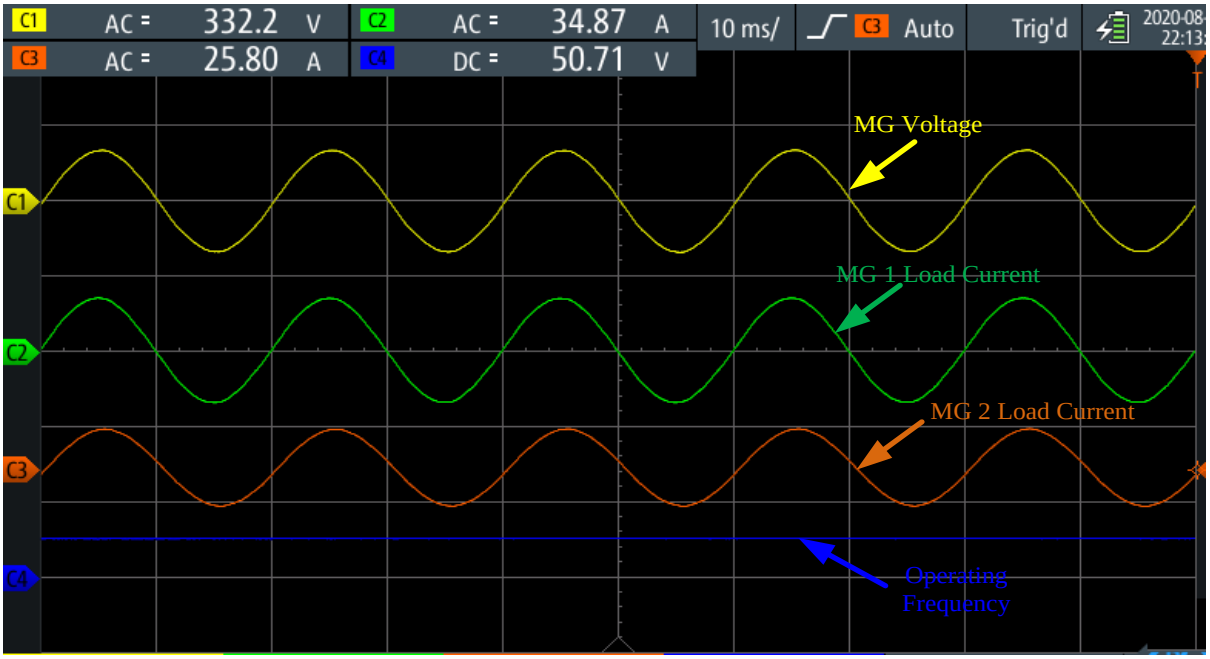


Figure 5.19 MG1 and MG2 are operating in islanded mode

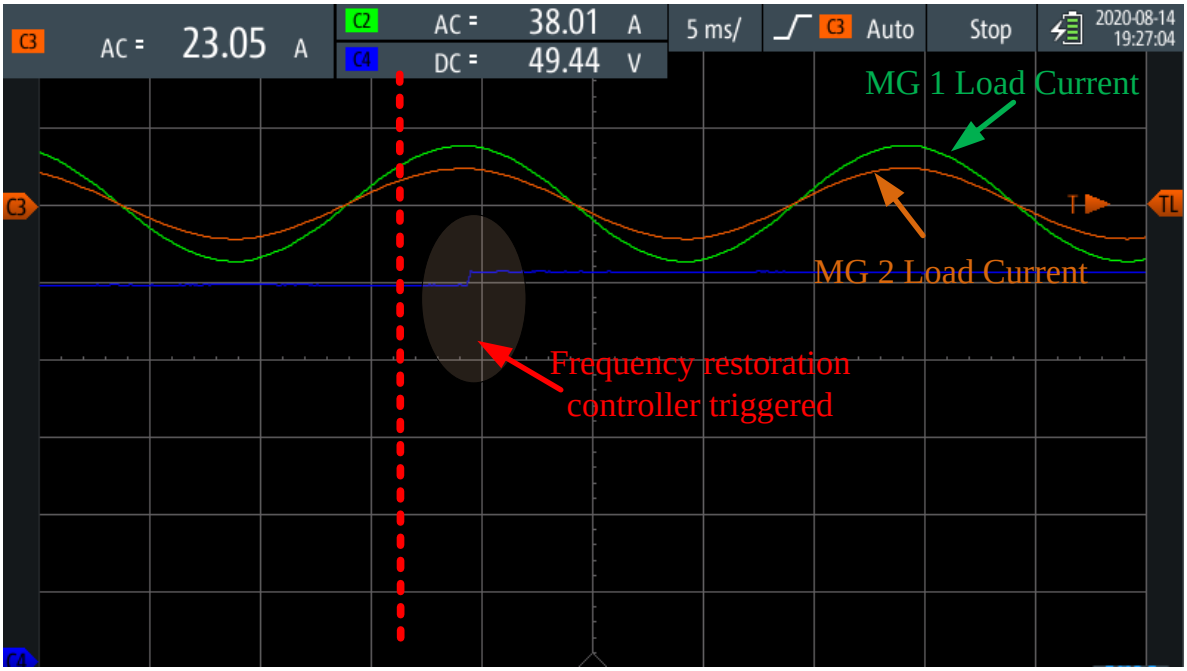


Figure 5.20 Illustration of frequency restoration controller

Now, in order to restore the frequency, the frequency restoration controller is triggered. As captured in Figure 5.20, the zoomed frequency plot shows, the frequency is restored to its nominal value. These experimental results provide a satisfactory test of frequency restoration controller.

### *5.7.2 Seamless coupling of MGs and power-sharing performance*

In this case study initially, both the MGs are delivering the required load demand separately, and after that, the coupling controller is triggered. As shown in Figure 5.21, both the microgrids are coupled seamlessly, without creating any sudden transient in voltage/current profile. It can also be observed that the frequency, measured in MG1 is also maintained within the acceptable limit. The power-sharing performance of the proposed droop controller is also verified in this case study. It can be observed that, after coupling, the total load current is shared equally between the MGs. This case study provides satisfactory testing of the proposed seamless coupling and droop controller performance.

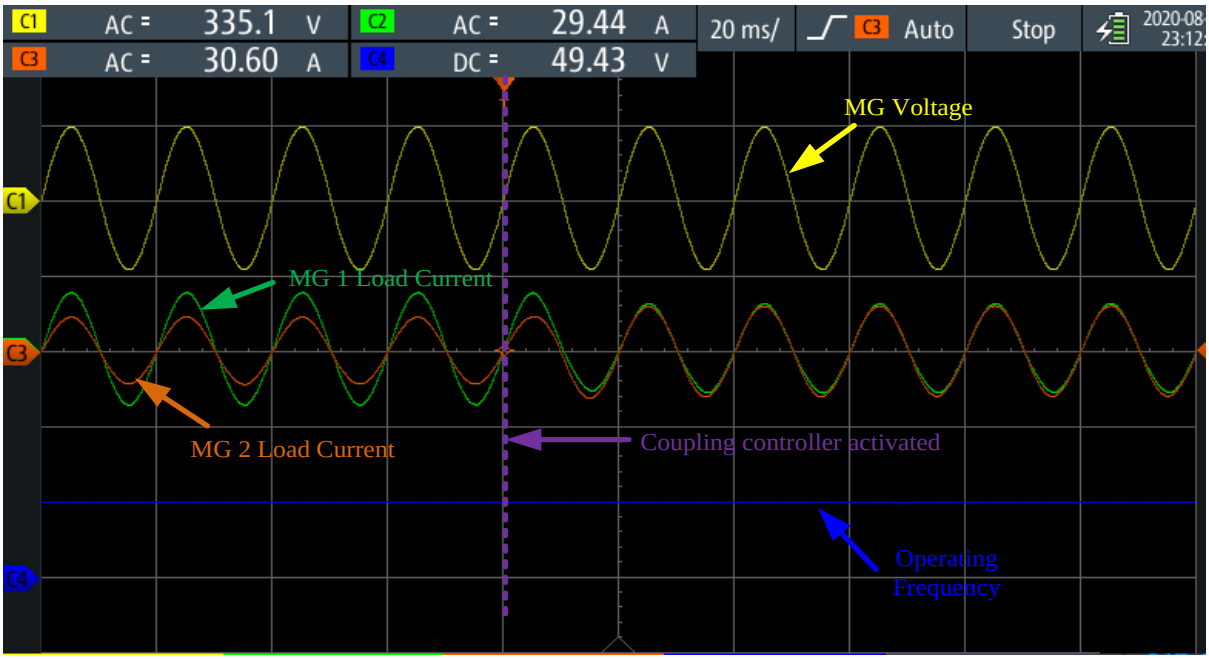


Figure 5.21 Illustration of seamless coupling of MGs

A comparative result has been captured, where MGs are coupled by using the forced breaker switching, without activating the coupling controller. The result, as shown in Figure 5.22, provides a clear idea of how the system can be unstable without a proper coupling controller. The sudden transient in load current and a voltage dip can collapse the total system.

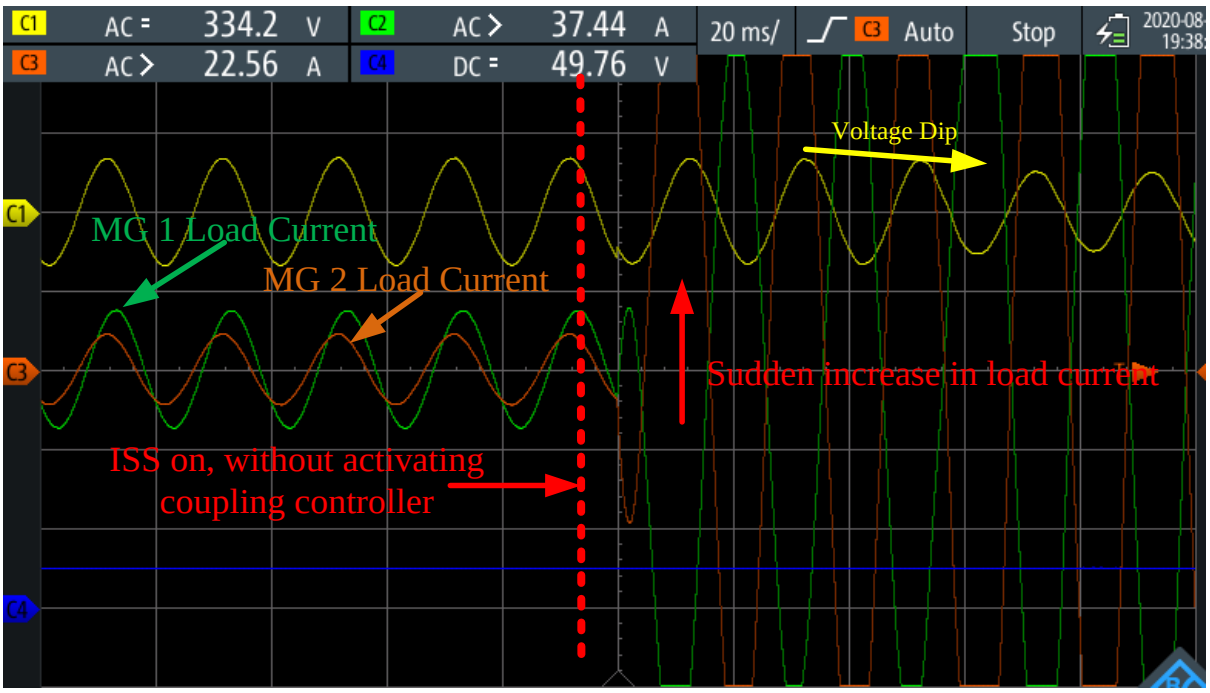


Figure 5.22 Illustration of MG coupling without activating the coupling controller

### *5.7.3 Seamless decoupling of MGs*

In this case study, a similar approach has been taken in order to verify the efficacy of the decoupling controller.

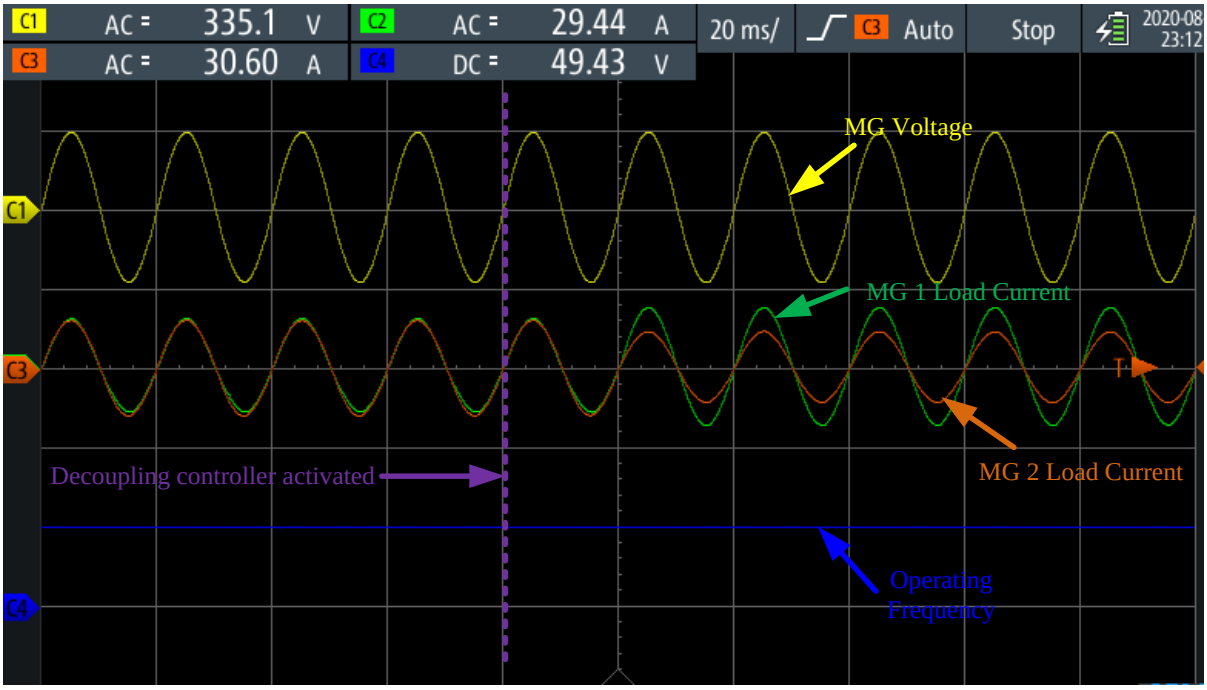


Figure 5.23 Illustration of seamless decoupling of MGs

Initially, both the MGs are in coupled condition, and the total load demand is shared equally between them. After activating the decoupling controller, MGs are separated and supplying the individual load demand. It can be observed from Figure 5.23 that the decoupling is achieved seamlessly, and the system stability is maintained without creating any sudden transient in voltage/current profile.

### *5.7.4 Reconnection after decoupling*

In this case study, a reconnection is attempted after decoupling and successfully achieved.

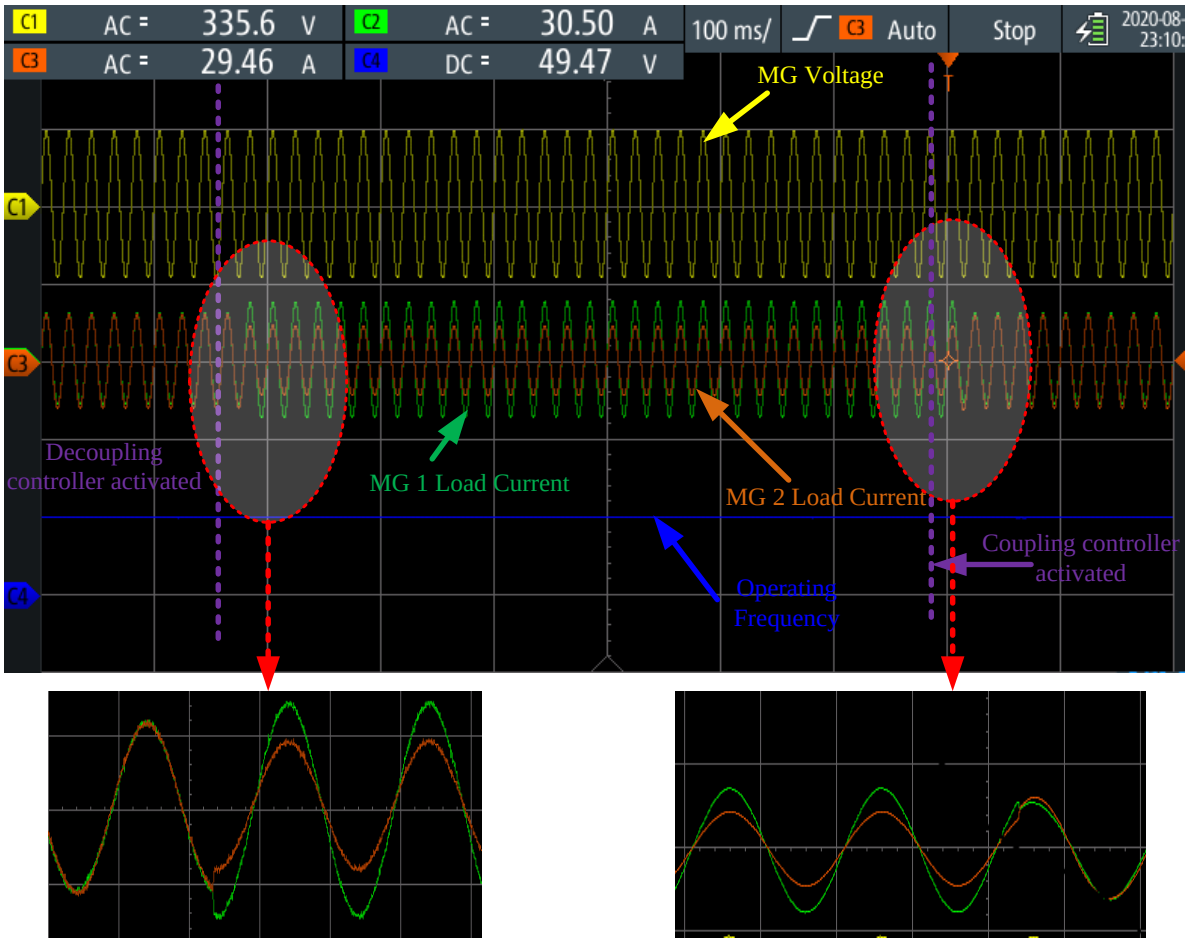


Figure 5.24 Illustration of seamless reconnection of MGs

A smooth transition between the standalone and interconnected mode is achieved without creating any stability issue in the system. The zoomed plot, as shown in Figure 5.24, proves the efficacy of the proposed controller. The capture results also show the

droop controller performance after reconnection. After re-connection loads are appropriately shared without creating any communication/computational delay.

## 5.8 Conclusion

An enhancement in droop control is proposed in this chapter to maintain the system voltage and frequency to its nominal value. An extra layer of control topology is proposed in droop control, which uses the d-axis component of the terminal voltage to maintain the system voltage and frequency. MATLAB based simulation and HIL based experimental results for a series of possible different case studies conclude the following:

- The improved droop control is able to keep the system voltage and frequency close to the nominal value. Different transient conditions like load change, coupling to other MG and decoupling are considered, and the efficiency of the proposed controller is shown in the simulation and real-time results in section 5.6 and 5.7.
- A coupling and decoupling controller is also implemented in this chapter. A seamless coupling and decoupling are achieved using the topology of proposed droop control. The proposed controller is also able to reconnect the neighbouring MG after decoupling seamlessly (case study 5.7.5). The power-sharing accuracy of the proposed droop control is not compromised during any transient situation.
- The unique hardware-in-loop experimental model has been developed, and the proposed controller has been tested successfully.

Chapter 6

# Stability Analysis of Autonomous Microgrid with Proposed Droop Control

## 6.1 Introduction

Load shedding and intelligent demand response can be implemented to avoid overloading in a rural, isolated MG. In order to minimise the load shedding, isolated rural MGs can be coupled together to support each other, if there is any available power in neighbouring MG. The concept of CMG is explored exclusively in the previous chapters. The proper utilisation of available resources in CMG to enhance the coupling advantage is achieved. To achieve the power-sharing, the steady-state voltage and frequency is differed from its nominal value and settled down within the acceptable limit for isolated MGs. Therefore, to restore the system voltage and frequency to its nominal value, a double layer droop control is proposed.

Lots of research has been conducted on the CMG, in order to support the rural, isolated power system during any grid fault, grid maintenance, or in any emergency overload condition [184]–[187]. Two or more neighbouring microgrid can be coupled together to support any contingency is proposed in [188]. The CMG can also be formed if the individual MGs are operating in Maximum Power Point Tracking (MPPT) mode as well [189]. Also, research has been conducted on a temporary connection to enhance resilience during any fault [190]. Centralised and decentralised approach [184], [191], [192], decision-making tools [185], economic concerns [193], optimal power exchange through robust optimization based control [194] also have been introduced to enhance the reliability, energy trading cost and reliability of CMG. Optimal power exchange

through a bi-directional or back to back converter [195], [196], high voltage dc line [197] is also introduced. The dynamic security and reliability aspect also has been evaluated [197]. Also, a small signal stability-based decision-making algorithm [198]–[200] is also presented for coupling the MGs. The stability analysis with different key factors is also evaluated in these research.

However, the impact of interconnecting tie-line in isolated MG is not addressed well by the research community. As in the rural, isolated MG, the X/R ratio is very low, and that can lead to a significant stability issue and voltage drop for coupling the MG. In this chapter, the stability of the proposed controller is studied using the eigenvalue analysis method. The Small Signal Model (SSM) of each converter with internal voltage and current control loop, droop control, double layer frequency restoration control and resistive rural network with different loads are analysed. This chapter will also illustrate the limitation of the coupling network with different tie-line parameters.

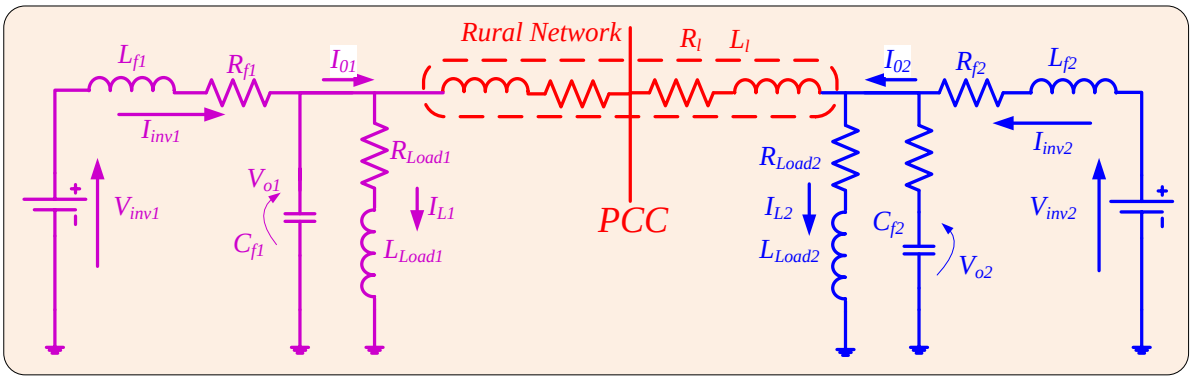


*Figure 6.1 Equivalent circuit and power flow of coupled MG*

## 6.2 Equivalent circuit diagram of coupled MG

Figure 6.1 shows the general structure of interconnected standalone MG. The equivalent circuit diagram consists of two voltage sources, LC filter, rural network and R, L loads. The complete controller structure with voltage and current control loop, droop control and double layer frequency restoration control is depicted in Figure 6.3. In the

following sections, the SSM of each individual component of the control structure is developed.

## 6.3 Inverter control structure of standalone MG

The active power control between the MGs is generally achieved by changing the phase angle between the MG inverters. This is usually accomplished by using droop control where the frequency is regulated by using droop equation (6.1)-

$$\omega_1 = \omega_0 - m_p \Delta P \tag{6.1}$$

Where $m_p$ is the droop gain, $\omega_1$ is the output frequency of the MG1, $\omega_0$ is the nominal frequency, and $\Delta P$ is the power supplied from MG1 to MG2 (or vice versa). The phase angle difference is modified according to the function of power supplies to another MG. The phase angle difference between the MGs can be defined as the following equation-

$$\Delta\delta_i = \int (\omega_i - \omega_j) dt \tag{6.2}$$

In the above equation, $\omega_i$ *and* $\omega_j$ are the final output frequency of MG1 and MG2 respectively. In the coupled system in case of any load change, the output frequency will change and will settle down in a steady-state frequency. The settled steady-state frequency are most likely to differ from the nominal value $\omega_n$. In order to restore the frequency, a restoration technique has been proposed in Chapter 5. Section 5.2 gives a comprehensive analysis of MG frequency restoration. The required amount of frequency component (let's say, $\omega_{req}$) to restore the frequency is determined by the d axis component of the output voltage. The output frequency of each inverter after restoration will be

$$\omega_{01} = \omega_1 + \omega_{req} \tag{6.3}$$

Each inverter of MGs has a voltage and current control loop implemented in *d-q* coordinates. A single-phase system can directly convert into *αβ* frame without any matrix transformation. An imaginary variable obtained by shifting the original signal (voltage/current) by 90 degrees and thus the original signal and imaginary signal represent the variable in αβ co-ordinates. Figure 6.2 shows the single-phase to d-q transformation.

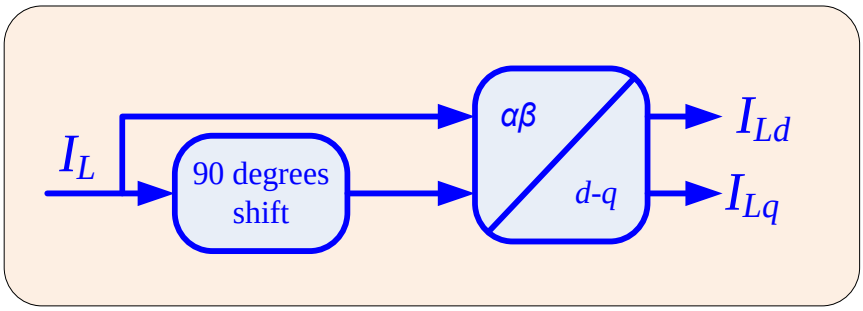


*Figure 6.2 Single-phase to d-q transformation*

The internal voltage control loop generates the d and q axis current references for the current controller. As both current and voltage control loop operates in d-q coordinates, a proportional-integral (PI) controller is implemented. It is to be noted that the current controller is usually ten times faster than the voltage controller. The electrical phase angle $\theta_{01}$ is generated by integrating the output frequency of the coupled system-

$$\theta_{01} = \int (\omega_1 + \omega_{req}) dt = \int \omega_{01} dt \qquad (6.4)$$

Figure 6.3 provides a complete architecture of the control topology implemented for each inverter in MG.

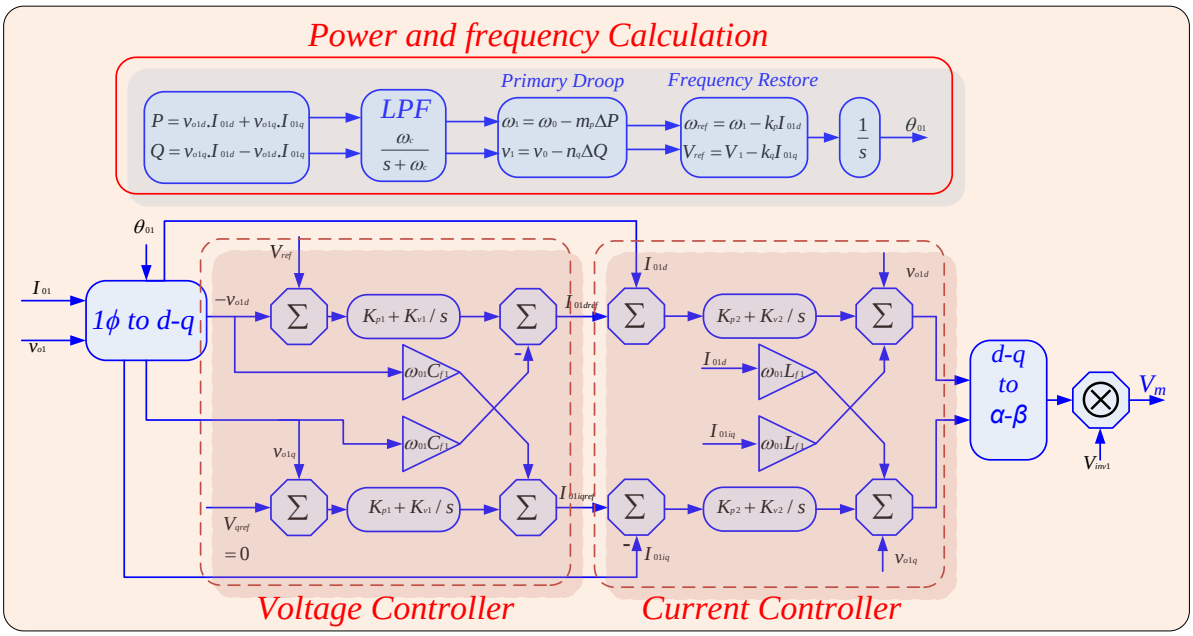


*Figure 6.3 Proposed standalone MG controller*

## 6.4 Small signal modelling of the proposed system

In this section, the state space equations of the proposed systems with all the proposed controllers are derived. The power circuit with the desired power flow is shown in Figure 6.2, whereas the proposed controller is shown in Figure 6.3. The state equations of the primary voltage and current controllers are already available in different literature [199], [201], [202]. In the following sections, a detailed analysis of all the controllers are presented.

As stated earlier the proposed controllers are designed in d-q reference frame, so-

$$I_{01} = I_{01\alpha} + jI_{01\beta} \tag{6.5}$$

$$I_{01}e^{-j\theta 01} = I_{01d} + jI_{01q} \tag{6.6}$$

$$I_{01} = (I_{01d} + jI_{01q})e^{j\theta 01} \tag{6.7}$$

The transformation of $\alpha$-$\beta$ frame to *d*-*q* frame is shown in the previous equation, where $\theta_{01}$ is obtained from 6.4 equation.

The state-space equations each inverter output current, filtered voltage and load current is shown below-

$$\Delta I_{inv1d} = \omega_{01}\Delta I_{inv1q} + \Delta\omega_{01} I_{inv1q} - \frac{R_{f1}}{L_{f1}}\Delta I_{inv1d} + \frac{\Delta v_{inv1d}}{L_{f1}} - \frac{\Delta v_{01d}}{L_{f1}} \tag{6.8}$$

$$\Delta I_{inv1q} = -\omega_{01}\Delta I_{inv1d} - \Delta\omega_{01} I_{inv1d} - \frac{R_{f1}}{L_{f1}}\Delta I_{inv1q} + \frac{\Delta v_{inv1q}}{L_{f1}} - \frac{\Delta v_{01q}}{L_{f1}} \tag{6.9}$$

$$\Delta \dot{I}_{L1d} = \omega_{01}\Delta I_{L1q} + \Delta\omega_{01} I_{L1q} - \frac{R_{Load1}}{L_{Load1}}\Delta I_{L1d} + \frac{\Delta v_{0d}}{L_{Load1}} \tag{6.10}$$

$$\Delta \dot{I}_{L1q} = -\omega_{01}\Delta I_{L1d} - \Delta\omega_{01} I_{L1d} - \frac{R_{Load1}}{L_{Load1}}\Delta I_{L1q} + \frac{\Delta v_{0q}}{L_{Load1}} \tag{6.11}$$

$$\Delta \dot{v}_{01d} = \omega_{01}\Delta v_{01q} + \Delta\omega_{01} v_{01q} + \frac{\Delta I_{inv1d}}{C_{f1}} - \frac{\Delta I_{01d}}{C_{f1}} \tag{6.12}$$

$$\Delta \dot{v}_{01q} = -\omega_{01}\Delta v_{01d} - \Delta\omega_{01} v_{01d} + \frac{\Delta I_{inv1q}}{C_{f1}} - \frac{\Delta I_{01q}}{C_{f1}} \tag{6.13}$$

The transmission line dynamics are shown in the following state space equations-

$$\Delta \dot{I}_{01d} = \omega_{01}\Delta I_{01q} + \Delta\omega_{01} I_{01q} - \frac{R_l}{L_l}\Delta I_{01d} + \left(\frac{1}{L_l} + \frac{1}{L_{Load}}\right)\Delta v_{01d} - \frac{v_{02d}}{L_l} + \left(\frac{R_l}{L_l} + \frac{R_{Load}}{L_{Load}}\right)\Delta I_{L1d} \tag{6.14}$$

$$\Delta \dot{I}_{01q} = -\omega_{01}\Delta I_{01d} - \Delta\omega_{01} I_{01d} - \frac{R_l}{L_l}\Delta I_{01q} + \left(\frac{1}{L_l} + \frac{1}{L_{Load}}\right)\Delta v_{01q} - \frac{v_{02q}}{L_l} + \left(\frac{R_l}{L_l} - \frac{R_{Load}}{L_{Load}}\right)\Delta I_{L1q} \tag{6.15}$$

The power calculation and droop equations are presented below:

$$P = v_{o1d}.I_{01d} + v_{o1q}.I_{01q} \tag{6.16}$$

$$Q = v_{o1q}.I_{01d} - v_{o1d}.I_{01q} \tag{6.17}$$

The power equations after filter can be written as the following, where $\omega_c$ is the filter cut-off frequency-

$$P_1 = \frac{\omega_c}{s+\omega_c}(v_{o1d}.I_{01d} + v_{o1q}.I_{01q}) \quad (6.18)$$

$$Q_1 = \frac{\omega_c}{s+\omega_c}(v_{o1q}.I_{01d} - v_{o1d}.I_{01q}) \quad (6.19)$$

$$\omega_1 = \omega_0 - m_p \Delta P \quad (6.20)$$

$$v_1 = v_0 - n_q \Delta Q \quad (6.21)$$

The double layered droop controller to restore the frequency

$$\omega_{ref} = \omega_1 - k_p I_{01d} \quad (6.22)$$

$$V_{ref} = V_1 - k_q I_{01q} \quad (6.23)$$

$$\omega_{01} = \omega_1 + \omega_{req} \quad (6.24)$$

$$\theta_{01} = \int (\omega_1 + \omega_{req}) dt \quad (6.25)$$

Considering all above equations, the state space matrix of a MG will be

$$X_1=[\Delta\delta_{01} \quad \Delta P_1 \quad \Delta Q_1 \quad \Delta I_{L1dq} \quad \Delta I_{inv1dq} \quad \Delta V_{01dq} \quad \Delta I_{01dq}]^T \quad (6.26)$$

Similarly, all the equations for another MG can be obtained and the state space matrix can be written as-

$$X_2=[\Delta\delta_{02} \quad \Delta P_2 \quad \Delta Q_2 \quad \Delta I_{L2dq} \quad \Delta I_{inv2dq} \quad \Delta V_{02dq} \quad \Delta I_{02dq}]^T \quad (6.27)$$

Finally, the state space matrix for coupled MG can be written as-

$$X = [X_1^T \quad X_2^T]^T \quad (6.28)$$

## 6.5 Eigenvalue analysis

The system parameters for eigenvalue analysis are provided in Table 6.1. With the provided parameters the systems are assured to operate in nominal operating condition. The eigenvalues are showing in the following plots are mainly sensitive to droop

controller parameters, load, demand, transmission line parameters and state feedback controllers. The dominant eigen values with the variation of different parameters are analysed in details in the following section.

*Table 6.1 Nominal system parameters*

| System Parameters | Values |
|---|---|
| DC Voltage ($V_{inv1}$ & $V_{inv2}$) | 400 V |
| Inverter 1 & 2 filter inductance ($L_{f1}$ & $L_{f2}$) | 6.5 *mH* |
| Inverter 1 & 2 filter capacitance ($C_{f1}$ & $C_{f2}$) | 25 µF |
| Active power droop coefficient ($m_p$) | 4.5 X $10^{-5}$ rad/W |
| Reactive power droop coefficient ($n_q$) | 2.5 X $10^{-4}$ V/Var |
| Inverter 1 & 2 filter resistance ($R_{f1}$ & $R_{f2}$) | 0.2 Ω |
| Resistance of line 1 & 2 ($R_{L1}$ & $R_{L2}$) | 3.83 Ω (R/X >2); 5.83 Ω (R/X<1) |
| Inductance of line 1 & 2 ($L_{L1}$ & $L_{L2}$) | 0.0053 H (R/X >2); 0.038 H (R/X<1) |
| Load resistance of MG1 & MG2 ($R_{Load1}$ & $R_{Load2}$) | 20 Ω |
| Load inductance of MG1 & MG2 ($L_{Load1}$ & $L_{Load2}$) | 0.5 *mH* |
| Low pass filter cutoff ($\omega_c$) | 31.4 rad/sec |

The coupled system is linearised around an operating point and all the eigenvalues are shown in the Table 6.2. The corresponding damping ratio is also calculated. All the eigenvalues can be divided into two groups- well damped eigenvalues and potentially problematic eigenvalues. The eigenvalues with damping ration less than 30% is considered as problematic eigenvalues, these are not damped quickly, and these oscillations created due to these values eventually affect the system performance. The consequences due to these oscillations can results in loss of efficiency, control system instability and mainly wear and tear on equipment. Oscillations in output voltage and

current can create harmonics and affect the power quality. The proposed controller reduces the no of problematic eigenvalues and maintain the system stability. In order to further improve the system stability a predictive/robust controller design is required.

*Table 6.2 System eigenvalues*

| Real | Img. | Damping Ratio |
|---|---|---|
| -870.913 | ±180.29 | 100 |
| -503.287 | ±1.09*10e4 | 13.71 |
| -293.616 | ±1.13*10e4 | 27.63 |
| -296.768 | ±39.46 | 89.16 |
| -101.544 | ±24.83 | 56.91 |
| -102.129 | ±6.894 | 61.73 |
| -49.725 | 0 | 98.9 |
| -880.21 | ±201.59 | 99.98 |
| -506.964 | ±1.171*10e4 | 27.67 |
| -291.569 | 1.276*10e4 | 27.4 |
| -295.619 | ±37.49 | 87.5 |
| -106.583 | ±33.73 | 58.6 |
| -104.237 | ±7.547 | 60.4 |
| -50.59 | 0 | 99.5 |

The locus of eigenvalues for the change of active power co-efficient ($m_p$) is shown in Figure 6.4. With a very high value of $m_p$ ($8.1 \times 10^{-5}$), the trajectory of eigenvalue reaches almost to the right-hand side of s-plane, which indicates low system stability. In the case of $m_p$=$8.5 \times 10^{-5}$, the eigenvalue crosses the imaginary axis and indicating an unstable operation. Similarly, Figure 6.5 shows the eigenvalues mapping with the change of reactive droop coefficient ($n_q$) value. It also has a significant contribution to system stability. With the value of $n_q = 3.0 \times 10^{-4}$, it reaches to the unstable region. It can be

concluded that with an improper selection of droop coefficients, can lead the system to an unstable region. In the case of, the power management-based droop control proposed in Chapter 4, is very important to maintain the system stability, especially in the case of asymmetric power-sharing.

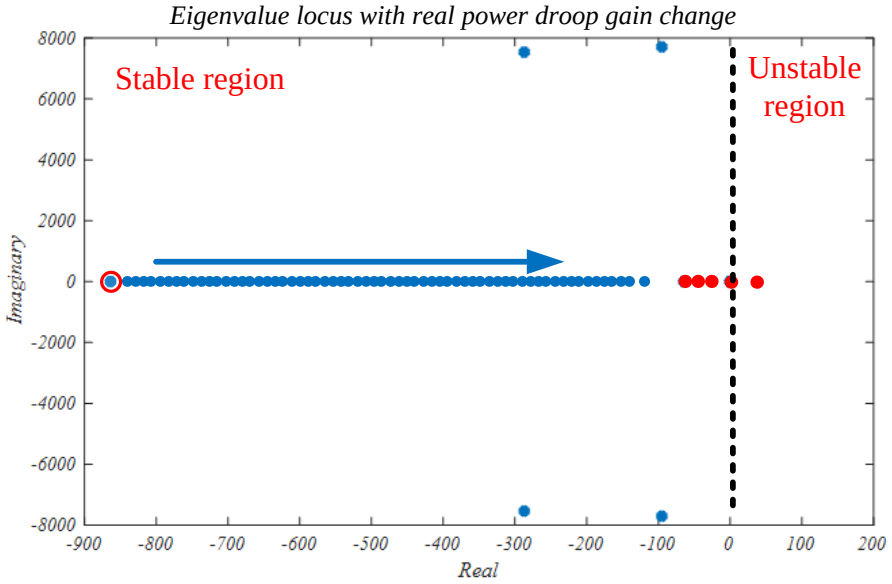


*Figure 6.4 Eigenvalue locus with real power droop gain change*

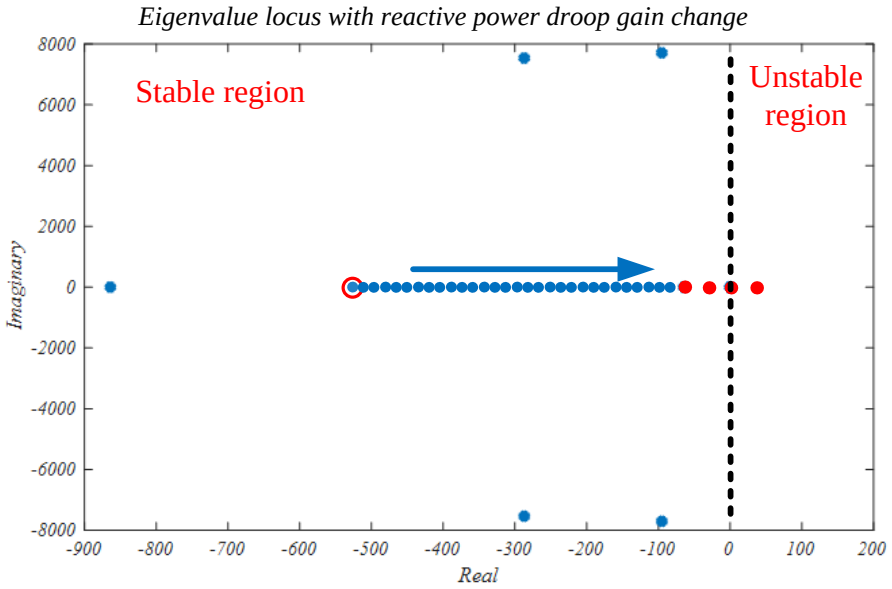


*Figure 6.5 Eigenvalue locus with reactive power droop gain change*

Figure 6.6 shows the eigenvalue trajectory with the change of load variation. It is obvious that, if the load demand increases and exceeds the total power rating of the MG, then the system will lead to instability. In this case, the load demand increases and when

it crosses beyond 10 kW, the system becomes unstable. The rural network also plays a very important role in system stability. The strong real and reactive power coupling due to the highly resistive line can create instability in state feedback controllers (voltage and current controller). It can be seen from Figure 6.7 that, with a value of R/X 3.25, the eigenvalue trajectory is leading to the imaginary axis.

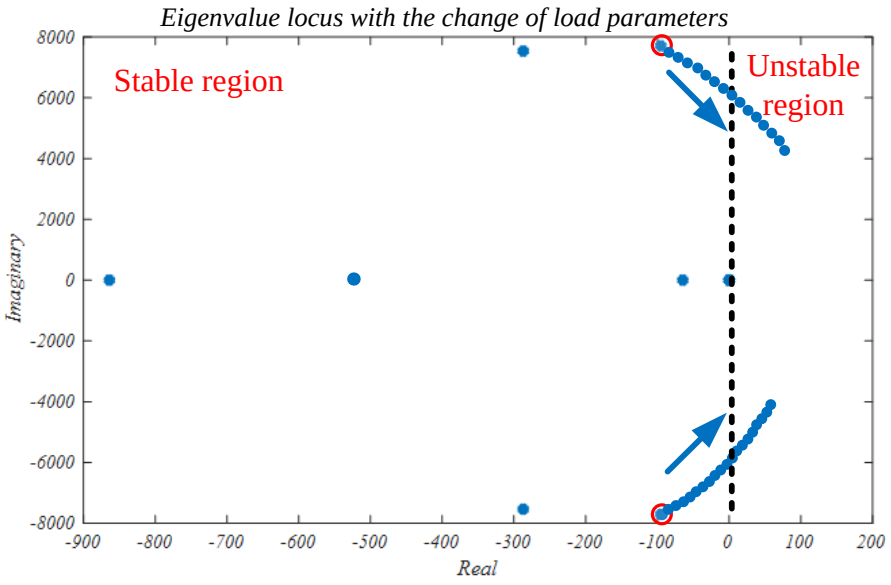


*Figure 6.6 Eigenvalue locus with load variation*

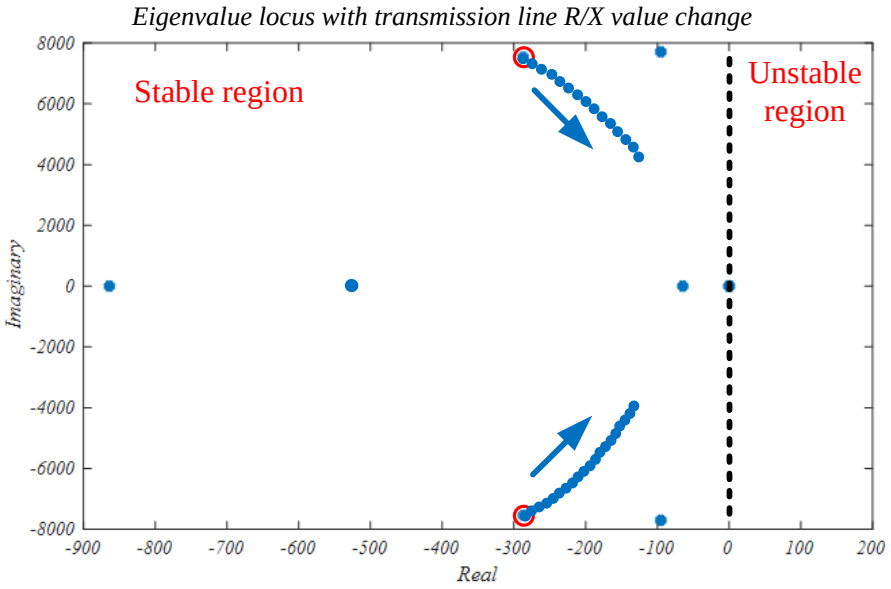


*Figure 6.7 Eigenvalue locus with the variation of transmission line parameter*

## 6.6 Simulation results

The effect of resistive line parameters and the variation of line length is shown in this section. The variation of line length can create the voltage drop in these standalone systems. So, it is very important to define the area of neighbouring MGs for available resources sharing. As the rural standalone network is mainly resistive, so it is very much vulnerable to voltage drop. The effect of line impedance on power-sharing, with proposed and conventional droop control, is also analysed. The simulation has been carried out in Matlab, and the system parameters are provided in Table 6.1.

### *6.6.1 Case Study 1: The effect of line length*

The effect of resistive line length and the associated voltage drop for coupling the neighbouring MGs is analysed in this section. The literature survey suggests that a maximum 5 % of voltage drop is allowed in standalone MG. The droop gains should be chosen in such a way that the voltage drop should be within the allowable range. In this case study, a rural network is considered with an R/X ratio of 2.5.

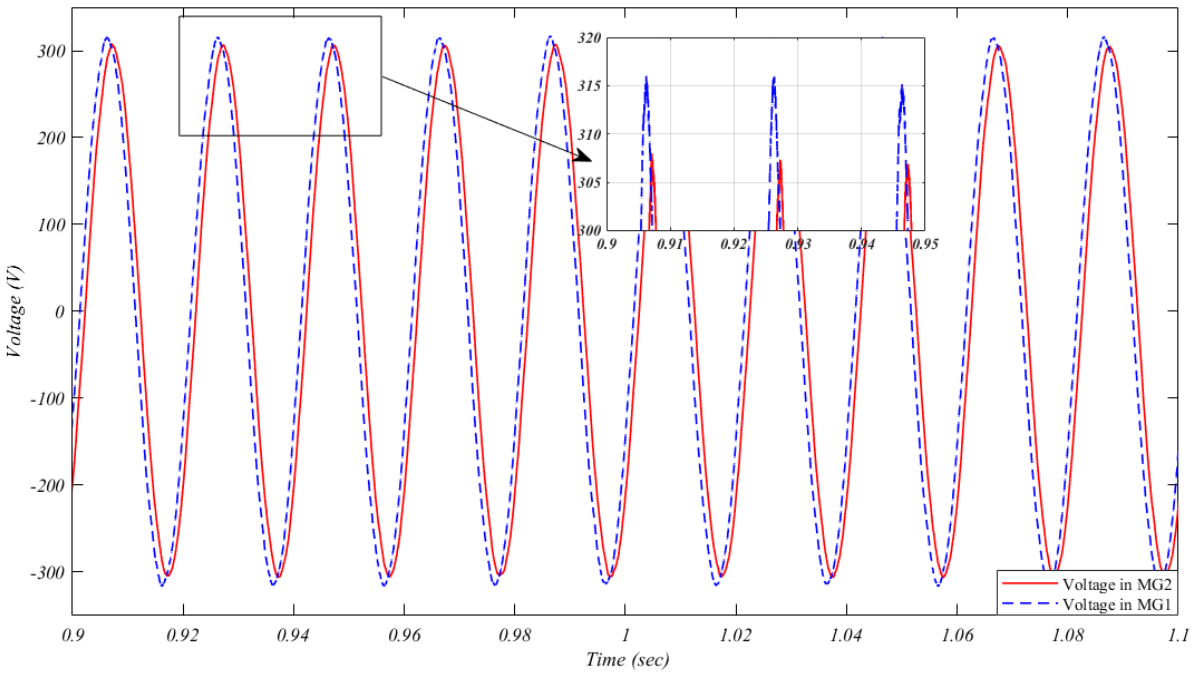


*Figure 6.8 Voltage drop analysis in a 50 KM rural network with an R/X ratio of 1.5*

Figure 6.8 shows an almost 10V voltage drop in a 50 km network, which is within the allowable range. With the increase of line length to 80 km the voltage-drop increases to 15V as illustrated in Figure 6.9. So, it is recommended with a value of 2.5, R/X ratio of a rural network; the power can be shared with the neighbouring MGs, which is within 75 km radius.

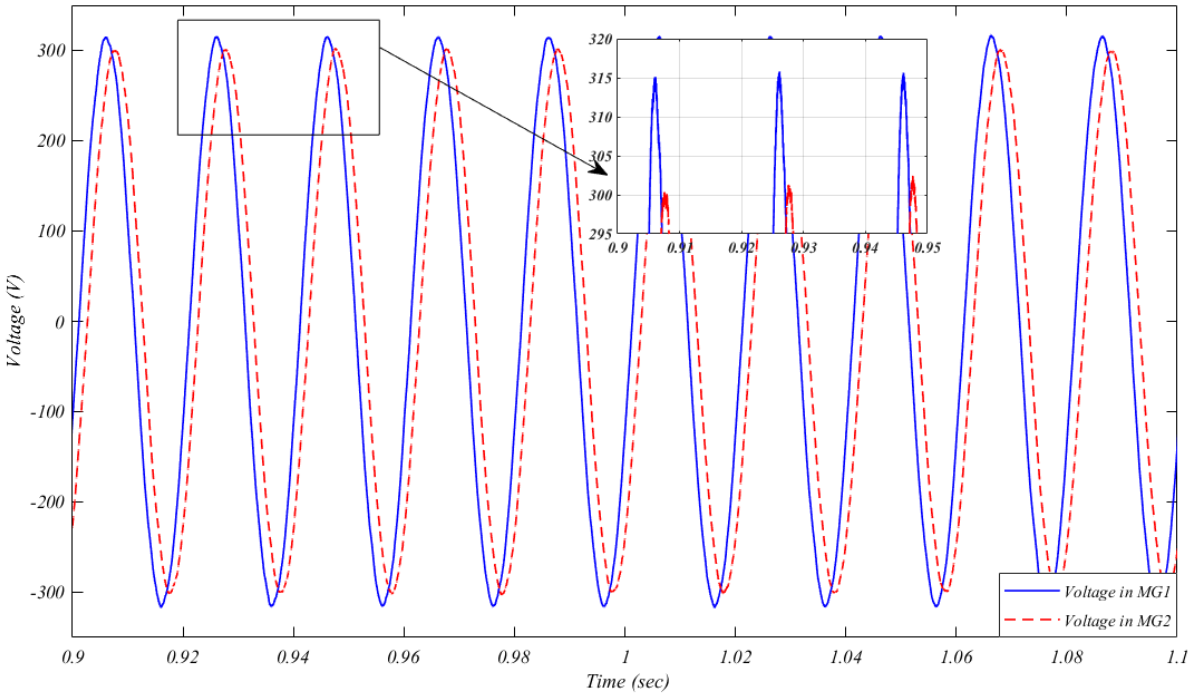


*Figure 6.9 Voltage drop analysis in an 80 KM rural network with an R/X ratio of 1.5*

### *6.6.2 Case Study 2: The effect of line impedance on power-sharing*

The line impedance (R/X ratio) plays a crucial role in power-sharing. In the case of a resistive rural network where R/X ratio is very high with a value of 3.5, the active power drooping gain should be chosen very high to achieve an accurate power-sharing. In the previous section (section 6.5), it has been shown a very high value to drooping gain can lead the system to an unstable region. So, a proper choice of drooping gain is essential for a stable mode of operation. The power management based asymmetric power-sharing proposed in Chapter 4, reduce the stress on a particular MG inverter and allows the inverter to share the power according to its availability and power rating. Figure 6.10

shows a comparison of power-sharing accuracy of proposed droop control with different R/X ratio. It can be shown that with the increase of line inductance, the power-sharing accuracy will also increase. A proper choice of drooping gain with different impedance can provide a better solution. Otherwise, a virtual impedance-based solution can be adopted to achieve better power-sharing. The virtual impedance-based solution is illustrated in different pieces of literature [171]–[173], and beyond the interest of this research.

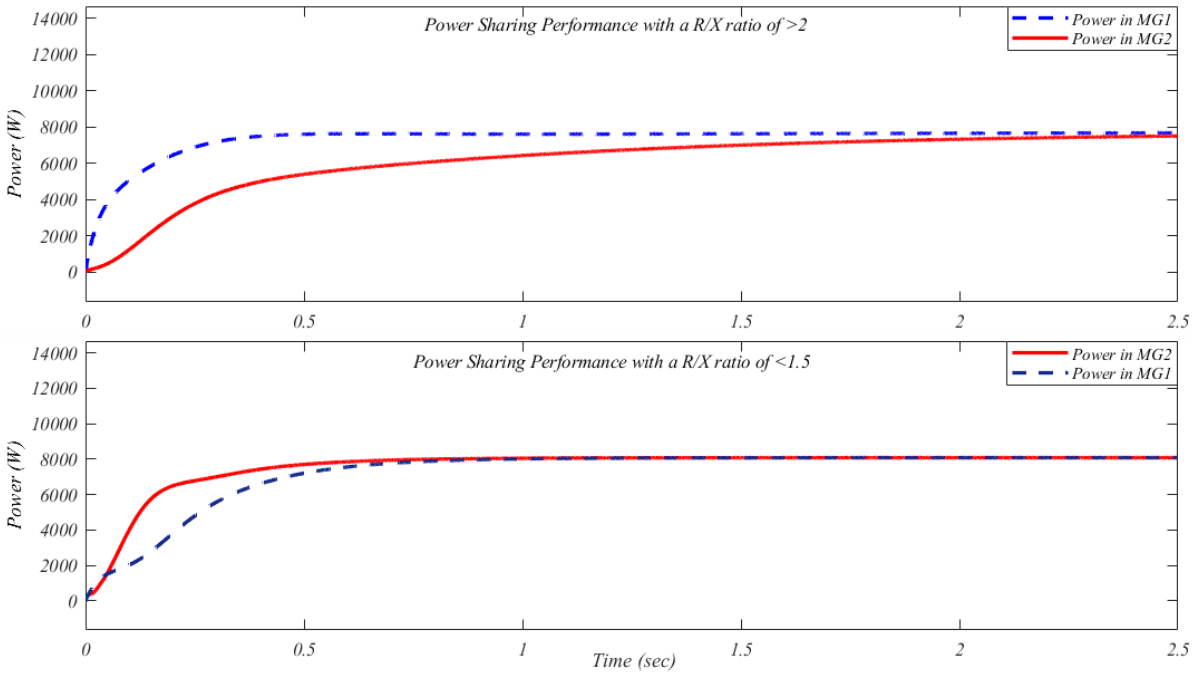


*Figure 6.10 Power sharing performance of MGs with different line impedance*

## 6.7 Conclusion

A linearized state-space model of inverter-based standalone MGs is presented in this Chapter. Further, an eigenvalue-based stability analysis has been carried out around a nominal operating point. A simulation-based analysis has also been carried out to check the power-sharing performance under different line impedance. The key finding of this chapter is summarised below-

- The eigenvalue analysis suggests that real and reactive power droop coefficients, line impedance, load demand play a significant role in system stability. A proper choice of droop coefficient is required to maintain the system stability in rural resistive network. This can be achieved by using the proposed power management-based droop control.
- The simulation-based study suggests that in the rural network (with an R/X ratio of 2.5) if the neighbouring MGs are within 75 KM radius, they can be coupled together for available power-sharing.
- It also can be concluded from the simulation study that power-sharing performance reduce with a high R/X ratio of the network. Further, a virtual impedance-based droop control can be proposed to achieve the accuracy of power-sharing performance.

Chapter 7

# Conclusions and Future Work

## 7.1 General conclusions

The inter-microgrid operation of power-sharing among the neighbouring MGs, a seamless operation between the standalone mode and interconnected mode and the stability analysis in both mode of operation has been analysed in this research work. It is essential to ensure the stability of each unit while sharing power. Additionally, it is also crucial to connected/disconnect the neighbouring MGs seamlessly for maintaining system stability under different load and generation condition. In this research work, advanced control topologies are presented in order to achieve the research objectives. The general conclusions of this research work are summarised below-

1. Coupling of neighbouring isolated MGs is a great solution (in terms of economically as well) to meet the increasing power demand. Different coupling issues between the neighbouring isolated MGs are analysed in this thesis.
2. An intensive literature survey has been presented for the renewable energy-based standalone MGs. Different power-sharing topologies have been reviewed, and pieces of literature suggest that droop control is the most commonly used wireless technique for power-sharing purpose. However, a lot of improvement is still required in case of asymmetric power-sharing and with a very high resistive rural network. Frequency control in a rural static microgrid is also an important issue to be addressed. The research objectives are discussed in detail in section 1.2.

3. A laboratory-scale MG is developed in order to prove the efficacy of the proposed controllers. LabView based sbRIO-9683 and TI based F28335 has been used to design the proposed controllers. Further, OPAL-RT and PLEXIM real-time simulators are also used to testing the controllers in HIL mode.
4. A power management based droop control in proposed to achieve the power sharing between the neighbouring MGs. The proposed controllers help the neighbouring MGs to couple most efficiently. An asymmetric power-sharing is achieved using this proposed controller, which does not restrict the inverters for equal sharing. It reduces the stress on the inverters of the MGs and provides better stability on the system. The frequency of the coupled system is also controlled within an acceptable range during standalone mode and coupled mode. The simulation and experimental work have been presented to verify the efficacy of the proposed controller.
5. Due to the absence of large power grid and intermittency of load demand and renewable generation, the frequency of the system deviates a lot from its nominal value. In the case of standalone static MG, it is vital to maintain the system frequency to its nominal value. A frequency restoration technique is presented in this research. The double-layered droop control uses the d-axis component of the terminal voltage to restore the system frequency.
6. The seamless transition between the standalone mode and coupled-mode should be achieved for the higher system stability and safety. When the total load demand of the coupled MG exceeds the total capacity, the MGs should be decoupled. In order to do that, a coupled and decoupled controller is proposed. Based on the double-layered droop control, when the frequency of

both the MGs is restored to the nominal value, they can be coupled/decoupled seamlessly. The proposed technique has been tested in F28335 microcontroller with an incorporation of OPAL-RT and PLEXIM real-time simulator.

7. A mathematical model of standalone MG is presented to analyse the stability of the proposed system and controllers. The state-space model of the coupled MG is also presented. An eigenvalue analysis suggests that the system stability is sensitive to parameters like- active and reactive power droop coefficients, rural network line parameters, state feedback controllers, load etc. The sensitivity analysis is presented to show the eigenvalue trajectory on state variable variations.
8. A stiff coupling between the active and reactive power components, in the presence of the resistive rural network, can lead the system to an unstable region, and it also deteriorates the power-sharing performance. A proper selection of drooping gain can solve this problem. The power management based asymmetric power-sharing solves the power-sharing issue and keep the frequency within an acceptable limit as well.
9. A comprehensive simulation-based study suggest that the neighbouring MGs can be coupled together (through a rural network with an R/X ratio of 1.5) for available power-sharing if they are within a radius of 75 KM. Otherwise, the voltage drop will exceed the allowable 5% limit.

## 7.2 Future work

With the increasing penetration of renewable energy sources, the implementation of standalone MGs are also increasing. The research community is more focused to provide

more advanced technology to ensure the robustness of the system. The research outcomes of this thesis also provide some more research questions. Further development of this research area is proposed as follows:

1. There is a possibility that in rural community microgrids sometimes grid power is also available. During any severe grid fault or during any unintentional/intention islanding the microgrid should detect the islanding robustly. A robust islanding detection technique can be very useful. Some specific research has also been carried out in this regard, which is included in Appendix 1. This has been published in IEEE Transaction on Industrial Electronics.
2. The research can be extended to multi microgrid model, where different type of renewable energy sources can be integrated together. A supervisory control development might be required to solve the power management issues.
3. A communication system would be ideal to receive the generation and load demand information from the neighbouring MG. The effect of communication delay could be investigated in depth, and the effect on droop control may be analysed.
4. The cyber-attack on the communication network and incorrect data insertion (false data can be transmitted due to the failure of any sensor as well) can reduce the system reliability. It could be an interesting and useful topic of research s to overcome the false data insertion in the network.
5. A robust virtual impedance-based droop control can be proposed in case of a highly resistive rural network. Different loads like constant power/constant current, constant impedance loads could be addressed as well.

6. The interaction between AD and DC rural MGs during both modes (standalone and coupled) can be considered. The AC and DC power flow between the MGs during coupled-mode exposes new challenges of modelling and practical work.

# Appendix A: Use of Signal Processing Methods for Efficient Islanding Detection in Static DG and a Parallel Comparison with DWT Method

## A.1 Introduction

In rural community MG where large grid power is available to support the local load, the intentional / non-intentional islanding detection topology has to be developed for a smooth operation. With addition to the previously discussed available power sharing topologies this research work also investigated for developing a robust islanding detection technique for a static generation-based MG. Islanding or non-islanding events in grid-connected distributed generation brings along a typical distinguishable transient signature in its frequency profile. Any kind of disturbances manifest transients in the system and the nature of these transients depend upon the type of disturbances. Frequency pattern at PCC is different for islanding and non-islanding events. The frequency waveform at PCC is shown in Figure A.1. For islanding events, the disturbance transients in the frequency waveform is growing or decaying for positive and negative power mismatch respectively [203], [204] whereas for non-islanding events, the disturbance transient is damped sinusoid. For non-islanding events, there is a participation from the grid towards damping these oscillations by sharing of active and/or reactive power appropriately. This demarcation leads to the development of a new islanding protection approach, which is based on the estimation of frequency waveform parameter (transient's frequency) by Matrix Pencil (MP) method.

As power mismatch increases, steepness of the frequency deviation curve also increases and this results in less number of cycles/ revolution within the particular time.

Thus, the disturbance 'transient's frequency' for islanding event increases as power mismatch decreases and it reaches up to its maximum value ($Th_2$) when power mismatch is zero and it will depend on the system configuration. This disturbance 'transient's frequency' for non-islanding event (load switching, capacitor bank switching, distribution line faults, etc.) is much higher than $Th_2$. The threshold value ($Th_2$) of disturbance transient's frequency is determined by performing a series of simulations with different possible case study scenario. Thus, it has been determined that islanding event occurs, when the disturbance 'transient's frequency' lies between zero to $Th_2$.

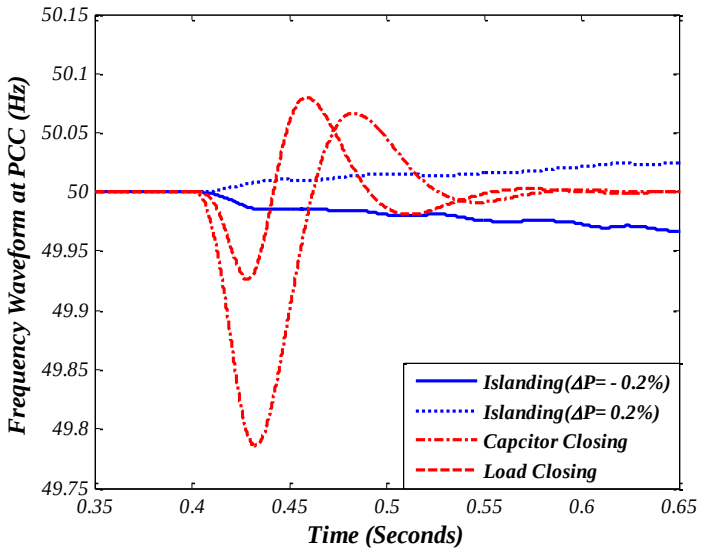


*Figure A.0.1 Behaviour of frequency at PCC*

# A.2 Proposed matrix pencil (MP) method and its application

Matrix pencil (MP) method is a class of mathematical approach to estimate signal parameters of a signal consisting of multiple damped sinusoids. In the context of identification of islanding events, the estimation of real-time frequency components is of interest and a formulation of MP approach is presented in the following.

In general, the waveform to be analysed from an islanding event can be expressed as

$$y(n) = \sum_{k=1}^{M} a_k e^{(-d_k + j2\pi f_k)n} + \eta(n) \qquad n = 0, 1, ...., N\text{-}1 \qquad \text{(A.1)}$$

Where $a_k, f_k, d_k$ ,are the complex amplitude, transient frequency and damping factor of the $k_{th}$ sinusoidal component, $M$ represents the number of the sinusoids present in the signal, $\eta$ accounts for the noise in the signal (assumed to be white) and $N$ is the total number of samples.

The estimation of the amplitude $|\alpha_k|$ is possible, using a least square formulation if the other parameters of the signal are known. However, the estimation of transient frequencies $f_k$ related to the estimation of the poles $-d_k + j2\pi f_k$ of the signal, can be obtained by different approaches and is a non-trivial matter. MP method is followed to estimate $f_k$ as outlined briefly by the following derivation.

MP method uses certain properties of the underlying signal. Let us define

$$\boldsymbol{y}_i = [y_i \quad y_{i+1} \quad \cdot\cdot \quad \cdot\cdot \quad y_{N-L+i-1}]^T \tag{A.2}$$

Data matrix of order $(N-L)(L+1)$ is directly obtained from the data sequence $y(n)$ as

$$\boldsymbol{Y}_{(N-L)\mathrm{x}(L+1)} = [\boldsymbol{y}_L \quad \boldsymbol{y}_{L-1} \quad \cdot\cdot \quad \cdot\cdot \quad \boldsymbol{y}_1 \; y0\,] \tag{A.3}$$

where, $L$ is called the pencil parameter. Some results from [203], [205] are used for transient frequency estimation in this chapter. To use some results from Theorem 2.1 in [203] two new matrices are formed. These two matrices $\boldsymbol{Y}_1$ and $\boldsymbol{Y}_2$ are derived from $\boldsymbol{Y}$ by deleting its last and first row respectively.

$$\boldsymbol{Y}_{1(N-L)\mathrm{x}L} = [\boldsymbol{y}_{L-1} \quad \boldsymbol{y}_{L-2} \quad \cdot\cdot \quad \cdot\cdot \quad \boldsymbol{y}_0] \tag{A.4}$$

$$\boldsymbol{Y}_{2(N-L)\mathrm{x}L} = [\boldsymbol{y}_L \quad \boldsymbol{y}_{L-1} \quad \cdot\cdot \quad \cdot\cdot \quad \boldsymbol{y}_1] \tag{A.5}$$

According to Cramer-Rao bound, $L$ is chosen between *N/3* and *2N/3* for the optimum estimator and efficient data filtering [205]–[208].

In this section, prior to applying the MP approach, singular value decomposition (*SVD*) is proposed to be performed on the matrix $Y$ for de-noising.

$$Y = U \sum V^H \text{ and } U^H Y V = \sum \tag{A.6}$$

Here, $(.)^H$ is hermitian operator, $U = YY^H$ and $V = Y^H Y$ are the unitary matrices, and main diagonal elements of $\sum$ represents the individual singular value $\sigma_i$ of the matrix *Y*. These eigenvalues are arranged in descending order $\sigma_1 \geq \sigma_2 \geq \cdots \geq \sigma_i \geq \cdots \geq \sigma_{min\{(L,\, N-L+1)\}}$. If the data is free from noise, $M = \max(i)$ for which $M = \max(i)$.

If noise is also present in the signal, the singular values smaller than a certain value ($\alpha$) are considered as noise and are filtered out by choosing a signal component number (*M*) such that $M = \max(i)$ for which $\frac{\sigma_i}{\sigma_{\max}} > \alpha$.

The value of $\alpha$ is chosen depending on the application. In the application in this research, since high frequency noises are to be eliminated, a low value (e.g. $10^{-3}$) is to be chosen.

After getting the value of *M*, *M*-dominant singular value vector of matrix *V* is selected to form new signal matrices *V*, and the rest *M+1* to *L* are discarded.

$\sum_s$ is obtained from the *M* columns of $\sum$ corresponding to the *M*-dominant singular values, $\boldsymbol{W_1}$ and $\boldsymbol{W_2}$ are derived from these two matrices as follows. Here, matrices $V_{1s}$ and $V_{2s}$ are formed from $V_s$ by deleting its last and first rows, respectively.

$$W_1 = U \sum_s V_{1s} \tag{A.7}$$

$$W_2 = U \sum_s V_{2s} \tag{A.8}$$

Eigenvalues $\lambda_k$ are the signal poles and can be found by using the concept of Moore-Penrose or pseudo-inverse as follows

$$\left(W_1^H W_1\right)^{-1} W_2 = \lambda I_{M \times M} \tag{A.9}$$

Frequency $f_k$ and damping coefficients $d_k$ of the signal components are estimated by using (10) and (11) respectively

$$f_k = \frac{\angle \lambda_k}{2\pi} \tag{A.10}$$

$$d_k = Re(log(\lambda_k)) \tag{A.11}$$

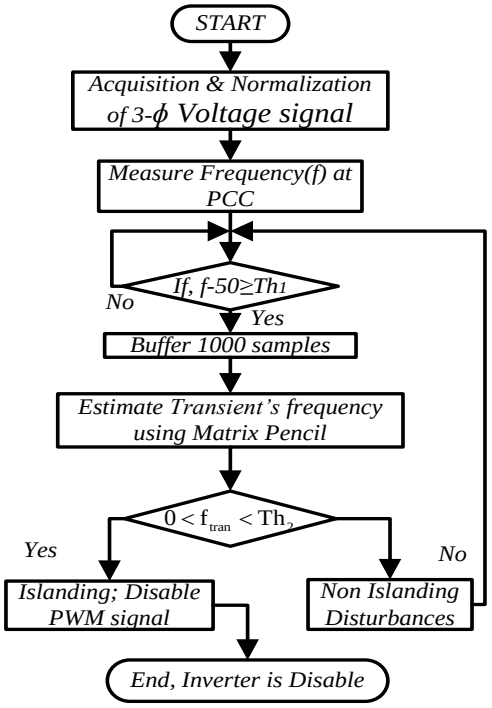


*Figure A.0.2 Flow chart of proposed islanding detection with MP method*

A flowchart of the proposed algorithm is shown in Figure A.2. In this case, the frequency of the PCC voltage signal is measured using phase locked loop (*PLL*) and sampled with a sampling rate of 10 kHz. Then the difference between measured and nominal frequency (50 Hz) is compared with a threshold ($Th_1$) to discriminate whether the system is in normal operating condition or not. If the difference between measured and nominal frequency crosses the threshold limit ($Th_1$), it means the system is subjected to noticeable disturbance, and subsequently it initiates data buffering. When buffered data samples are equal to 1000 samples, it goes to the transient frequency estimation block. In transient frequency estimation block, Matrix pencil function is embedded into

MATLAB Simulink to estimate the transient frequency. Estimated transient frequency is compared with threshold ($Th_2$) in order to discriminate the islanding and non-islanding events. When estimated transient frequency lies between zero and $Th_2$ (indicative of islanding event), the islanding detection block disables the PWM signals to stop further DG generation. If transient frequency lies outside the upper and $Th_2$ (indicating non-islanding event), PWM signal remains enabled and DG generation continues until further detection of disturbances. The algorithm continues to check the frequency difference to distinguish between islanding and non-islanding events.

## A.3 DWT-based islanding detection method

DWT has the ability to analyse signals in both time and frequency domains simultaneously. DWT decomposes the signal into different frequency bands. This helps in reducing the computational burden, extracting the features and eliminating the noise. The energy of the DWT coefficients depends upon the number of frequency components and their strength that lies within the frequency band of DWT coefficients. DWT based islanding detection employs the concept of change in frequency components from grid connected to islanded mode. According to that change, it sets up thresholds to detect islanding events. This feature makes it powerful in the detection of islanding events, but it can also mal-operate when frequency change for other disturbance is analogous to islanding events.

Authors in [209]–[213] presented a DWT based passive island detection technique. In this research, PCC voltage signal is acquired with sampling frequency 5 kHz. Daubechies 4 (*DB4*) is used as mother wavelet to evaluate DWT coefficients of PCC voltage signal. PCC voltage signal is decomposed up to four level $d_1$ (1250-2500 Hz), $d_2$ (625-1250 Hz), $d_3$ (312.5-625 Hz) and $d_4$ (156.25-312.5 Hz) using the multi-resolution

analysis.

The characteristic of different DWT coefficient for normal and islanding condition are analysed when the grid is free from harmonics. It is found that difference in energy of $d_2$ level coefficient for grid connected, and islanded mode is maximum as compared to other levels. Thus, the $d_2$ level is selected for islanding and non-islanding discrimination. Discrimination based on a change in magnitude of wavelet coefficient may lead to nuisance tripping to other transients (load change, capacitor switching, etc.). Thus, to avoid such situation root mean absolute of second level wavelet coefficient (*RMAC*) [209] is used to develop DWT based islanding algorithm, and its flow chart is shown in Figure A.3.

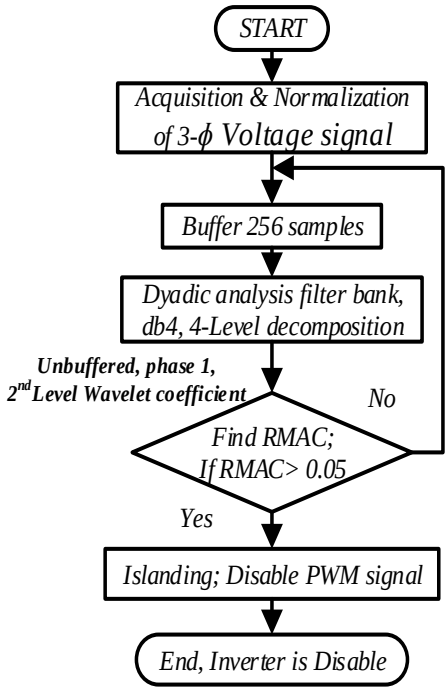


*Figure A.0.3 Flow chart of DWT based islanding detection method*

## A.4 System under investigation

To test the effectiveness of the proposed algorithm, the system shown in Figure A.4 (a) and the control topology adopted to generate the PWM signal is shown in Figure A.4 (b). The proposed system is simulated in a MATLAB/Simulink platform. Further, the

same system has been realised in OPAL-RT platform to demonstrate the effectiveness of the proposed algorithm in real time environment. The system consists of an inverter-based DG, a three-phase RLC load, transformer and the grid. The DG unit contains a three-phase PWM inverter, DC voltage source of 400V and LCL filter. The islanding is created with the opening of the grid circuit breaker (CB1).

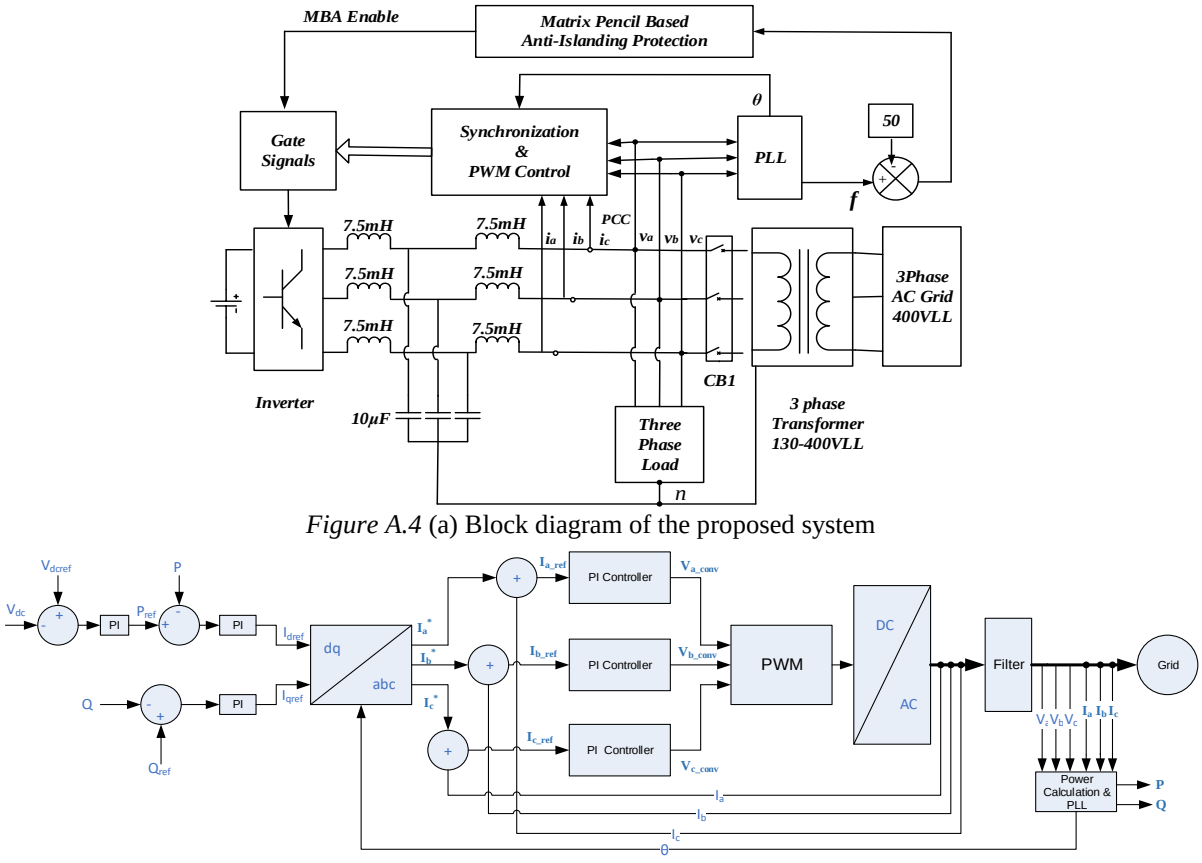


*Figure A.4* (a) Block diagram of the proposed system

*Figure A.4* (b). PWM generation for Inverter

*Figure A.0.4 System configuration and control strategy of inverter*

In this system, the voltage signal is sensed at the PCC. RMS and peak value of the voltage signal is continuously calculated to normalise it to 1V peak–peak such that any distortion can be reflected in this normalised signal. PLL is used to measure frequency and phase of normalised voltage. Synchronisation and PWM control estimates required peak inverter voltage ($V_{inv\ peak}$) and lead angle ($\delta$) using standard power flow theory and generate a sinusoidal reference signal for PWM pulse generation to control the inverter output. As presented in Table A.1 gives the full system parameters for this study.

*Table A.1 Parameters of the studied system*

| **Grid Parameters** | |
|---|---|
| Line–line voltage | 400 V |
| Nominal frequency | 50 Hz |
| **Load parameters** | |
| Linear Resistive Load | Rated Power =1.4 kW |
| Load with Qf=1 | Rated Active Power =1.4 kW,<br>Rated Reactive Power=2.8 kVar |
| Load with Qf=3 | Rated Active Power =1.4 kW,<br>Rated Reactive Power=4.2 kVar |
| Load with Qf=5 | Rated Active Power =1.4 kW,<br>Rated Reactive Power=7 kVar |
| Non-Linear Load (Rectifier Fed Resistive load) | Rated Power =0.685 kW<br>Resistance =22 Ω |
| **DG parameters** | |
| Rated Power | 1.4 kW |
| AC Terminal Voltage | 230V per phase |
| DC Voltage | 400V |
| Filter parameter | L= 15mH/ phase<br>C=10µF/phase |

# A.5 Simulated results with discussion

In this section, DWT and proposed MP method performance are tested based on simulation results under various scenarios. Table A.2 in the appendix gives a summary of the power mismatch considered and the estimated transient's frequency. Individual cases are elaborated below.

*Table A.2 Power mismatch and estimated parameters*

| **Case** | **ΔP** | **ΔQ** | **Voltage (pu)** | **Frequency (Hz)** | **Estimated Transient** |
|---|---|---|---|---|---|
| **Close Power Mismatch** | 0.20% | 0% | 0.996 | 49.98 | 4 |
| **Large Power Mismatch** | 10.70% | 0% | 0.903 | 49.62 | 3.75 |

## *A.5.1 Islanding event of large power mismatch*

In this condition, local load demand is 1.55 kW, inverter-based DG supplies 1.4 kW and the grid supplies rest of the power demand. When the grid is disconnected, there is 150 W negative power mismatch between the load demand and DG which is more than

10% of the DG power. To check the efficacy of islanding detection methods under this condition, grid circuit breaker is opened at the instant 0.4 second. This leads to the formation of islanding situation with large power mismatch. Results of proposed MP method and DWT in the context of comparative performance are shown in Figure A.5(a) and A.5(b) respectively.

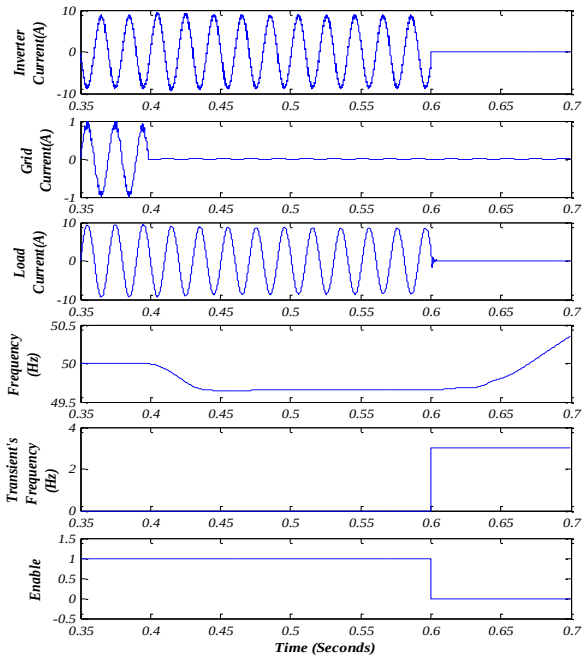


*Figure A.5(a)*

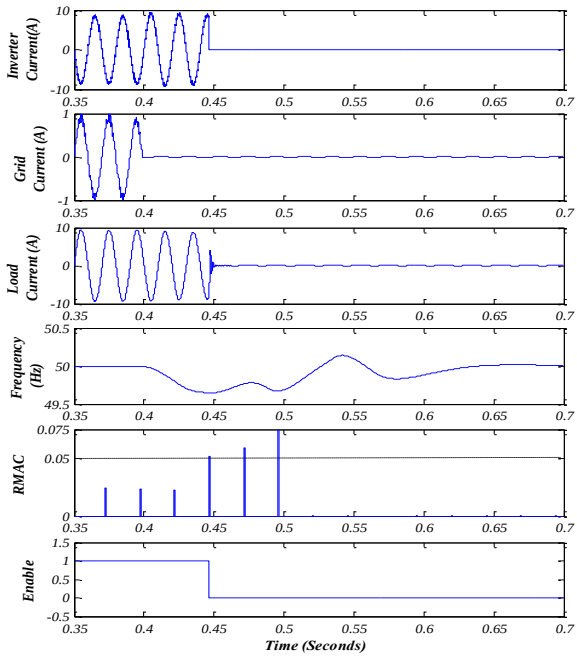


*Figure A.*5(b)

*Figure A.0.5 Simulation result of large negative power mismatch with (a) proposed MP method (b) DWT method*

From Figure A.5 (a), it is clear that the frequency of the PCC voltage signal starts decreasing monotonically, and transient frequency estimated by the proposed MP method lies between the 0 to 5 Hz. Thus, the proposed MP method sends disable signal to cut-off the supply from DG.

RMAC value determined by the DWT based method also crosses the threshold level and sends disable signal to stop the supply from DG.

From the results and discussion, it is clear that both techniques are capable to detect islanding event in case of large power mismatch. It is noteworthy to mention that in the proposed MP method, the detection time is equal to 0.2 second, which is large as

compared to DWT based method detection time of 0.05 second as shown in Figure A.5 (a) and A.5(b) of MATLAB simulation result, though both of them comply to the limit of IEEE Std. 1547 requirement of detection within 2 seconds.

### *A.5.2 Islanding event of close to zero power mismatch*

In this case study inverter-based DG source generates 1.4 kW, which is almost same as the load demand of 1.402kW. Thus, in this condition, the power mismatch is nearly zero. To check the efficacy of islanding detection methods under this condition, grid circuit breaker is opened at the instant 0.4 second. The simulation results of proposed MP method and DWT are shown in Figure A.6(a) and A.6(b) respectively.

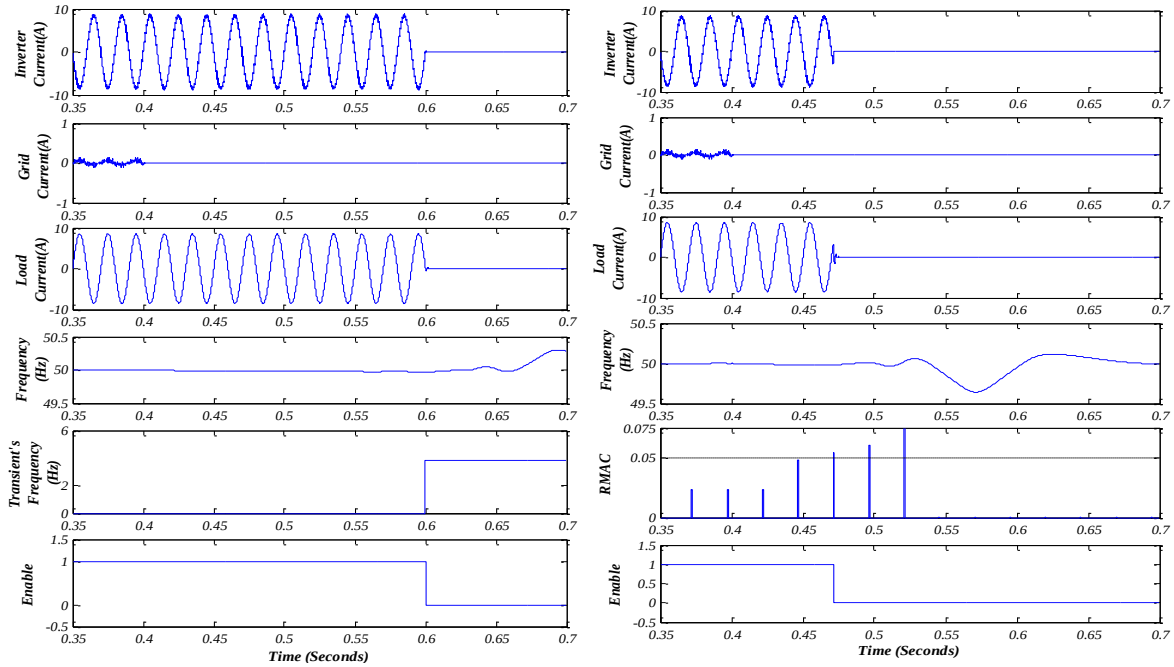


*Figure A.*6(a) *Figure A.*6(b)

*Figure A.0.6 Simulation result of close to zero power mismatch with (a) proposed MP method and (b) DWT method*

It is reflected from the results, that both techniques are capable of detecting islanding events. Detection time of the proposed MP and DWT based methods are 0.2 second and 0.07 second. It is noteworthy to mention that detection time of DWT based islanding detection method increase with the decrease in power mismatch whereas the detection time of proposed MP method is constant. NDZ of proposed method is equal to 0.18

percent of active power mismatch because below this level frequency deviation is too small to cross the threshold of $Th_1$.

### *A.5.3 Linear Load switching*

In this condition, inverter based DG generates 1.4 kW and injects total generated power to the grid because local load demand is zero. Suddenly, at the instant 0.4 second, local demand increases to 1.4 kW. This event acts as a transient disturbance to the system. Simulation results of proposed MP method and DWT for these transient situations are shown in Figure A.7(a) and A.7(b) respectively. From the result shown in Figure A.7(a), it is clear that the frequency of the PCC voltage signal starts oscillating and the transient frequency estimated by the MP method is greater than 10 Hz. Therefore, DG supply remains enabled. RMAC value of DWT method is also below the preset threshold value of 0.05. Thus, both techniques are capable of distinguishing this transient as a non-islanding event.

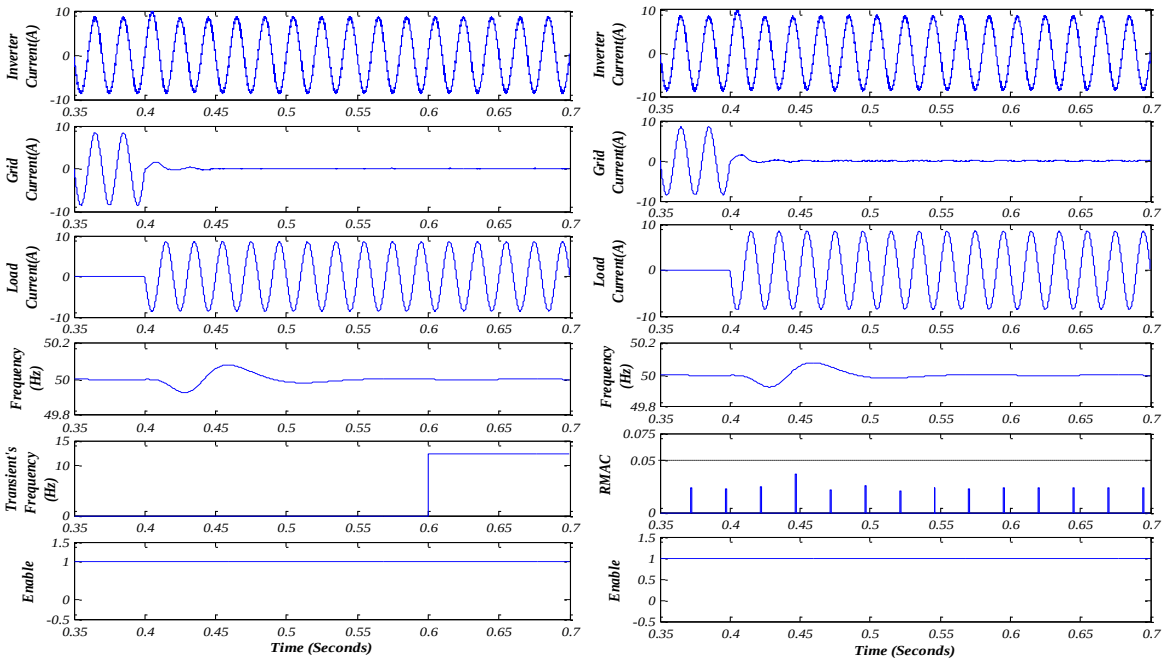


*Figure A.*7(a) *Figure A.*7(b)

*Figure A.0.7 load switching (non-islanding event) with (a) proposed MP method and (b) DWT method*

### *A.5.4 Nonlinear load Switching*

In this section, the reliability of the proposed MP method and DWT based islanding detection method is tested when a nonlinear load is added at the instant 0.4 second. MP method and DWT in the context of comparative performance are shown in Figure A.8(a) and A.8(b) respectively. From the results, it is clear that proposed MP technique outperforms and accurately detects it as a non-islanding event even if the switched load is nonlinear in nature. Whereas, in the case of DWT method, RMAC value crosses the threshold level, which leads to mal-operation as shown in Figure A.8 (b). To avoid mal-operation, the threshold value of RMAC must be set at a higher level. It is undesirable to increase the threshold level because it will result in larger NDZ.

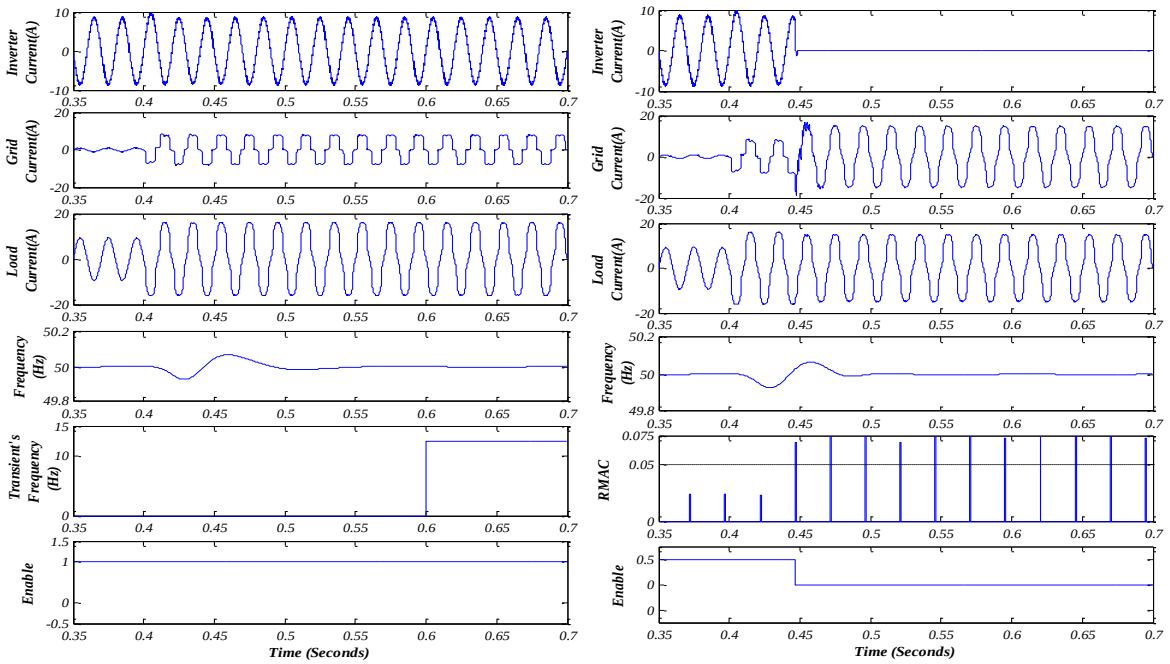


*Figure A.*8(a) *Figure A.*8(b)

*Figure A.0.8 Simulation result of nonlinear load switching with (a) proposed MP method and (b) DWT method*

### *A.5.5 Capacitor switching*

In this case, before the capacitive load switching, DG feeds power to 1.4 kW local load thus power exchange from the grid is almost negligible (grid current is zero). In the event of capacitive load switching, power has been drawn from the grid (grid current

value increases from zero) to meet the additional power requirement of the capacitive load. To study the efficacy of islanding detection algorithm under such scenario, a 450 VAR of capacitive load is added at the instance 0.4 second, which results in a switching type non-islanding event. Result in Figure A.9(a) shows that frequency of PCC voltage signal starts oscillating from the instant 0.4 second and estimated transient frequency is greater than the $Th_2$. Thus, DG supply remains enabled.

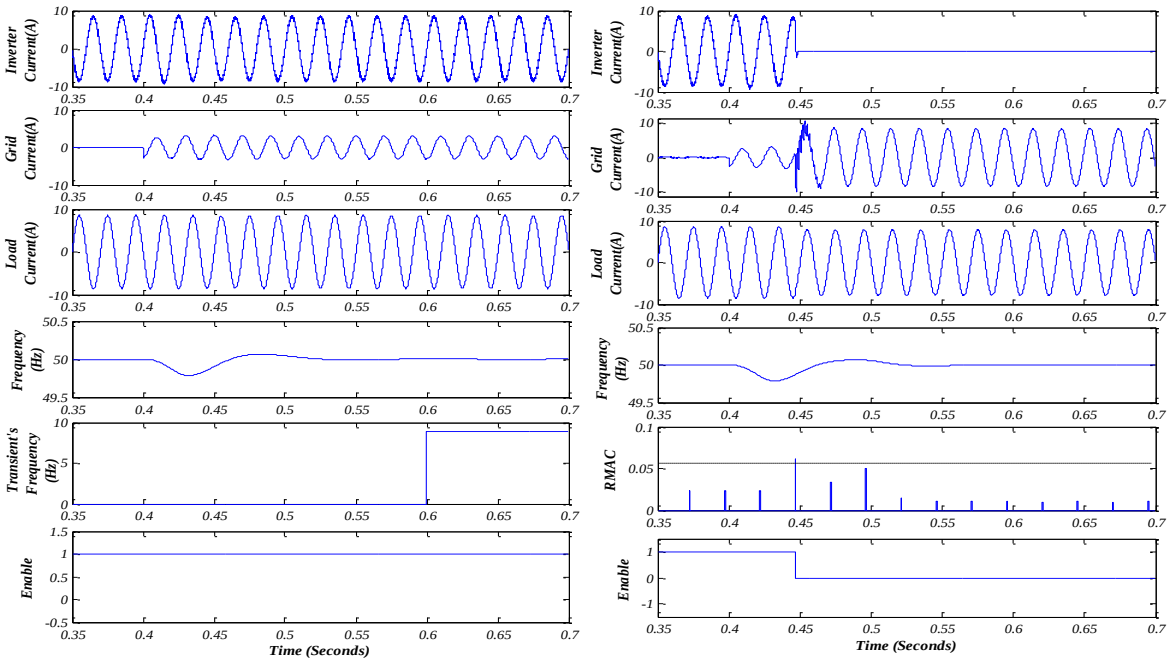


*Figure A.*9 (a) *Figure A.*9 (b)

*Figure A.0.9 Capacitor switching (non-islanding event) with (a) proposed MP method and (b) DWT method*

In the case of DWT based method, RMAC value increase from the preset threshold value of 0.05 as shown in Figure A.9 (b), recognises it as islanding event and disables the DG power supply. This is a practical case example where the proposed MP method is more reliable than that of DWT method for proper discrimination between islanding and non-islanding events. It is noteworthy to mention that 450 VAR capacitive load acts as a threshold, below which the wavelet based relay, operate perfectly but exhibits mal-operation for 450 VAR and above capacitive load switching. This situation occurs because the energy of the wavelet coefficients are found to be too low to reach the

threshold 0.05 for cases lower than 450 VAR capacitive load switching. Proposed MP method has also been tested for different ratings higher and lower than the 450 VAR but does not show any malfunction.

### *A.5.6 Effect of grid-voltage harmonics on islanding detection*

To demonstrate the effect of grid harmonics effect on the performance of the proposed MP and DWT based technique an analysis has been presented in this section (Figure A.10). Grid harmonics can also affect some DWT based technique performance. This is due to the fact that DWT decomposes the signal in frequency bands as mentioned in section A.3. In the present study, the $d_2$ level band is used for the islanding detection. Variation in harmonics component that lies within this frequency band may lead to malfunctioning of DWT based island detection algorithm. Thus, to check the performance of DWT and proposed MP method, harmonics of order 13 and 17 are added to grid voltage at the instance 0.4 seconds. The magnitude of added harmonics is quite small. It is equal to 0.58 % and 0.68% of the fundamental for harmonics order 13 and 17 respectively, which is much lower than the permissible limit of IEEE Std. 519.

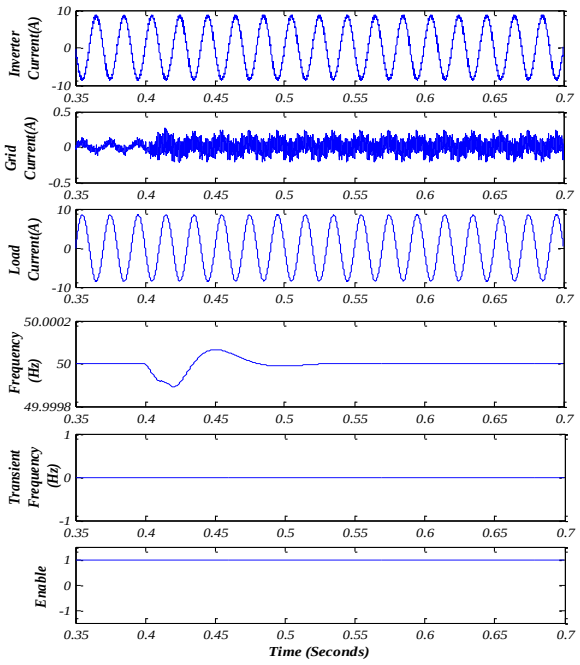


*Figure A.*10(a)

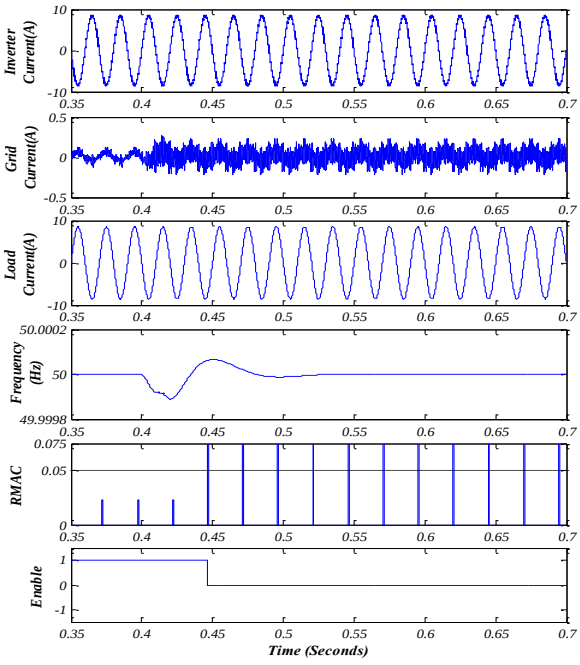


*Figure A.*10(b)

*Figure A.0.10 Effect of 13 and 17 order harmonics on (a) proposed MP method and (b) DWT method*

It is found from Figure A.10(b), RMAC values crosses the set thresholds and interpret it as islanding event. This situation occurs because the energy of $d_2$ level is increased due to the addition of harmonics of order 13 and 17. To avoid the malfunction of DWT based islanding detection technique, it needs a measurement of grid voltage harmonics, and the threshold has to be appropriately adjusted. It also introduces a remarkable delay for the regular update of thresholds, which is not a feasible solution. Proposed MP technique performance is not affected by the harmonics variation. The simulation results are shown in Figure A.10(a) and A.10 (b) confirm the superiority of the proposed MP technique over DWT in the presence of grid harmonics.

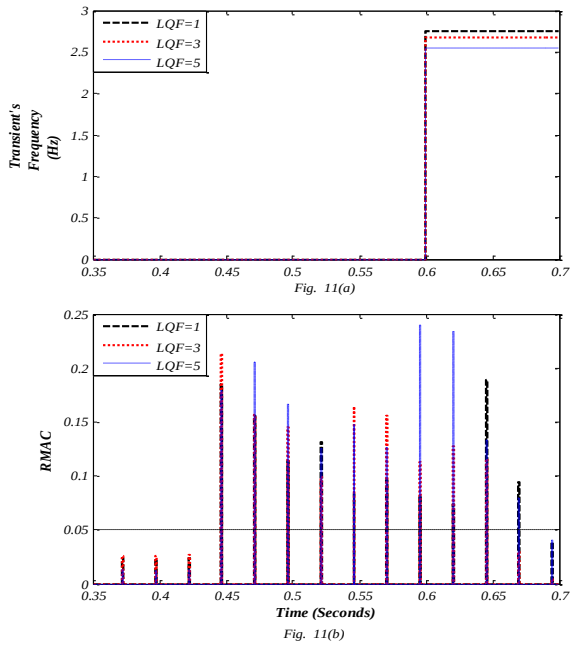


*Figure A.0.11 Effect of load quality on (a) proposed MP method (b) DWT method*

## *A.5.7 Effect of Load Quality Factor on islanding Detection*

Load quality factor also affects the islanding detection. Islanding detection becomes difficult for the RLC load having quality factor greater than the 2.5 [209]. Proposed MP and DWT based islanding detection method are tested for three different values of load quality factor. It can be seen from Figure A.11 that for all the three cases, the proposed

MP method and DWT method exhibit accurate islanding detection. From Figure A.11(a) it is clear that as the load quality factor increases, estimated transient's frequency by MP method decreases. Thus, load quality factor does not affect the islanding detection property of the proposed MP method. DWT method also detects the islanding condition correctly as shown in Figure A.11(b).

## A.6 Real-time results with discussion

The proposed system is implemented in RT-LAB simulator (OP5600), which uses field programmable gate array (FPGA) architecture with Xilinx system generator toolbox to realise the virtual prototype of the system. The laboratory setup diagram is shown in Figure A.12. The virtual prototype of the system, which is in 'software in the loop (SIL)' is almost similar to the 'hardware in the loop (HIL)' as it is implemented with the proper delay management of actual signals and control signals. The communication between CPUs (PC & OPAL-RT) is controlled by the FPGA architecture and the console PC. All the real-time results obtained from OPAL-RT are scaled down by 10 in magnitude.

In this section, real-time validation of proposed MP method and its comparison with wavelet transform is presented for the critical cases such as zero power mismatch (Figure A.13). Effect of non-linear load variation and presence of grid harmonics are presented in the Figure A.14, and A.15 respectively.

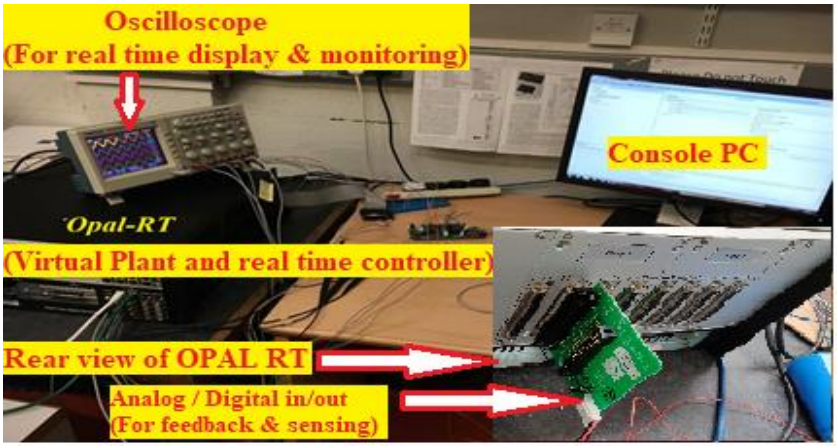


*Figure A.0.12 Opal- RT laboratory setup*

It has been observed from the Figure A.13 (a), islanding detection time of proposed MP method is reduced to 0.1 second in comparison to detection time of 0.2 second in a simulated environment. It means the computational burden of proposed method is not very significant in the OPAL-RT environment. Thus, it is well suited for the real-time islanding detection. Wavelet based method detection time (0.03 second) in real time also reduced as compared to the detection time (0.07 second) in simulated case. From the result shown in Figure A.13, it is clear that both the methods are capable to detect islanding accurately.

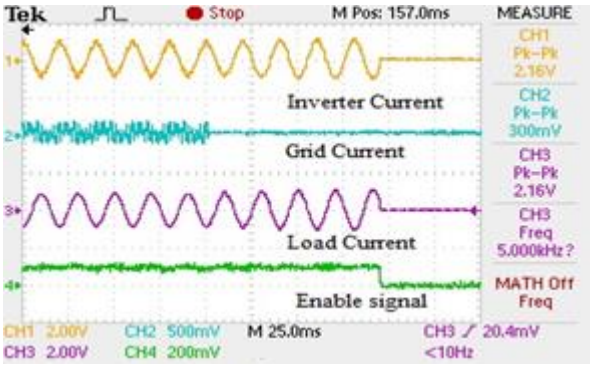


*Figure A.13(a)*

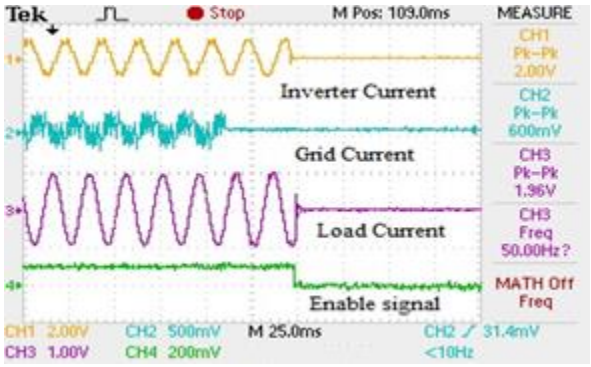


*Figure A.13 (b)*

*Figure A.0.13 Real-time result of close to zero power mismatch with (a) proposed MP method (b) DWT method*

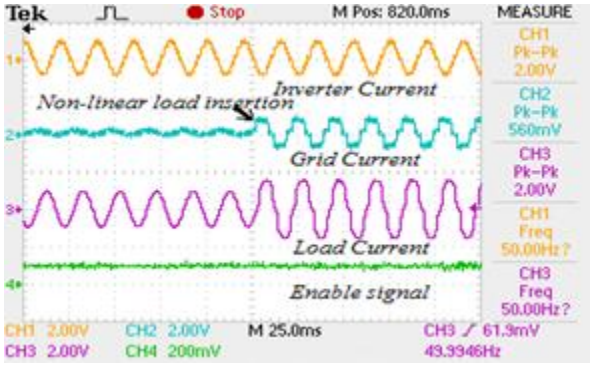


*Figure A.*14 (a)

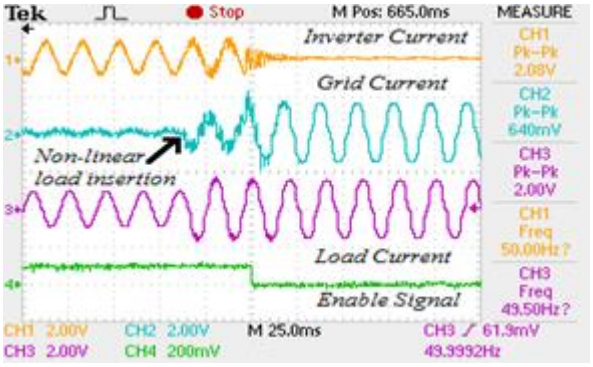


*Figure A.*14 (b)

*Figure A.0.14 Real time result of the effect of non-linear load (non-islanding event) with (a) proposed MP method (b) DWT method*

From the results shown in Figure A.14 (a)(similar to case study A.5.4 in section A.5 non-linear load switching) and Figure A.15 (a)( similar to case study A.5.5 in section A.5 presence of voltage harmonics in grid), it is clear that in real time environment, proposed MP method clearly discriminate these events as non-islanding disturbances and continues the DG supply. Whereas DWT method shows malfunctions to these events as shown in Figure A.14(b) and Figure A.15(b) and stops the DG supply.

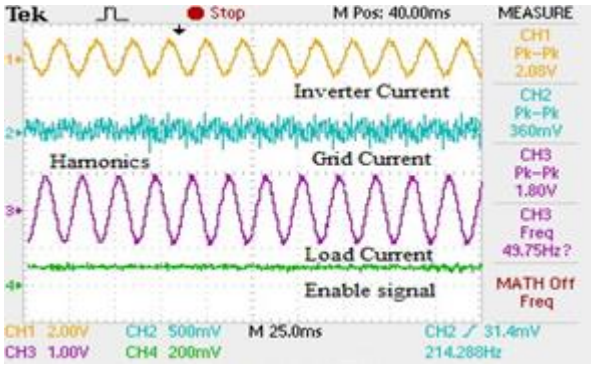


*Figure A.*15(a)

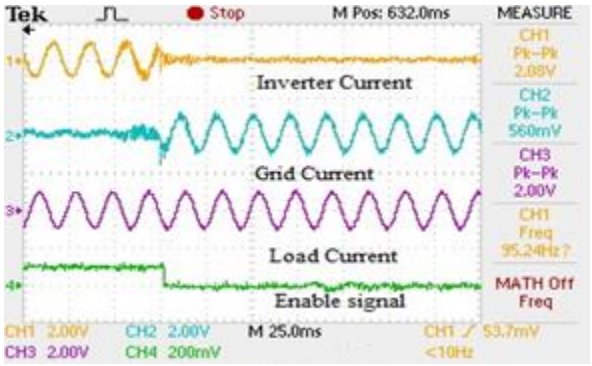


*Figure A.*15 (b)

*Figure A.0.15 Real time result of effect of 13 and 17 order harmonics on (a) proposed MP method and (b) DWT method*

## A.7 Conclusion

In this research work disturbance transient's frequency estimation is treated as the dominant criteria to discriminate islanding and non-islanding events. In the case of islanding events, frequency variation will monotonically increase or decrease. On the other hand, in the case of non-islanding events, the frequency will be oscillating in

nature. This basic difference is exploited with MP algorithm to address the discrimination between two events. To position the new algorithm in the context of popular passive methods used, the proposed MP method has been compared with DWT based technique. In the unusual event of only exact zero power mismatch, it is acknowledged that this passive MP method may not work alone, but that will be an extremely rare event. Even for minimal power mismatch (0.2% difference), the decomposition of signal subspace and noise subspace in the context of frequency estimation concept is being exploited as the estimation objective which is also suitable for real-time implementation with the less computational burden. From the presented 7 different case studies, it is concluded that the proposed MP technique in comparison to the DWT based technique is more robust and does not trigger any mal-operation in the event of grid harmonic pollution and other non-islanding switching transient cases where it can affect the grid voltage harmonics. However, detection time (0.2 sec in case of simulated and 0.1 sec in real-time) is large as compared with DWT based technique, but then again it is much lower than the IEEE std. 1547 permissible limit of two second.

# Appendix B: Detail Control Technique of Inverters

## B.1 Detail inverter control topology

A detail control technique of the proposed microgrid (MG) inverters are given in this section. The proposed converter can regulate the system voltage and frequency in islanded mode with no need to connect another synchronizing converter / generator. In this proposed control system, the active and reactive power delivered by the converter is the function of system frequency and voltage. The power sharing of the converter is achieved by implementing the communication less droop control. Fig. B.1 is showing the detail control topology of the microgrid inverter when it is operating in the standalone mode. Whereas the Fig. B.2 is representing the detail control topology of the inverters, operating in a interconnected mode. The operation of the MG2 inverter is controlled by the maximum power point controller/ power management controller, which define the power reference values for the inverter. As shown in the picture, the voltage and frequency reference for the MG 2 inverter is taken from MG1, which mainly helps to synchronise the system.

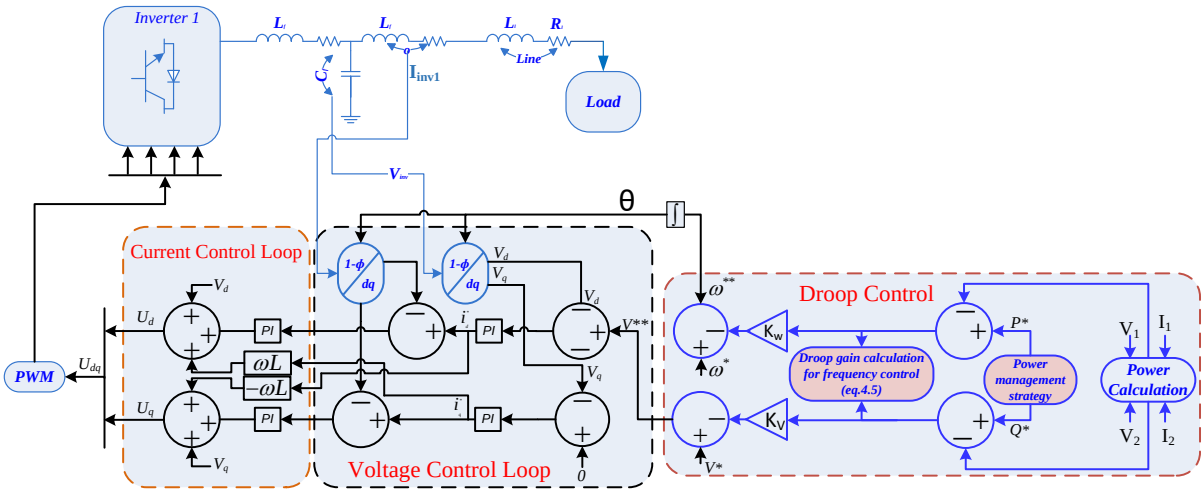


*Figure B.0.1 Detail inverter control topology for the standalone mode of operation*

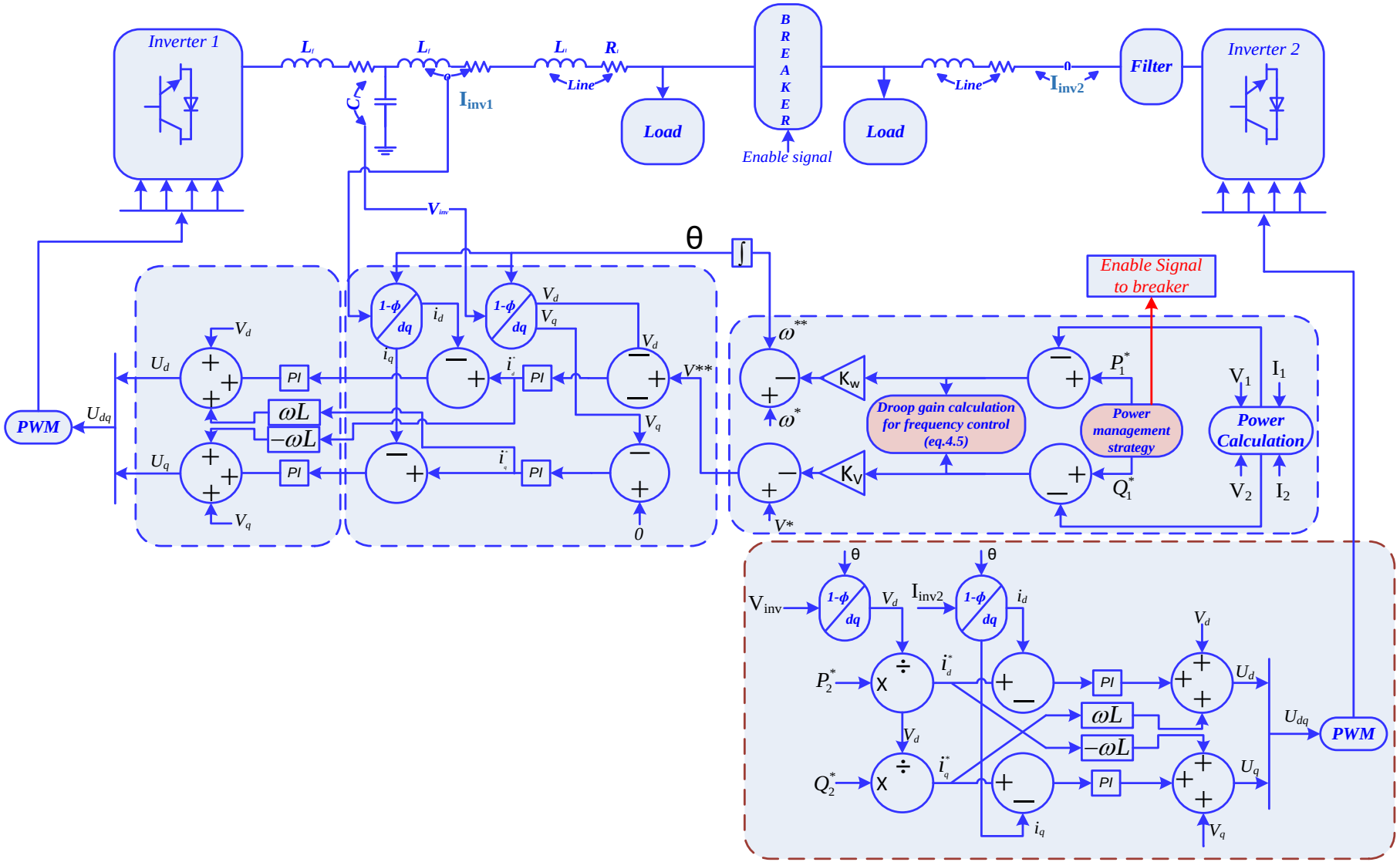


*Figure B.0.2 Detail inverter control topology for the interconnected mode of operation*

# Appendix C: List of Publication

## Published:

[1] S. Agrawal, S. Patra, S. R. Mohanty, V. Agarwal, and M. Basu, “Use of Matrix-Pencil Method for efficient islanding detection in Static DG and a parallel comparison with DWT method,” IEEE Transactions on Industrial Electronics. pp. 1–1, 2018.

[2] S. Patra, S. Agrawal, S. R. Mohanty, V. Agarwal and M. Basu, "ESPRIT based robust anti-islanding algorithm for grid-tied inverter," 2017 IEEE Students’ Technology Symposium (TechSym), Kharagpur, 2017, pp. 90-95.

[3] Sreedhar M, S. Patra, M. Basu “Hardware Based Intrusion Detection in E-LAN based Distributed DC Microgrid: A Virtual Sensor Approach” IET Renewable Power Generation Conference-Dublin 2021- to appear

[4] S. Patra, S. Madichetty, and M. Basu, “Development of a Smart Energy Community by Coupling Neighbouring Community Microgrids for Enhanced Power Sharing Using Customised Droop Control,” Energies, vol. 14, no. 17, p. 5383, Aug. 2021, doi: 10.3390/en14175383.

[5] S. Patra and M. Basu, "Double Layered Droop Control based Frequency Restoration and Seamless Reconnection of Isolated Neighbouring Microgrids for Power Sharing," in *IEEE Journal of Emerging and Selected Topics in Power Electronics*, 2022, doi: 10.1109/JESTPE.2022.3197729.

## Under Review/Ready to Submit:

[1] Sreedhar M, S. Patra, M. Basu, “A Robust Predictive Current Control Approach for Three Phase Inverter (Two / Multi Level) Under Parameter Uncertainties- A Generalized Approach” Ready to submit in IEEE Transaction on Industrial Electronics.

## In Progress:

[1] S. Patra, Sreedhar M, M. Basu , “Modelling, Analysis and Performance evaluation of DC Microgrid: An experiment-based literature review” Renewable and Sustainable Energy Reviews

[2] Sreedhar M, S. Patra, M. Basu, “Observer Based Cyber Attack Detection in Distributed DC Microgrid- A Priority Attack Detection Method” in IEEE Transaction in Smart Grid.

[3] S. Patra, M. Basu, “Coupling of isolated neighbouring microgrids: A literature Review” Renewable and Sustainable Energy Reviews.

# References


[1] "Climate Action Plan 2019 - To Tackle Climate Breakdown," Ireland, 2019. Accessed: Nov. 10, 2020. [Online]. Available: https://www.gov.ie/en/publication/ccb2e0-the-climate-action-plan-2019/.

[2] microgridknowledge.com(Elisa Wood), "How Many Microgrids Are There Exactly? Here's a Tally from Navigant," 2018. https://microgridknowledge.com/how-many-microgrids/ (accessed Aug. 26, 2018).

[3] C. Lo Prete and B. F. Hobbs, "A cooperative game theoretic analysis of incentives for microgrids in regulated electricity markets," *Appl. Energy*, vol. 169, pp. 524–541, May 2016, doi: 10.1016/J.APENERGY.2016.01.099.

[4] "GTM Report Forecasts $12.5B Microgrid Investment within US by 2022." https://microgridknowledge.com/microgrid-investment-gtm/ (accessed Nov. 10, 2020).

[5] "Press Release | Microgrid Deployment Tracker 2Q19." https://guidehouseinsights.com/news-and-views/navigant-research-has-identified-4475-microgrid-projects-representing-nearly-27-gw-of-planned-and-in (accessed Nov. 10, 2020).

[6] "Low Carbon Off-Grid Communities (LOGiC) | Interreg NWE." https://www.nweurope.eu/projects/project-search/low-carbon-off-grid-communities-logic/#tab-4 (accessed Nov. 10, 2020).

[7] A. Kyritsis *et al.*, "Evolution of PV systems in Greece and review of applicable solutions for higher penetration levels," *Renew. Energy*, vol. 109, pp. 487–499, Aug. 2017, doi: 10.1016/J.RENENE.2017.03.066.

[8] "IEEE 1547-2018 - IEEE Standard for Interconnection and Interoperability of Distributed Energy Resources with Associated Electric Power Systems Interfaces." https://standards.ieee.org/standard/1547-2018.html (accessed Feb. 24, 2021).

[9] H. Nikkhajoei and R. H. Lasseter, "Distributed Generation Interface to the CERTS Microgrid," *IEEE Trans. Power Deliv.*, vol. 24, no. 3, pp. 1598–1608, Jul. 2009, doi: 10.1109/TPWRD.2009.2021040.

[10] F. Otieno, N. Williams, and P. McSharry, "Forecasting Energy Demand for Microgrids Over Multiple Horizons," in *2018 IEEE PES/IAS PowerAfrica*, Jun. 2018, pp. 457–462, doi: 10.1109/PowerAfrica.2018.8521063.

[11] S. Bouzarovski, "Understanding Energy Poverty, Vulnerability and Justice," in *Energy Poverty*, Cham: Springer International Publishing, 2018, pp. 9–39.

[12] P. A. Trotter, M. C. McManus, and R. Maconachie, "Electricity planning and implementation in sub-Saharan Africa: A systematic review," *Renew. Sustain. Energy Rev.*, vol. 74, pp. 1189–1209, Jul. 2017, doi: 10.1016/J.RSER.2017.03.001.

[13] J. Balakrishnan, "Renewable Energy and Distributed Generation in Rural Villages," in *First International Conference on Industrial and Information Systems*, Aug. 2006, pp. 190–195, doi: 10.1109/ICIIS.2006.365662.

[14] M. Sadiqi, A. Pahwa, and R. D. Miller, "Basic design and cost optimization of a hybrid power system for rural communities in Afghanistan," in *2012 North American Power Symposium (NAPS)*, Sep. 2012, pp. 1–6, doi: 10.1109/NAPS.2012.6336333.

[15] "Remote Communities in Canada," Canada, 2011. Accessed: Nov. 10, 2020. [Online]. Available: https://www.nrcan.gc.ca/sites/www.nrcan.gc.ca/files/canmetenergy/files/pubs/2013-118_en.pdf.

[16] Y.-Y. Hong, M.-C. Hsiao, Y.-R. Chang, Y.-D. Lee, and H.-C. Huang, "Multiscenario Underfrequency Load Shedding in a Microgrid Consisting of Intermittent Renewables," *IEEE Trans. Power Deliv.*, vol. 28, no. 3, pp. 1610–1617, Jul. 2013, doi: 10.1109/TPWRD.2013.2254502.

[17] S. Bahramirad, W. Reder, and A. Khodaei, "Reliability-Constrained Optimal Sizing of Energy Storage System in a Microgrid," *IEEE Trans. Smart Grid*, vol. 3, no. 4, pp. 2056–2062, Dec. 2012, doi: 10.1109/TSG.2012.2217991.

[18] S. A. Arefifar and Y. A.-R. I. Mohamed, "DG Mix, Reactive Sources and Energy Storage Units for Optimizing Microgrid Reliability and Supply Security," *IEEE Trans. Smart Grid*, vol. 5, no. 4, pp. 1835–1844, Jul. 2014, doi: 10.1109/TSG.2014.2307919.

[19] R. Majumder, A. Ghosh, G. Ledwich, and F. Zare, "Power Management and Power Flow Control With Back-to-Back Converters in a Utility Connected Microgrid," *IEEE Trans. Power Syst.*, vol. 25, no. 2, pp. 821–834, May 2010, doi: 10.1109/TPWRS.2009.2034666.

[20] R. H. Lasseter, “Smart Distribution: Coupled Microgrids,” *Proc. IEEE*, vol. 99, no. 6, pp. 1074–1082, Jun. 2011, doi: 10.1109/JPROC.2011.2114630.

[21] J. Kumar, A. Agarwal, and V. Agarwal, “A review on overall control of DC microgrids,” *J. Energy Storage*, vol. 21, pp. 113–138, Feb. 2019, doi: 10.1016/J.EST.2018.11.013.

[22] W. Javed *et al.*, “System Configuration, Fault Detection, Location, Isolation and Restoration: A Review on LVDC Microgrid Protections,” *Energies*, vol. 12, no. 6, p. 1001, Mar. 2019, doi: 10.3390/en12061001.

[23] D. Kumar and F. Zare, “A Comprehensive Review of Maritime Microgrids: System Architectures, Energy Efficiency, Power Quality, and Regulations,” *IEEE Access*, vol. 7, pp. 67249–67277, 2019.

[24] A. Singh and S. Suhag, “Trends in Islanded Microgrid Frequency Regulation – A Review,” *Smart Sci.*, vol. 7, no. 2, pp. 91–115, Apr. 2019, doi: 10.1080/23080477.2018.1540380.

[25] A. Mohammed, S. S. Refaat, S. Bayhan, and H. Abu-Rub, “AC Microgrid Control and Management Strategies: Evaluation and Review,” *IEEE Power Electron. Mag.*, vol. 6, no. 2, pp. 18–31, Jun. 2019.

[26] A. Hirsch, Y. Parag, and J. Guerrero, “Microgrids: A review of technologies, key drivers, and outstanding issues,” *Renew. Sustain. Energy Rev.*, vol. 90, pp. 402–411, Jul. 2018, doi: 10.1016/J.RSER.2018.03.040.

[27] J. A. Laghari, H. Mokhlis, A. H. A. Bakar, and H. Mohamad, “Application of computational intelligence techniques for load shedding in power systems: A review,” *Energy Convers. Manag.*, vol. 75, pp. 130–140, Nov. 2013, doi: 10.1016/J.ENCONMAN.2013.06.010.

[28] V. Tamilselvan and T. Jayabarathi, “A hybrid method for optimal load shedding and improving voltage stability,” *Ain Shams Eng. J.*, vol. 7, no. 1, pp. 223–232, Mar. 2016, doi: 10.1016/J.ASEJ.2015.11.003.

[29] N. R. Tummuru, U. Manandhar, A. Ukil, H. B. Gooi, S. K. Kollimalla, and S. Naidu, “Control strategy for AC-DC microgrid with hybrid energy storage under different operating modes,” *Int. J. Electr. Power Energy Syst.*, vol. 104, pp. 807–816, Jan. 2019, doi: 10.1016/J.IJEPES.2018.07.063.

[30] A. A. Khodadoost Arani, G. B. Gharehpetian, and M. Abedi, “Review on Energy Storage Systems Control Methods in Microgrids,” *Int. J. Electr. Power Energy Syst.*, vol. 107, pp. 745–757, May 2019.

[31] S. Kotra and M. Mahesh K., “Design and Stability Analysis of DC Microgrid with Hybrid Energy Storage System,” *IEEE Trans. Sustain. Energy*, pp. 1–1, 2019, doi: 10.1109/TSTE.2019.2891255.

[32] M. Yousif *et al.*, “Dataset for Scheduling Strategies for Microgrids Coupled with Natural Gas Networks,” *Data*, vol. 4, no. 1, p. 24, Feb. 2019, doi: 10.3390/data4010024.

[33] B. John, A. Ghosh, M. Goyal, and F. Zare, “A DC Power Exchange Highway Based Power Flow Management for Interconnected Microgrid Clusters,” *IEEE Syst. J.*, pp. 1–11, 2019.

[34] M. N. Alam, S. Chakrabarti, and A. Ghosh, “Networked Microgrids: State-of-the-Art and Future Perspectives,” *IEEE Trans. Ind. Informatics*, vol. 15, no. 3, pp. 1238–1250, Mar. 2019.

[35] J. Qiu, J. Zhao, H. Yang, D. Wang, and Z. Y. Dong, “Planning of solar photovoltaics, battery energy storage system and gas micro turbine for coupled micro energy grids,” *Appl. Energy*, vol. 219, pp. 361–369, Jun. 2018, doi: 10.1016/J.APENERGY.2017.09.066.

[36] F. Shahnia, “Interconnected Microgrid Systems for Remote Areas,” in *Sustainable Development in Energy Systems*, Cham: Springer International Publishing, 2017, pp. 39–63.

[37] S. Bourbour and F. Shahnia, “Impact of the weightings of different criteria in selecting the suitable microgrids when forming a system of coupled microgrids,” in *2016 IEEE Innovative Smart Grid Technologies - Asia (ISGT-Asia)*, Nov. 2016, pp. 1151–1156, doi: 10.1109/ISGT-Asia.2016.7796548.

[38] F. Shahnia, S. Bourbour, and A. Ghosh, “Coupling Neighboring Microgrids for Overload Management Based on Dynamic Multicriteria Decision-Making,” *IEEE Trans. Smart Grid*, pp. 1–1, 2015, doi: 10.1109/TSG.2015.2477845.

[39] Q. Liu, T. Caldognetto, and S. Buso, “Flexible Control of Interlinking Converters for DC Microgrids Coupled to Smart AC Power Systems,” *IEEE Trans. Ind. Electron.*, vol. 66, no. 5, pp. 3477–3485, May 2019, doi: 10.1109/TIE.2018.2856210.

[40] M. Jafari, Z. Malekjamshidi, and J. Zhu, “Copper Loss Analysis of a Multiwinding High-Frequency Transformer for a Magnetically-Coupled Residential Microgrid,” *IEEE Trans. Ind. Appl.*, vol. 55, no. 1, pp. 283–297, Jan. 2019, doi: 10.1109/TIA.2018.2864170.

[41] M. Jafari, Z. Malekjamshidi, and J. Zhu, “A magnetically coupled multi-port, multi-operation-mode micro-grid with a predictive dynamic programming-based energy management for residential applications,” *Int. J. Electr. Power Energy Syst.*, vol. 104, pp. 784–796, Jan. 2019, doi: 10.1016/J.IJEPES.2018.07.040.

[42] F. Shahnia and S. Bourbour, “A practical and intelligent technique for coupling multiple neighboring

microgrids at the synchronization stage," *Sustain. Energy, Grids Networks*, vol. 11, pp. 13–25, Sep. 2017, doi: 10.1016/J.SEGAN.2017.06.002.

[43] R. H. Lasseter, "Smart Distribution: Coupled Microgrids," *Proc. IEEE*, vol. 99, no. 6, pp. 1074–1082, Jun. 2011, doi: 10.1109/JPROC.2011.2114630.

[44] "SolarPower Europe - Leading the Energy Transition." http://www.solarpowereurope.org/ (accessed Jun. 20, 2019).

[45] L. Moretti, M. Astolfi, C. Vergara, E. Macchi, J. I. Pérez-Arriaga, and G. Manzolini, "A design and dispatch optimization algorithm based on mixed integer linear programming for rural electrification," *Appl. Energy*, vol. 233–234, pp. 1104–1121, Jan. 2019, doi: 10.1016/J.APENERGY.2018.09.194.

[46] G. Pathak, B. Singh, and B. K. Panigrahi, "Wind–Hydro Microgrid and Its Control for Rural Energy System," *IEEE Trans. Ind. Appl.*, vol. 55, no. 3, pp. 3037–3045, May 2019, doi: 10.1109/TIA.2019.2897659.

[47] D. F. Gómez-Hernández, B. Domenech, J. Moreira, N. Farrera, A. López-González, and L. Ferrer-Martí, "Comparative evaluation of rural electrification project plans: A case study in Mexico," *Energy Policy*, vol. 129, pp. 23–33, Jun. 2019, doi: 10.1016/J.ENPOL.2019.02.004.

[48] N. Narayan *et al.*, "Quantifying the Benefits of a Solar Home System-Based DC Microgrid for Rural Electrification," *Energies*, vol. 12, no. 5, p. 938, Mar. 2019, doi: 10.3390/en12050938.

[49] A. Saxena and D. S. Chauhan, "Rural Electrification Using Microgrids and Its Performance Analysis with the Perspective of Single-Phase Inverter as Its Main Constituent," Springer, Singapore, 2019, pp. 425–437.

[50] S. Numminen and P. D. Lund, "Evaluation of the reliability of solar micro-grids in emerging markets – Issues and solutions," *Energy Sustain. Dev.*, vol. 48, pp. 34–42, Feb. 2019, doi: 10.1016/J.ESD.2018.10.006.

[51] J. N. Balls and H. W. Fischer, "Electricity-Centered Clientelism and the Contradictions of Private Solar Microgrids in India," *Ann. Am. Assoc. Geogr.*, vol. 109, no. 2, pp. 465–475, Mar. 2019, doi: 10.1080/24694452.2018.1535312.

[52] J. Kumar, B. V. Suryakiran, A. Verma, and T. S. Bhatti, "Analysis of techno-economic viability with demand response strategy of a grid-connected microgrid model for enhanced rural electrification in Uttar Pradesh state, India," *Energy*, vol. 178, pp. 176–185, Jul. 2019, doi: 10.1016/J.ENERGY.2019.04.105.

[53] J. Rocabert, A. Luna, F. Blaabjerg, and P. Rodríguez, "Control of Power Converters in AC Microgrids," *IEEE Trans. Power Electron.*, vol. 27, no. 11, pp. 4734–4749, Nov. 2012, doi: 10.1109/TPEL.2012.2199334.

[54] P. Arboleya *et al.*, "An improved control scheme based in droop characteristic for microgrid converters," *Electr. Power Syst. Res.*, vol. 80, no. 10, pp. 1215–1221, Oct. 2010, doi: 10.1016/J.EPSR.2010.04.003.

[55] E. Mojica-Nava, C. A. Macana, and N. Quijano, "Dynamic Population Games for Optimal Dispatch on Hierarchical Microgrid Control," *IEEE Trans. Syst. Man, Cybern. Syst.*, vol. 44, no. 3, pp. 306–317, Mar. 2014, doi: 10.1109/TSMCC.2013.2266117.

[56] L. Meng, F. Tang, M. Savaghebi, J. C. Vasquez, and J. M. Guerrero, "Tertiary Control of Voltage Unbalance Compensation for Optimal Power Quality in Islanded Microgrids," *IEEE Trans. Energy Convers.*, vol. 29, no. 4, pp. 802–815, Dec. 2014, doi: 10.1109/TEC.2014.2363687.

[57] F. Shahnia, A. Ghosh, S. Rajakaruna, and R. P. S. Chandrasena, "Primary control level of parallel distributed energy resources converters in system of multiple interconnected autonomous microgrids within self-healing networks," *IET Gener. Transm. Distrib.*, vol. 8, no. 2, pp. 203–222, Feb. 2014, doi: 10.1049/iet-gtd.2013.0126.

[58] B. Jiang and Y. Fei, "Smart Home in Smart Microgrid: A Cost-Effective Energy Ecosystem With Intelligent Hierarchical Agents," *IEEE Trans. Smart Grid*, vol. 6, no. 1, pp. 3–13, Jan. 2015, doi: 10.1109/TSG.2014.2347043.

[59] X. Wu, X. Wang, and C. Qu, "A Hierarchical Framework for Generation Scheduling of Microgrids," *IEEE Trans. Power Deliv.*, vol. 29, no. 6, pp. 2448–2457, Dec. 2014, doi: 10.1109/TPWRD.2014.2360064.

[60] D. E. Olivares *et al.*, "Trends in Microgrid Control," *IEEE Trans. Smart Grid*, vol. 5, no. 4, pp. 1905–1919, Jul. 2014, doi: 10.1109/TSG.2013.2295514.

[61] B. M. Eid, N. A. Rahim, J. Selvaraj, and A. H. El Khateb, "Control Methods and Objectives for Electronically Coupled Distributed Energy Resources in Microgrids: A Review," *IEEE Syst. J.*, vol. 10, no. 2, pp. 446–458, Jun. 2016, doi: 10.1109/JSYST.2013.2296075.

[62] H. Mahmood, D. Michaelson, and J. Jiang, "Decentralized Power Management of a PV/Battery Hybrid Unit in a Droop-Controlled Islanded Microgrid," *IEEE Trans. Power Electron.*, vol. 30, no. 12, pp. 7215–7229, Dec. 2015, doi: 10.1109/TPEL.2015.2394351.

[63] Y. Karimi, H. Oraee, and J. M. Guerrero, "Decentralized Method for Load Sharing and Power Management in a Hybrid Single/Three-Phase-Islanded Microgrid Consisting of Hybrid Source PV/Battery Units," *IEEE Trans. Power Electron.*, vol. 32, no. 8, pp. 6135–6144, Aug. 2017, doi: 10.1109/TPEL.2016.2620258.

[64] H. Mahmood and J. Jiang, "Autonomous Coordination of Multiple PV/Battery Hybrid Units in Islanded Microgrids," *IEEE Trans. Smart Grid*, pp. 1–1, 2017, doi: 10.1109/TSG.2017.2709550.

[65] S. Adhikari and F. Li, "Coordinated V-f and P-Q Control of Solar Photovoltaic Generators With MPPT and Battery Storage in Microgrids," *IEEE Trans. Smart Grid*, vol. 5, no. 3, pp. 1270–1281, May 2014, doi: 10.1109/TSG.2014.2301157.

[66] S. Bae and A. Kwasinski, "Dynamic Modeling and Operation Strategy for a Microgrid With Wind and Photovoltaic Resources," *IEEE Trans. Smart Grid*, vol. 3, no. 4, pp. 1867–1876, Dec. 2012, doi: 10.1109/TSG.2012.2198498.

[67] Z. Yi, W. Dong, and A. H. Etemadi, "A Unified Control and Power Management Scheme for PV-Battery-Based Hybrid Microgrids for Both Grid-Connected and Islanded Modes," *IEEE Trans. Smart Grid*, pp. 1–1, 2017, doi: 10.1109/TSG.2017.2700332.

[68] W. Du, Q. Jiang, M. J. Erickson, and R. H. Lasseter, "Voltage-Source Control of PV Inverter in a CERTS Microgrid," *IEEE Trans. Power Deliv.*, vol. 29, no. 4, pp. 1726–1734, Aug. 2014, doi: 10.1109/TPWRD.2014.2302313.

[69] H. Mahmood, D. Michaelson, and Jin Jiang, "Strategies for Independent Deployment and Autonomous Control of PV and Battery Units in Islanded Microgrids," *IEEE J. Emerg. Sel. Top. Power Electron.*, vol. 3, no. 3, pp. 742–755, Sep. 2015, doi: 10.1109/JESTPE.2015.2413756.

[70] T. Lu, Q. Ai, and Z. Wang, "Interactive game vector: A stochastic operation-based pricing mechanism for smart energy systems with coupled-microgrids," *Appl. Energy*, vol. 212, pp. 1462–1475, Feb. 2018, doi: 10.1016/J.APENERGY.2017.12.096.

[71] M. Yousif *et al.*, "Application of Particle Swarm Optimization to a Scheduling Strategy for Microgrids Coupled with Natural Gas Networks," *Energies*, vol. 11, no. 12, p. 3499, Dec. 2018, doi: 10.3390/en11123499.

[72] N. Bazmohammadi, A. Tahsiri, A. Anvari-Moghaddam, and J. M. Guerrero, "A hierarchical energy management strategy for interconnected microgrids considering uncertainty," *Int. J. Electr. Power Energy Syst.*, vol. 109, pp. 597–608, Jul. 2019, doi: 10.1016/J.IJEPES.2019.02.033.

[73] N. A. El-Taweel, H. Khani, and H. E. Z. Farag, "Voltage regulation in active power distribution systems integrated with natural gas grids using distributed electric and gas energy resources," *Int. J. Electr. Power Energy Syst.*, vol. 106, pp. 561–571, Mar. 2019, doi: 10.1016/J.IJEPES.2018.10.037.

[74] M. Batool, S. M. Islam, and F. Shahnia, "Master control unit based power exchange strategy for interconnected microgrids," in *2017 Australasian Universities Power Engineering Conference (AUPEC)*, Nov. 2017, pp. 1–6, doi: 10.1109/AUPEC.2017.8282475.

[75] Y. Han and J.-I. Ha, "Droop Control Using Impedance of Grid-Integrated DFIG within Microgrid," *IEEE Trans. Energy Convers.*, vol. 34, no. 1, pp. 88–97, Mar. 2019, doi: 10.1109/TEC.2018.2861819.

[76] A. A. Khodadoost Arani, G. B. Gharehpetian, and M. Abedi, "Review on Energy Storage Systems Control Methods in Microgrids," *Int. J. Electr. Power Energy Syst.*, vol. 107, pp. 745–757, May 2019, doi: 10.1016/J.IJEPES.2018.12.040.

[77] H. Han, X. Hou, J. Yang, J. Wu, M. Su, and J. M. Guerrero, "Review of Power Sharing Control Strategies for Islanding Operation of AC Microgrids," *IEEE Trans. Smart Grid*, vol. 7, no. 1, pp. 200–215, Jan. 2016, doi: 10.1109/TSG.2015.2434849.

[78] M. F. Zia, E. Elbouchikhi, and M. Benbouzid, "Microgrids energy management systems: A critical review on methods, solutions, and prospects," *Appl. Energy*, vol. 222, pp. 1033–1055, Jul. 2018, doi: 10.1016/J.APENERGY.2018.04.103.

[79] H. Liu, N. Mahmoudi, K. Chen, H. Liu, N. Mahmoudi, and K. Chen, "Microgrids Real-Time Pricing Based on Clustering Techniques," *Energies*, vol. 11, no. 6, p. 1388, May 2018, doi: 10.3390/en11061388.

[80] H. Moazami Goodarzi and M. H. Kazemi, "An optimal autonomous microgrid cluster based on distributed generation droop parameter optimization and renewable energy sources using an improved grey wolf optimizer," *Eng. Optim.*, vol. 50, no. 5, pp. 819–839, May 2018, doi: 10.1080/0305215X.2017.1355970.

[81] J. He and Y. W. Li, “An Enhanced Microgrid Load Demand Sharing Strategy,” *IEEE Trans. Power Electron.*, vol. 27, no. 9, pp. 3984–3995, Sep. 2012, doi: 10.1109/TPEL.2012.2190099.

[82] L. Hongpeng, L. Xiaoxi, Z. Wei, and W. Wei, “An Improved Harmonic Power Sharing Scheme of Paralleled Inverter System,” in *2018 International Power Electronics Conference (IPEC-Niigata 2018 - ECCE Asia)*, May 2018, pp. 2969–2972, doi: 10.23919/IPEC.2018.8507542.

[83] P. H. Divshali, A. Alimardani, S. H. Hosseinian, and M. Abedi, “Decentralized Cooperative Control Strategy of Microsources for Stabilizing Autonomous VSC-Based Microgrids,” *IEEE Trans. Power Syst.*, vol. 27, no. 4, pp. 1949–1959, Nov. 2012, doi: 10.1109/TPWRS.2012.2188914.

[84] X. Meng, J. Liu, and Z. Liu, “A Generalized Droop Control for Grid-Supporting Inverter Based on Comparison Between Traditional Droop Control and Virtual Synchronous Generator Control,” *IEEE Trans. Power Electron.*, vol. 34, no. 6, pp. 5416–5438, Jun. 2019, doi: 10.1109/TPEL.2018.2868722.

[85] H. Sun *et al.*, “Review of Challenges and Research Opportunities for Voltage Control in Smart Grids,” *IEEE Trans. Power Syst.*, vol. 34, no. 4, pp. 2790–2801, Jul. 2019, doi: 10.1109/TPWRS.2019.2897948.

[86] R. Wang, Q. Sun, D. Ma, and Z. Liu, “The Small-Signal Stability Analysis of the Droop-Controlled Converter in Electromagnetic Timescale,” *IEEE Trans. Sustain. Energy*, pp. 1–1, 2019, doi: 10.1109/TSTE.2019.2894633.

[87] J. M. Guerrero, J. Matas, L. Garcia de Vicuna, M. Castilla, and J. Miret, “Decentralized Control for Parallel Operation of Distributed Generation Inverters Using Resistive Output Impedance,” *IEEE Trans. Ind. Electron.*, vol. 54, no. 2, pp. 994–1004, Apr. 2007, doi: 10.1109/TIE.2007.892621.

[88] J. Pan, S. Yu, and M. Ma, “Model Predictive Load Frequency Control of Isolated Micro-Grid with Electrical Vehicles,” in *2018 37th Chinese Control Conference (CCC)*, Jul. 2018, pp. 3588–3593, doi: 10.23919/ChiCC.2018.8482678.

[89] B. John, A. Ghosh, and F. Zare, “Load Sharing in Medium Voltage Islanded Microgrids With Advanced Angle Droop Control,” *IEEE Trans. Smart Grid*, vol. 9, no. 6, pp. 6461–6469, Nov. 2018, doi: 10.1109/TSG.2017.2713452.

[90] H. Moussa, A. Shahin, J.-P. Martin, S. Pierfederici, and N. Moubayed, “Optimal Angle Droop for Power Sharing Enhancement With Stability Improvement in Islanded Microgrids,” *IEEE Trans. Smart Grid*, vol. 9, no. 5, pp. 5014–5026, Sep. 2018, doi: 10.1109/TSG.2017.2678686.

[91] B. Wei, A. Marzabal, R. Ruiz, J. M. Guerrero, and J. C. Vasquez, “DAVIC: A New Distributed Adaptive Virtual Impedance Control for Parallel-Connected Voltage Source Inverters in Modular UPS System,” *IEEE Trans. Power Electron.*, vol. 34, no. 6, pp. 5953–5968, Jun. 2019, doi: 10.1109/TPEL.2018.2869870.

[92] Y. Li and Y. W. Li, “Power Management of Inverter Interfaced Autonomous Microgrid Based on Virtual Frequency-Voltage Frame,” *IEEE Trans. Smart Grid*, vol. 2, no. 1, pp. 30–40, Mar. 2011, doi: 10.1109/TSG.2010.2095046.

[93] Y. Cao, Z. Li, Z. Lu, Z. Chen, and X. Liu, “A full-dq based adaptive virtual impedance compensation in virtual power frame for droop-controlled parallel inverters under unbalanced conditions,” in *IECON 2017 - 43rd Annual Conference of the IEEE Industrial Electronics Society*, Oct. 2017, pp. 8710–8715, doi: 10.1109/IECON.2017.8217531.

[94] Yan Li and Yun Wei Li, “Decoupled power control for an inverter based low voltage microgrid in autonomous operation,” in *2009 IEEE 6th International Power Electronics and Motion Control Conference*, May 2009, pp. 2490–2496, doi: 10.1109/IPEMC.2009.5157823.

[95] C. Dou, Z. Zhang, D. Yue, and M. Song, “Improved droop control based on virtual impedance and virtual power source in low-voltage microgrid,” *IET Gener. Transm. Distrib.*, vol. 11, no. 4, pp. 1046–1054, Mar. 2017, doi: 10.1049/iet-gtd.2016.1492.

[96] S. Sahoo, S. Mishra, S. Jha, and B. Singh, “A Cooperative Adaptive Droop Based Energy Management & Optimal Voltage Regulation Scheme for DC Microgrids,” *IEEE Trans. Ind. Electron.*, pp. 1–1, 2019, doi: 10.1109/TIE.2019.2910037.

[97] N. Vazquez, S. S. Yu, T. K. Chau, T. Fernando, and H. H.-C. Iu, “A Fully Decentralized Adaptive Droop Optimization Strategy for Power Loss Minimization in Microgrids With PV-BESS,” *IEEE Trans. Energy Convers.*, vol. 34, no. 1, pp. 385–395, Mar. 2019, doi: 10.1109/TEC.2018.2878246.

[98] S. Chowdhury, M. O. Badawy, Y. Sozer, and A. De Abreu, “A Novel Battery Management System Using a Duality of the Adaptive Droop Control Theory,” *IEEE Trans. Ind. Appl.*, pp. 1–1, 2019, doi: 10.1109/TIA.2019.2919497.

[99] A. Yogarathinam and N. R. Chaudhuri, “Stability-Constrained Adaptive Droop for Power Sharing in AC-

MTDC Grids," *IEEE Trans. Power Syst.*, vol. 34, no. 3, pp. 1955–1965, May 2019, doi: 10.1109/TPWRS.2018.2890296.

[100] M. Davari and Y. A.-R. I. Mohamed, "Robust Droop and DC-Bus Voltage Control for Effective Stabilization and Power Sharing in VSC Multiterminal DC Grids," *IEEE Trans. Power Electron.*, vol. 33, no. 5, pp. 4373–4395, May 2018, doi: 10.1109/TPEL.2017.2715039.

[101] N. M. Dehkordi, N. Sadati, and M. Hamzeh, "Robust tuning of transient droop gains based on Kharitonov's stability theorem in droop-controlled microgrids," *IET Gener. Transm. Distrib.*, vol. 12, no. 14, pp. 3495–3501, Aug. 2018, doi: 10.1049/iet-gtd.2017.1767.

[102] D. J. Perreault, R. L. Selders, and J. G. Kassakian, "Frequency-based current-sharing techniques for paralleled power converters," *IEEE Trans. Power Electron.*, vol. 13, no. 4, pp. 626–634, Jul. 1998, doi: 10.1109/63.704128.

[103] A. Tuladhar, Hua Jin, T. Unger, and K. Mauch, "Control of parallel inverters in distributed AC power systems with consideration of line impedance effect," *IEEE Trans. Ind. Appl.*, vol. 36, no. 1, pp. 131–138, 2000, doi: 10.1109/28.821807.

[104] S.-J. Ahn, J.-W. Park, I.-Y. Chung, S.-I. Moon, S.-H. Kang, and S.-R. Nam, "Power-Sharing Method of Multiple Distributed Generators Considering Control Modes and Configurations of a Microgrid," *IEEE Trans. Power Deliv.*, vol. 25, no. 3, pp. 2007–2016, Jul. 2010, doi: 10.1109/TPWRD.2010.2047736.

[105] P. Ge *et al.*, "Extended-State-Observer-Based Distributed Robust Secondary Voltage and Frequency Control for an Autonomous Microgrid," *IEEE Trans. Sustain. Energy*, pp. 1–1, 2018, doi: 10.1109/TSTE.2018.2888562.

[106] S. Institution of Engineering and Technology and B. Subudhi, *IET smart grid*. IET Digital Library, 2019.

[107] F. Doost Mohammadi, H. Keshtkar Vanashi, and A. Feliachi, "State-Space Modeling, Analysis, and Distributed Secondary Frequency Control of Isolated Microgrids," *IEEE Trans. Energy Convers.*, vol. 33, no. 1, pp. 155–165, Mar. 2018, doi: 10.1109/TEC.2017.2757012.

[108] C. Ahumada, R. Cardenas, D. Saez, and J. M. Guerrero, "Secondary Control Strategies for Frequency Restoration in Islanded Microgrids With Consideration of Communication Delays," *IEEE Trans. Smart Grid*, vol. 7, no. 3, pp. 1430–1441, May 2016, doi: 10.1109/TSG.2015.2461190.

[109] L. Xing *et al.*, "Dual-consensus-based Distributed Frequency Control for Multiple Energy Storage Systems," *IEEE Trans. Smart Grid*, pp. 1–1, 2019, doi: 10.1109/TSG.2019.2904075.

[110] Y.-Q. Bao, C. Shen, Q. Wang, and J.-L. Zhang, "Demand Response Based on Kalman-Filtering for the Frequency Control," *J. Electr. Eng. Technol.*, vol. 14, no. 3, pp. 1087–1094, May 2019, doi: 10.1007/s42835-019-00139-4.

[111] A. K. Barik and D. C. Das, "Proficient load-frequency regulation of demand response supported bio-renewable cogeneration based hybrid microgrids with quasi-oppositional selfish-herd optimisation," *IET Gener. Transm. Distrib.*, vol. 13, no. 13, pp. 2889–2898, Jul. 2019, doi: 10.1049/iet-gtd.2019.0166.

[112] C. Gouveia, J. Moreira, C. L. Moreira, and J. A. Pecas Lopes, "Coordinating Storage and Demand Response for Microgrid Emergency Operation," *IEEE Trans. Smart Grid*, vol. 4, no. 4, pp. 1898–1908, Dec. 2013, doi: 10.1109/TSG.2013.2257895.

[113] K. Liu, J. He, Z. Luo, X. Shen, X. Liu, and T. Lu, "Secondary Frequency Control of Isolated Microgrid Based on LADRC," *IEEE Access*, vol. 7, pp. 53454–53462, 2019, doi: 10.1109/ACCESS.2019.2911911.

[114] M.-H. Khooban, T. Niknam, M. Shasadeghi, T. Dragicevic, and F. Blaabjerg, "Load Frequency Control in Microgrids Based on a Stochastic Noninteger Controller," *IEEE Trans. Sustain. Energy*, vol. 9, no. 2, pp. 853–861, Apr. 2018, doi: 10.1109/TSTE.2017.2763607.

[115] M. H. Khooban, T. Niknam, F. Blaabjerg, and T. Dragičević, "A new load frequency control strategy for micro-grids with considering electrical vehicles," *Electr. Power Syst. Res.*, vol. 143, pp. 585–598, Feb. 2017, doi: 10.1016/J.EPSR.2016.10.057.

[116] A. Abazari, H. Monsef, and B. Wu, "Coordination strategies of distributed energy resources including FESS, DEG, FC and WTG in load frequency control (LFC) scheme of hybrid isolated micro-grid," *Int. J. Electr. Power Energy Syst.*, vol. 109, pp. 535–547, Jul. 2019, doi: 10.1016/J.IJEPES.2019.02.029.

[117] M. Gheisarnejad and M. H. Khooban, "Secondary load frequency control for multi-microgrids: HiL real-time simulation," *Soft Comput.*, vol. 23, no. 14, pp. 5785–5798, Jul. 2019, doi: 10.1007/s00500-018-3243-5.

[118] Y. Shi, B. Xu, D. Wang, and B. Zhang, "Using Battery Storage for Peak Shaving and Frequency Regulation: Joint Optimization for Superlinear Gains," *IEEE Trans. Power Syst.*, vol. 33, no. 3, pp. 2882–2894, May 2018, doi: 10.1109/TPWRS.2017.2749512.

[119] A. Khorshidi, T. Niknam, and B. Bahmani, “Robust Multi-Agent Asynchronously Compensated Decentralized Frequency Synchronization Control Scheme for Microgrids,” *J. Electr. Eng. Technol.*, pp. 1–10, Apr. 2019, doi: 10.1007/s42835-019-00170-5.

[120] L. Xing *et al.*, “Dual-consensus-based Distributed Frequency Control for Multiple Energy Storage Systems,” *IEEE Trans. Smart Grid*, pp. 1–1, 2019, doi: 10.1109/TSG.2019.2904075.

[121] A. Aderibole, H. H. Zeineldin, M. Al Hosani, and E. F. El-Saadany, “Demand Side Management Strategy for Droop-Based Autonomous Microgrids Through Voltage Reduction,” *IEEE Trans. Energy Convers.*, vol. 34, no. 2, pp. 878–888, Jun. 2019, doi: 10.1109/TEC.2018.2877750.

[122] X. Liu, Y. Zhang, and K. Y. Lee, “Coordinated Distributed MPC for Load Frequency Control of Power System With Wind Farms,” *IEEE Trans. Ind. Electron.*, vol. 64, no. 6, pp. 5140–5150, Jun. 2017, doi: 10.1109/TIE.2016.2642882.

[123] M. Lotfy *et al.*, “A Frequency Control Approach for Hybrid Power System Using Multi-Objective Optimization,” *Energies*, vol. 10, no. 1, p. 80, Jan. 2017, doi: 10.3390/en10010080.

[124] F. Guo, C. Wen, J. Mao, and Y.-D. Song, “Distributed Secondary Voltage and Frequency Restoration Control of Droop-Controlled Inverter-Based Microgrids,” *IEEE Trans. Ind. Electron.*, vol. 62, no. 7, pp. 4355–4364, Jul. 2015, doi: 10.1109/TIE.2014.2379211.

[125] E. Pashajavid, F. Shahnia, and A. Ghosh, “Interconnection of two neighboring autonomous microgrids based on small signal analysis,” in *2015 9th International Conference on Power Electronics and ECCE Asia (ICPE-ECCE Asia)*, Jun. 2015, pp. 213–220, doi: 10.1109/ICPE.2015.7167789.

[126] J. Guo, T. Zhao, W. Liu, and J. Zhang, “Reliability Modeling and Assessment of Isolated Microgrid Considering Influences of Frequency Control,” *IEEE Access*, vol. 7, pp. 50362–50371, 2019, doi: 10.1109/ACCESS.2019.2909153.

[127] J. Kim *et al.*, “Supercapacitor to Provide Ancillary Services with Control Coordination,” *IEEE Trans. Ind. Appl.*, pp. 1–1, 2019, doi: 10.1109/TIA.2019.2924859.

[128] A. A. Khodadoost Arani, G. B. Gharehpetian, and M. Abedi, “A Novel Control Method Based on Droop for Cooperation of Flywheel and Battery Energy Storage Systems in Islanded Microgrids,” *IEEE Syst. J.*, pp. 1–8, 2019, doi: 10.1109/JSYST.2019.2911160.

[129] S. P. Melo, U. Brand, T. Vogt, J. S. Telle, F. Schuldt, and K. v. Maydell, “Primary frequency control provided by hybrid battery storage and power-to-heat system,” *Appl. Energy*, vol. 233–234, pp. 220–231, Jan. 2019, doi: 10.1016/J.APENERGY.2018.09.177.

[130] U. Datta, A. Kalam, and J. Shi, “Battery Energy Storage System Control for Mitigating PV Penetration Impact on Primary Frequency Control and State-of-Charge Recovery,” *IEEE Trans. Sustain. Energy*, pp. 1–1, 2019, doi: 10.1109/TSTE.2019.2904722.

[131] S. Weng, D. Yue, C. Dou, J. Shi, and C. Huang, “Distributed Event-Triggered Cooperative Control for Frequency and Voltage Stability and Power Sharing in Isolated Inverter-Based Microgrid,” *IEEE Trans. Cybern.*, vol. 49, no. 4, pp. 1427–1439, Apr. 2019, doi: 10.1109/TCYB.2018.2803754.

[132] Y. Guo, H. Gao, H. Xing, Q. Wu, and Z. Lin, “Decentralized Coordinated Voltage Control for VSC-HVDC Connected Wind Farms Based on ADMM,” *IEEE Trans. Sustain. Energy*, vol. 10, no. 2, pp. 800–810, Apr. 2019, doi: 10.1109/TSTE.2018.2848467.

[133] Q. Sun, Q. Sun, D. Qin, Q. Sun, Q. Sun, and D. Qin, “Adaptive Fuzzy Droop Control for Optimized Power Sharing in an Islanded Microgrid,” *Energies*, vol. 12, no. 1, p. 45, Dec. 2018, doi: 10.3390/en12010045.

[134] P. Sreekumar and O. Al Trad, “Optimisation of Harmonic Droop Coefficient to Minimize Power Losses in an Islanded Microgrid,” in *2019 Advances in Science and Engineering Technology International Conferences (ASET)*, Mar. 2019, pp. 1–5, doi: 10.1109/ICASET.2019.8714574.

[135] K. Lu, W. Zhou, G. Zeng, and Y. Zheng, “Constrained population extremal optimization-based robust load frequency control of multi-area interconnected power system,” *Int. J. Electr. Power Energy Syst.*, vol. 105, pp. 249–271, Feb. 2019, doi: 10.1016/J.IJEPES.2018.08.043.

[136] M. Gheisarnejad, “An effective hybrid harmony search and cuckoo optimization algorithm based fuzzy PID controller for load frequency control,” *Appl. Soft Comput.*, vol. 65, pp. 121–138, Apr. 2018, doi: 10.1016/J.ASOC.2018.01.007.

[137] S. T. Cady, M. Zholbaryssov, A. D. Dominguez-Garcia, and C. N. Hadjicostis, “A Distributed Frequency Regulation Architecture for Islanded Inertialess AC Microgrids,” *IEEE Trans. Control Syst. Technol.*, vol. 25, no. 6, pp. 1961–1977, Nov. 2017, doi: 10.1109/TCST.2016.2640940.

[138] P. Vorobev, D. M. Greenwood, J. H. Bell, J. W. Bialek, P. C. Taylor, and K. Turitsyn, “Deadbands, Droop, and Inertia Impact on Power System Frequency Distribution,” *IEEE Trans. Power Syst.*, vol. 34, no. 4,

pp. 3098–3108, Jul. 2019, doi: 10.1109/TPWRS.2019.2895547.

[139] S. T. Cady, C. N. Hadjicostis, and A. D. Dominguez-Garcia, “Distributed frequency control of inertia-less AC microgrids,” in *2015 54th IEEE Conference on Decision and Control (CDC)*, Dec. 2015, pp. 2018–2023, doi: 10.1109/CDC.2015.7402503.

[140] Y. S. Kim, E. S. Kim, and S. Il Moon, “Distributed Generation Control Method for Active Power Sharing and Self-Frequency Recovery in an Islanded Microgrid,” *IEEE Trans. Power Syst.*, vol. 32, no. 1, pp. 544–551, Jan. 2017, doi: 10.1109/TPWRS.2016.2543231.

[141] M. Kosari and S. H. Hosseinian, “Decentralized Reactive Power Sharing and Frequency Restoration in Islanded Microgrid,” *IEEE Trans. Power Syst.*, vol. 32, no. 4, pp. 2901–2912, Jul. 2017, doi: 10.1109/TPWRS.2016.2621033.

[142] K. De Brabandere, B. Bolsens, J. Van den Keybus, A. Woyte, J. Driesen, and R. Belmans, “A voltage and frequency droop control method for parallel inverters,” *IEEE Trans. Power Electron.*, vol. 22, no. 4, pp. 1107–1115, Jul. 2007, doi: 10.1109/TPEL.2007.900456.

[143] Z. Shuai *et al.*, “Microgrid stability: Classification and a review,” *Renew. Sustain. Energy Rev.*, vol. 58, pp. 167–179, May 2016, doi: 10.1016/J.RSER.2015.12.201.

[144] M. Naderi, Y. Khayat, Q. Shafiee, T. Dragicevic, H. Bevrani, and F. Blaabjerg, “Interconnected Autonomous AC Microgrids via Back-to-Back Converters—Part I: Small-Signal Modeling,” *IEEE Trans. Power Electron.*, pp. 1–1, Sep. 2019, doi: 10.1109/tpel.2019.2943996.

[145] E. A. A. Coelho *et al.*, “Small-Signal Analysis of the Microgrid Secondary Control Considering a Communication Time Delay,” *IEEE Trans. Ind. Electron.*, vol. 63, no. 10, pp. 6257–6269, Oct. 2016, doi: 10.1109/TIE.2016.2581155.

[146] A. M. Egwebe, M. Fazeli, P. Igic, and P. M. Holland, “Implementation and Stability Study of Dynamic Droop in Islanded Microgrids,” *IEEE Trans. Energy Convers.*, vol. 31, no. 3, pp. 821–832, Sep. 2016, doi: 10.1109/TEC.2016.2540922.

[147] H. Moussa, A. Shahin, J.-P. Martin, B. Nahid-Mobarakeh, S. Pierfederici, and N. Moubayed, “Harmonic Power Sharing With Voltage Distortion Compensation of Droop Controlled Islanded Microgrids,” *IEEE Trans. Smart Grid*, vol. 9, no. 5, pp. 5335–5347, Sep. 2018, doi: 10.1109/TSG.2017.2687058.

[148] IEEE Standard, “2030.8-2018 - 2030.8-2018 - IEEE Standard for the Testing of Microgrid Controllers - IEEE Standard,” 2018. Accessed: Nov. 11, 2020. [Online]. Available: https://ieeexplore.ieee.org/document/8444947.

[149] “MITSUBISHI ELECTRIC Semiconductors & Devices: IPMs(Intelligent Power Modules) L1 series PM25CL1A120.” http://www.mitsubishielectric.com/semiconductors/php/eTypeNoProfile.php?TYPENO=PM25CL1A120&FOLDER=/product/powermodule/ipm/l1_series (accessed Mar. 18, 2020).

[150] “Powerex Product: BP7B-LB.” http://www.pwrx.com/Product/BP7B-LB (accessed Mar. 18, 2020).

[151] “LV 25-1000 | LEM.” https://www.lem.com/en/lv-251000 (accessed Mar. 18, 2020).

[152] “LA 55-P/SP1 | LEM.” https://www.lem.com/en/la-55psp1 (accessed Mar. 18, 2020).

[153] “sbRIO-9606 - National Instruments.” https://www.ni.com/en-ie/support/model.sbrio-9606.html (accessed Mar. 19, 2020).

[154] “NI 9683 User Manual and Specifications - National Instruments.”

[155] “TMS320F28335 C2000™ 32-bit MCU with 150 MIPS, FPU, 512 KB Flash, EMIF, 12b ADC | TI.com.” http://www.ti.com/product/TMS320F28335 (accessed Mar. 19, 2020).

[156] “Real time digital simulator │ Real time system │ OP5600.” https://www.opal-rt.com/simulator-platform-op5600/ (accessed Mar. 19, 2020).

[157] “RT Box | Plexim.” https://www.plexim.com/products/rt_box (accessed Mar. 19, 2020).

[158] “Renewable Energy – Recast to 2030 (RED II) | EU Science Hub.” https://ec.europa.eu/jrc/en/jec/renewable-energy-recast-2030-red-ii (accessed Nov. 17, 2020).

[159] A. Lahnaoui, P. Stenzel, and J. Linssen, “Techno-economic analysis of photovoltaic battery system configuration and location☆,” *Appl. Energy*, vol. 227, pp. 497–505, Oct. 2018, doi: 10.1016/J.APENERGY.2017.09.093.

[160] Prabha Kundur, *Power System Stability And Control*. New York: McGraw-Hill, 1994.

[161] J. D. Glover, T. J. (Thomas J. Overbye, and M. S. Sarma, *Power system analysis and design*. Stamford, CT, USA: Cengage Learning, 2012.

[162] J. He, Y. W. Li, J. M. Guerrero, F. Blaabjerg, and J. C. Vasquez, “An islanding Microgrid power sharing

approach using enhanced virtual impedance control scheme," *IEEE Trans. Power Electron.*, vol. 28, no. 11, pp. 5272–5282, 2013, doi: 10.1109/TPEL.2013.2243757.

[163] X. Meng, J. Liu, and Z. Liu, "A Generalized Droop Control for Grid-Supporting Inverter Based on Comparison between Traditional Droop Control and Virtual Synchronous Generator Control," *IEEE Trans. Power Electron.*, vol. 34, no. 6, pp. 5416–5438, Jun. 2019, doi: 10.1109/TPEL.2018.2868722.

[164] Y. Han, H. Li, P. Shen, E. A. A. Coelho, and J. M. Guerrero, "Review of Active and Reactive Power Sharing Strategies in Hierarchical Controlled Microgrids," *IEEE Transactions on Power Electronics*, vol. 32, no. 3. Institute of Electrical and Electronics Engineers Inc., pp. 2427–2451, Mar. 01, 2017, doi: 10.1109/TPEL.2016.2569597.

[165] U. B. Tayab, M. A. Bin Roslan, L. J. Hwai, and M. Kashif, "A review of droop control techniques for microgrid," *Renewable and Sustainable Energy Reviews*, vol. 76. Elsevier Ltd, pp. 717–727, Sep. 01, 2017, doi: 10.1016/j.rser.2017.03.028.

[166] K. Ş. Parlak, M. Özdemir, and M. T. Aydemir, "Active and reactive power sharing and frequency restoration in a distributed power system consisting of two UPS units," *Int. J. Electr. Power Energy Syst.*, vol. 31, no. 5, pp. 220–226, Jun. 2009, doi: 10.1016/j.ijepes.2009.01.006.

[167] J. M. Rey, C. X. Rosero, M. Velasco, P. Marti, J. Miret, and M. Castilla, "Local Frequency Restoration for Droop-Controlled Parallel Inverters in Islanded Microgrids," *IEEE Trans. Energy Convers.*, 2018, doi: 10.1109/TEC.2018.2886267.

[168] F. Guo, C. Wen, J. Mao, and Y. D. Song, "Distributed Secondary Voltage and Frequency Restoration Control of Droop-Controlled Inverter-Based Microgrids," *IEEE Trans. Ind. Electron.*, vol. 62, no. 7, pp. 4355–4364, Jul. 2015, doi: 10.1109/TIE.2014.2379211.

[169] M. Eskandari, L. Li, M. H. Moradi, P. Siano, and F. Blaabjerg, "Active Power Sharing and Frequency Restoration in an Autonomous Networked Microgrid," *IEEE Trans. Power Syst.*, vol. 34, no. 6, pp. 4706–4717, Nov. 2019, doi: 10.1109/TPWRS.2019.2923797.

[170] G. Chen and Z. Guo, "Distributed secondary and optimal active power sharing control for islanded microgrids with communication delays," *IEEE Trans. Smart Grid*, vol. 10, no. 2, pp. 2002–2014, Mar. 2019, doi: 10.1109/TSG.2017.2785811.

[171] S. Prakash, S. Member, V. Nougain, and S. Mishra, "Adaptive Droop based Control for Active Power Sharing in Autonomous Microgrid for Improved Transient Performance," *IEEE J. Emerg. Sel. Top. Power Electron.*, pp. 1–1, Apr. 2020, doi: 10.1109/jestpe.2020.2988712.

[172] W. Deng, N. Dai, K.-W. Lao, and J. M. Guerrero, "A Virtual-Impedance Droop Control for Accurate Active Power Control and Reactive Power Sharing Using Capacitive-Coupling Inverters," *IEEE Trans. Ind. Appl.*, pp. 1–1, Jul. 2020, doi: 10.1109/tia.2020.3012934.

[173] L. Zhang, H. Zheng, Q. Hu, B. Su, and L. Lyu, "An Adaptive Droop Control Strategy for Islanded Microgrid Based on Improved Particle Swarm Optimization," *IEEE Access*, vol. 8, pp. 3579–3593, 2020, doi: 10.1109/ACCESS.2019.2960871.

[174] Y. Zhu, F. Zhuo, F. Wang, B. Liu, R. Gou, and Y. Zhao, "A virtual impedance optimization method for reactive power sharing in networked microgrid," *IEEE Trans. Power Electron.*, vol. 31, no. 4, pp. 2890–2904, Apr. 2016, doi: 10.1109/TPEL.2015.2450360.

[175] R. Rosso, S. Engelken, and M. Liserre, "Robust stability analysis of synchronverters operating in parallel," *IEEE Trans. Power Electron.*, vol. 34, no. 11, pp. 11309–11319, Nov. 2019, doi: 10.1109/TPEL.2019.2896707.

[176] Z. Shuai, W. Huang, Z. J. Shen, A. Luo, and Z. Tian, "Active Power Oscillation and Suppression Techniques between Two Parallel Synchronverters during Load Fluctuations," *IEEE Trans. Power Electron.*, vol. 35, no. 4, pp. 4127–4142, Apr. 2020, doi: 10.1109/TPEL.2019.2933628.

[177] Z. Li, Y. Xu, X. Feng, and Q. Wu, "Optimal Stochastic Deployment of Heterogeneous Energy Storage in a Residential Multi-Energy Microgrid with Demand-Side Management," *IEEE Trans. Ind. Informatics*, pp. 1–1, Feb. 2020, doi: 10.1109/tii.2020.2971227.

[178] A. Micallef, M. Apap, C. Spiteri-Staines, and J. M. Guerrero, "Single-Phase Microgrid with Seamless Transition Capabilities between Modes of Operation," *IEEE Trans. Smart Grid*, vol. 6, no. 6, pp. 2736–2745, Nov. 2015, doi: 10.1109/TSG.2015.2444912.

[179] C. Sun *et al.*, "Design and Real-Time Implementation of a Centralized Microgrid Control System with Rule-Based Dispatch and Seamless Transition Function," *IEEE Trans. Ind. Appl.*, vol. 56, no. 3, pp. 3168–3177, May 2020, doi: 10.1109/TIA.2020.2979790.

[180] A. Vukojevic and S. Lukic, "Microgrid Protection and Control Schemes for Seamless Transition to Island

and Grid Synchronization," *IEEE Trans. Smart Grid*, vol. 11, no. 4, pp. 2845–2855, Jul. 2020, doi: 10.1109/TSG.2020.2975850.

[181] S. Mishra, D. Ramasubramanian, and P. C. Sekhar, "A seamless control methodology for a grid connected and isolated PV-diesel microgrid," *IEEE Trans. Power Syst.*, vol. 28, no. 4, pp. 4393–4404, 2013, doi: 10.1109/TPWRS.2013.2261098.

[182] L. G. Meegahapola, D. Robinson, A. P. Agalgaonkar, S. Perera, and P. Ciufo, "Microgrids of commercial buildings: Strategies to manage mode transfer from grid connected to islanded mode," *IEEE Trans. Sustain. Energy*, vol. 5, no. 4, pp. 1337–1347, Oct. 2014, doi: 10.1109/TSTE.2014.2305657.

[183] Y. A. R. I. Mohamed and A. A. Radwan, "Hierarchical control system for robust microgrid operation and seamless mode transfer in active distribution systems," *IEEE Trans. Smart Grid*, vol. 2, no. 2, pp. 352–362, Jun. 2011, doi: 10.1109/TSG.2011.2136362.

[184] E. Pashajavid, A. Ghosh, and F. Zare, "A Multimode Supervisory Control Scheme for Coupling Remote Droop-Regulated Microgrids," *IEEE Trans. Smart Grid*, vol. 9, no. 5, pp. 5381–5392, Sep. 2018, doi: 10.1109/TSG.2017.2688475.

[185] F. Shahnia, S. Bourbour, and A. Ghosh, "Coupling Neighboring Microgrids for Overload Management Based on Dynamic Multicriteria Decision-Making," *IEEE Trans. Smart Grid*, vol. 8, no. 2, pp. 969–983, Mar. 2017, doi: 10.1109/TSG.2015.2477845.

[186] E. Pashajavid, F. Shahnia, and A. Ghosh, "Development of a Self-Healing Strategy to Enhance the Overloading Resilience of Islanded Microgrids," *IEEE Trans. Smart Grid*, vol. 8, no. 2, pp. 868–880, Mar. 2017, doi: 10.1109/TSG.2015.2477601.

[187] S. M. Ferdous, G. M. Shafiullah, F. Shahnia, R. M. Elavarasan, and U. Subramaniam, "Dynamic Frequency and Overload Management in Autonomous Coupled Microgrids for Self-Healing and Resiliency Improvement," *IEEE Access*, vol. 8, pp. 116796–116811, 2020, doi: 10.1109/ACCESS.2020.3004185.

[188] R. H. Lasseter, "Smart distribution: Coupled microgrids," in *Proceedings of the IEEE*, 2011, vol. 99, no. 6, pp. 1074–1082, doi: 10.1109/JPROC.2011.2114630.

[189] A. Khodaei, "Provisional Microgrids," *IEEE Trans. Smart Grid*, vol. 6, no. 3, pp. 1107–1115, May 2015, doi: 10.1109/TSG.2014.2358885.

[190] S. Bourbour and F. Shahnia, "A suitable mechanism for the interconnection phase of temporary coupling of adjacent microgrids," in *IEEE PES Innovative Smart Grid Technologies Conference Europe*, Dec. 2016, pp. 624–629, doi: 10.1109/ISGT-Asia.2016.7796457.

[191] A. Arefi and F. Shahnia, "Tertiary controller-based optimal voltage and frequency management technique for multi-microgrid systems of large remote towns," *IEEE Trans. Smart Grid*, vol. 9, no. 6, pp. 5962–5974, Nov. 2018, doi: 10.1109/TSG.2017.2700054.

[192] M. A. Shoeb, F. Shahnia, and G. Shafiullah, "A Multilayer and Event-triggered Voltage and Frequency Management Technique for Microgrid’s Central Controller Considering Operational and Sustainability Aspects," *IEEE Transactions on Smart Grid*, Institute of Electrical and Electronics Engineers Inc., 2018.

[193] M. A. Hayat, F. Shahnia, and G. M. Shafiullah, "Replacing Flat Rate Feed-In Tariffs for Rooftop Photovoltaic Systems with a Dynamic One to Consider Technical, Environmental, Social, and Geographical Factors," *IEEE Trans. Ind. Informatics*, vol. 15, no. 7, pp. 3831–3844, Jul. 2019, doi: 10.1109/TII.2018.2887281.

[194] C. Feng, F. Wen, S. You, Z. Li, F. Shahnia, and M. Shahidehpour, "Coalitional Game-Based Transactive Energy Management in Local Energy Communities," *IEEE Trans. Power Syst.*, vol. 35, no. 3, pp. 1729–1740, May 2020, doi: 10.1109/TPWRS.2019.2957537.

[195] A. J. Datta, A. Ghosh, and S. Rajakaruna, "Power sharing in a hybrid microgrid with bidirectional switch," in *IEEE Power and Energy Society General Meeting*, Jan. 2018, vol. 2018-January, pp. 1–5, doi: 10.1109/PESGM.2017.8274281.

[196] J. Susanto, F. Shahnia, A. Ghosh, and S. Rajakaruna, "Interconnected microgrids via back-to-back converters for dynamic frequency support," Nov. 2014, doi: 10.1109/AUPEC.2014.6966616.

[197] B. John, A. Ghosh, M. Goyal, and F. Zare, "A DC Power Exchange Highway Based Power Flow Management for Interconnected Microgrid Clusters," *IEEE Syst. J.*, vol. 13, no. 3, pp. 3347–3357, Sep. 2019, doi: 10.1109/JSYST.2019.2911625.

[198] E. Pashajavid, F. Shahnia, and A. Ghosh, "Interconnection of two neighboring autonomous microgrids based on small signal analysis," in *9th International Conference on Power Electronics - ECCE Asia:*

*"Green World with Power Electronics", ICPE 2015-ECCE Asia*, Jul. 2015, pp. 213–220, doi: 10.1109/ICPE.2015.7167789.

[199] F. Shahnia, "Stability and eigenanalysis of a sustainable remote area microgrid with a transforming structure," *Sustain. Energy, Grids Networks*, vol. 8, pp. 37–50, Dec. 2016, doi: 10.1016/j.segan.2016.09.005.

[200] Y. Zhang, L. Xie, and Q. Ding, "Interactive Control of Coupled Microgrids for Guaranteed System-Wide Small Signal Stability," *IEEE Trans. Smart Grid*, vol. 7, no. 2, pp. 1088–1096, Mar. 2016, doi: 10.1109/TSG.2015.2495233.

[201] J. Sun, "Impedance-based stability criterion for grid-connected inverters," *IEEE Trans. Power Electron.*, vol. 26, no. 11, pp. 3075–3078, 2011, doi: 10.1109/TPEL.2011.2136439.

[202] Y. Han *et al.*, "Modeling and Stability Analysis of $LCL$ -Type Grid-Connected Inverters: A Comprehensive Overview," *IEEE Access*, vol. 7, pp. 114975–115001, Aug. 2019, doi: 10.1109/access.2019.2935806.

[203] Y. Hua and T. K. Sarkar, "Matrix pencil method for estimating parameters of exponentially damped/undamped sinusoids in noise," *IEEE Trans. Acoust.*, vol. 38, no. 5, pp. 814–824, May 1990, doi: 10.1109/29.56027.

[204] M. Bakhshi, R. Noroozian, and G. B. Gharehpetian, "Anti-Islanding Scheme for Synchronous DG Units Based on Tufts–Kumaresan Signal Estimation Method," *IEEE Trans. Power Deliv.*, vol. 28, no. 4, pp. 2185–2193, Oct. 2013, doi: 10.1109/TPWRD.2013.2271837.

[205] T. K. Sarkar and O. Pereira, "Using the matrix pencil method to estimate the parameters of a sum of complex exponentials," *IEEE Antennas Propag. Mag.*, vol. 37, no. 1, pp. 48–55, Feb. 1995, doi: 10.1109/74.370583.

[206] J. E. Fernandez del Rio and T. K. Sarkar, "Comparison between the Matrix Pencil Method and the Fourier Transform Technique for High-Resolution Spectral Estimation," *Digit. Signal Process.*, vol. 6, no. 2, pp. 108–125, Apr. 1996, doi: 10.1006/dspr.1996.0011.

[207] S. Agrawal, S. R. Mohanty, and V. Agarwal, "Harmonics and interharmonics estimation of wind power plant using sliding window matrix pencil," in *IECON 2015 - 41st Annual Conference of the IEEE Industrial Electronics Society*, Nov. 2015, pp. 004984–004989, doi: 10.1109/IECON.2015.7392882.

[208] M. Bhuiyan, E. V. Malyarenko, M. A. Pantea, F. M. Seviaryn, and R. Gr. Maev, "Advantages and Limitations of Using Matrix Pencil Method for the Modal Analysis of Medical Percussion Signals," *IEEE Trans. Biomed. Eng.*, vol. 60, no. 2, pp. 417–426, Feb. 2013, doi: 10.1109/TBME.2012.2227318.

[209] M. Hanif, M. Basu, and K. Gaughan, "Development of EN50438 compliant wavelet-based islanding detection technique for three-phase static distributed generation systems," *IET Renew. Power Gener.*, vol. 6, no. 4, p. 289, 2012, doi: 10.1049/iet-rpg.2011.0290.

[210] A. Samui and S. R. Samantaray, "Wavelet Singular Entropy-Based Islanding Detection in Distributed Generation," *IEEE Trans. Power Deliv.*, vol. 28, no. 1, pp. 411–418, Jan. 2013, doi: 10.1109/TPWRD.2012.2220987.

[211] M. S. ElNozahy, E. F. El-Saadany, and M. M. A. Salama, "A robust wavelet-ANN based technique for islanding detection," in *2011 IEEE Power and Energy Society General Meeting*, Jul. 2011, pp. 1–8, doi: 10.1109/PES.2011.6039158.

[212] S. Alshareef, S. Talwar, and W. G. Morsi, "A New Approach Based on Wavelet Design and Machine Learning for Islanding Detection of Distributed Generation," *IEEE Trans. Smart Grid*, vol. 5, no. 4, pp. 1575–1583, Jul. 2014, doi: 10.1109/TSG.2013.2296598.

[213] H. T. Do, X. Zhang, N. V. Nguyen, S. Li, and T. T.-T. Chu, "Passive islanding detection method using Wavelet Packet Transform in Grid Connected Photovoltaic Systems," *IEEE Trans. Power Electron.*, pp. 1–1, 2015, doi: 10.1109/TPEL.2015.2506464.